Final Report for the project HARPOL:
Harmonizing and advancing retrieval approaches for present and future polarimetric space-borne atmospheric missions

ESA Open Call EO for Science & Society
February 2021 – December 2022

document number	SRON-ESG-RP-2021-006
authors	Otto Hasekamp, Pavel Litvinov, Cheng Chen, Oleg Dubovik, Guangliang Fu, et al.
ESA Technical Officer	Christian Retscher
CI identification	: None
issue	: 4.3
date	: 2022-12-16
status	: final

Issue	Date	Changed Section	Description of Change
1.0	2021-06-24	all	First issue. Contains WP1 report (Chapter 2).
2.0	2021-11-15	Chapter 1 &3	Added WP2 report (Chapter 3) and introduction (Chapter 1).
2.1	2021-12-20	all	Addressed ESA comments in Chapter 2 & 3
3.0	2022-06-22	Chapter 4	Added the WP3 report as Chapter 4.
3.1	2022-07-12	Chapter 4	Addressed ESA comments in Chapter 4
4.0	2022-10-23	Chapter 5,6,7	Included WP4 report as Chapter 5. Included summary (chapter 6) and recommendation (chapter 7)
4.1	2022-11-10	Chapter 5	Added MODIS comparison.
4.2	2022-11-17	Chapter 5	Added Figure 5-17, Figure 5-19, Figure 5-21, and Figure 5-22 and explanatory text.
4.3	2022-12-16	all	Addressed ESA comments

List of Abbreviations

AAOD	Absorption Aerosol Optical Depth
AOD	Aerosol Optical Depth
AE	Angstrom Exponent
AERONET	Aerosol Robotic Network
BRDF	Bi-directional Reflection Distribution Function
BPDF	Bi-directional Polarization Distribution Function
GRASP	Generalized Retrieval of Aerosol and Surface Properties
GRASP-CC	GRASP – Chemical Components
GRASP-HP	GRASP- High Performance
HARPOL	Harmonizing and advancing retrieval approaches for present and future polarimetric space-borne atmospheric missions
LOA	Laboratory of Atmospheric Optics
MAE	Mean Absolute Error
MODIS	Moderate Resolution Imaging Spectroradiometer
MODIS-DB	MODIS-Deep Blue
MODIS-DT	MODIS- Dark Target
POLDER	Polarization and Directionality of Earth Reflectances
PARASOL	Polarization & Anisotropy of Reflectances for Atmospheric Sciences coupled with Observations from a Lidar
WP	Work Package
RemoTAP	Remote sensing of Trace gas and Aerosol Products
RMSE	Root Mean Square Error
RMSD	Root Mean Square Difference
SSA	Single Scattering Albedo
SRON	Netherlands Institute for Space Research

Table of Contents

1 Introduction

Atmospheric aerosol particles strongly influence climate by scattering and absorbing light (direct forcing) and by changing cloud properties (indirect forcing). The corresponding radiative forcing represents one of the most uncertain radiative forcing terms as reported by the Intergovernmental Panel on Climate Change (IPCC). To improve our understanding of the effect of aerosols on climate and air quality, measurements of aerosol chemical composition, size distribution, optical properties like Aerosol Optical Thickness (AOT) and Single Scattering Albedo (SSA), as well as the aerosol height profile are of crucial importance. It has been demonstrated by studies on synthetics measurements, airborne measurements, and space-borne measurements that Multi-Angle Polarimetric (MAP) measurements are needed to provide information about detailed aerosol properties like size distribution, refractive index, SSA, in addition to the AOT.

The only MAP instrument that has provided a multi-year data set (2005-2013) in the past has been the French POLDER-3 instrument on the PARASOL mission. Now space agencies realize the large potential of MAP instrumentation, in the 2020s several of such instruments will be launched, e.g. 3MI on METOP-SG (ESA-2023), SPEXone and HARP-2 on PACE (NASA-2023), and a MAP on the CO2-Monitoring mission (ESA-2025) and A-CCP (NASA-2028). To cope with the increased information content on aerosols of MAP instrumentation and to assess the climatic effect of aerosols, new tools for retrieval need to be (further) developed. So far, this development has lagged the instrument development, which is the reason for the under-exploitation of the existing POLDER-3/PARASOL data sets.

Currently, there are two algorithms that have demonstrated capability at a global scale to exploit the rich information content of MAP measurements: the Generalized Retrieval of Aerosol and Surface Properties (GRASP) algorithm, developed at the Laboratory of Atmospheric Optics (LOA) of the University of Lille and the GRASP-sas company, and the Remote Sensing of Trace gases and Aerosol Properties (RemoTAP) algorithm developed at SRON – Netherlands Institute for Space Research. Both algorithms show good performance against ground based AERONET measurements and already important scientific advancement has been made using the corresponding data products. Nevertheless, when looking at global maps, significant differences are apparent between the two algorithms. In order to improve retrieval products from PARASOL and the upcoming missions containing MAP instrumentation (3MI/METOP-SG, SPEXone/PACE, HARP2/PACE, MAP/CO2M) it is essential to understand the reasons for the differences between the GRASP and RemoTAP algorithms.

Therefore, in the HARPOL (Harmonizing and advancing retrieval approaches for present and future polarimetric space-borne atmospheric missions) project we perform a comparison between the two algorithms. We expect this will lead to optimized algorithm choices for both algorithms leading to better aerosol products and error characterization.

The HARPOL project consists of different Work Packages (WPs):

- WP-1: Intercomparison of existent products
- WP-2: Intercomparison and harmonization using synthetic data
- WP-3: Intercomparison and harmonization using real data
- WP-4: Global processing using harmonized retrieval settings

This document contains the reports of the work performed in the different WPs. It is a living document where new sections are added when a new WP has been completed.

2 WP1 Report: Intercomparison of existent POLDER-3/SRON and POLDER-3/GRASP aerosol and surface products

2.1 Purpose and objective

The chapter is the report of intercomparison of existent POLDER-3/SRON and POLDER-3/GRASP aerosol and surface products in the frame of the harmonizing and advancing retrieval approaches for present and future polarimetric space-borne atmospheric missions (HARPOL) project working package 1. The purpose of this report is to present and evaluate the difference between the existent SRON and GRASP POLDER-3/PARASOL aerosol and surface products globally based on the intercomparison and validation with AERONET.

2.2 Chapter overview

The structure of this WP1 report is as follows. The description of the existent POLDER-3/SRON and POLDER-3/GRASP products used in this report are described in Section 3, followed by the description of the reference measurements and matchup methodology used for validation and intercomparison in Section 4. Section 5 describes the aerosol validation using reference measurements, compares the validation results and intercompares the SRON and GRASP aerosol products globally. Section 6 describes the surface intercomparison between the SRON and GRASP products as well as independent MODIS surface products. Section 7 concludes the activities conducted in WP1.

2.3 Description of POLDER-3/SRON and POLDER-3/GRASP products

The POLDER-3/PARASOL imager has 3 gaseous absorption channels (763, 765 and 910 nm), in addition to 6 channels (443, 490, 565, 670, 865 and 1020 nm) measuring the total radiance, and 3 channels (490, 670 and 865 nm) measuring the polarization. The number of viewing angles is similar for all spectral channels varying from 14 to 16 depending on the location of the pixel on the CCD. PARASOL provided global coverage about every 2 days with a nadir spatial resolution ~6 km.

SRON and GRASP algorithms are developed to retrieve aerosol and surface parameters simultaneously based on the online radiative transfer. Specifically, the algorithms search the

solution of aerosol microphysical properties (size, refractive index, column, shape etc.) and surface bidirectional reflection distribution function (BRDF) parameter in a continuous parameter space, and then derive aerosol optical properties based on the microphysical properties (Hasekamp et al., 2007, 2009; Dubovik et al., 2011, 2014; Fu and Hasekamp, 2018).

GRASP algorithm. The Generalized Retrieval of Aerosol and Surface Properties is a new-generation algorithm developed for deriving extensive aerosol properties from diverse pace-borne and ground-based instruments. The bigger the information content is in the remote sensing instrument the higher performance the GRASP algorithm will demonstrate. The overall concept of the algorithm is described by Dubovik et al. [2014] , while specific aspects are detailed in Dubovik et al. [2011]. An open-source GRASP-OPEN software version and documentation are available from https://www.grasp-open.com . The algorithm is based on highly advanced statistically optimized fitting implemented as multi- term least square minimization [Dubovik, 2004] that had earlier been successfully implemented (e.g., see Refs. (Dubovik and King, 2000, Dubovik et al., 2000, 2002, 2006) for aerosol retrievals from ground-based AERONET radiometers. POLDER/GRASP shares its methodology with AERONET retrievals. For example, for each individual pixel it uses multiple a priori constraints such as smoothness limitations on the retrieved continuous functions including the size distribution, spectral dependencies of the refractive index, and BRDF parameters. At the same time, the POLDER/GRASP concept is more flexible, includes several original features, and enables the implementation of advanced retrieval scenarios. For example, it retrieves both aerosol and underlying surface properties simultaneously from satellite observations using additional a priori constraints on the spectral variability of the land BRDF. The more essential novelty is that the POLDER/GRASP retrieval is implemented as a multi-pixel concept wherein the optimized retrieval is performed simultaneously for a large group of pixels [Dubovik et al., 2011] . This feature brings additional possibilities for improving the accuracy of retrievals by using known constraints on the inter-pixel variability of retrieved aerosol and surface reflectance parameters. The GRASP retrieval design allows for a stable retrieval using a unique global set of constraints (no location-specific assumptions) starting from a single initial guess globally. As a result, GRASP provides reliable retrievals of detailed aerosol properties that have traditionally been difficult to obtain from satellites, such as aerosol absorption and type. POLDER/GRASP retrieval utilizes radiances in six wavelengths and polarized radiances in three wavelengths and performs radiative-transfer modeling fully accounting for multiple interactions of the scattered solar light in the atmosphere at the native POLDER-1 and -2 ~7 km and POLDER-3 ~6-km resolution. Since these complex computations are done on-line, significant efforts have been focused on the optimization and acceleration of the GRASP routines and on adapting the code for operational processing of voluminous datasets.

The GRASP is a very flexible algorithm and allows a variety of different possibilities on modeling aerosol and surface. Currently, there are three archives of POLDER/PARASOL data processed by GRASP:

(1) PARASOL/GRASP «optimized» (in the sense that radiative transfer calculations were optimize to best trade-off between speed of processing and accuracy of results);

(2) PARASOL/GRASP «high-precision» (the accurate radiative transfer calculations were used).

(3) PARASOL/GRASP «models» (the aerosol is assumed as an external mixture of several aerosol components).

The «optimized» and «high-precision» are different only by the precision of RT calculations, while conceptually they are the same: aerosol size distribution, spectral values of complex index of refraction, fraction of spherical particles and and the Aerosol Layer Height (ALH), and the spectral parameters of surface BRDF and BPDF parameters are retrieved simultaneously. The retrievals were performed using one aerosol component model with 5 size bins size distribution and spectrally dependent complex refractive index. The aerosol vertical distribution was modelled using exponential profile and scale height retrieved.

The «models» approach uses different assumption for modeling aerosol properties (surface properties model is the same): the aerosol is assumed as external mixture of several aerosol components and only concentrations are retrieved together with the Aerosol Layer Height (ALH) and spectral parameters of surface BRDF and BPDF. The size distribution, complex refractive index and non-sphericity parameter for each aerosol component are derived from the results of AERONET aerosol climatology for the main distinct aerosol types [Dubovik et al., 2002] and improved in a series of sensitivity tests with satellite data. For retrievals over land both GRASP approaches, like in the SRON algorithm (see below), the Ross-Li and Maignan models have been used, with the difference that the directional and polarization effects are not assumed strictly spectrally neutral but only spectrally smooth. For retrievals over ocean the wind speed and a spectrally dependent Lambertian albedo are being included in the state vector.

SRON algorithm. The development of the SRON algorithm was initiated with the goal to make full use of the information content of multi-angle photo-polarimetric observations. The retrieval is based on an iterative fitting of a linearized radiative transfer model (Hasekamp and Landgraf, 2005) to the POLDER data, using a cost function containing a misfit term between the forward model and measurement and a regularization term using a priori estimates of values of some of the retrieved parameters. The algorithm has large flexibility in defining the aerosol properties included in the retrieval state vector (Fu and Hasekamp, 2018). The aerosol size distribution is described by the sum of an arbitrary number log-normal functions, called modes, where for each mode the effective radius, effective variance, aerosol column number, real and imaginary parts of the refractive index (in the form of coefficients of spectrally dependent functions), fraction of spherical particles, and the Aerosol Layer Height (ALH) can be retrieved in principle. For retrievals over ocean, reflection on the ocean surface is described by Fresnel reflection on surface facets, where the distribution of surface-facet orientations depends on wind-speed and direction. The contribution from the ocean body is modeled by a NN that was trained by RT calculations in the

ocean body for different Chlorophyll-a concentrations. In addition, a spectrally dependent Lambertian albedo can be added to the ocean reflection matrix. For retrievals over land, two models are implemented for the Bi-directional Reflectance Distribution Function (BRDF), namely the Ross-Li kernel based model and the Rahman-Pinty-Verstrate (RPV) model (Litvinov et al., 2011). For the polarized component of the surface reflection the models of Maignan et al. (2009) and Litvinov et al. (2011) have been implemented. Here, the directional and polarization effects of surface reflection are assumed to be spectrally neutral. So far, retrievals for two different types of aerosol descriptions in the state vector have been performed: a parametric 2-mode and a multi-mode description. The parametric 2-mode setup uses a bimodal aerosol description where all above-mentioned aerosol parameters are retrieved for both modes, except for the fraction of spheres which is only retrieved for the coarse mode, and the ALH for which one value for both modes is retrieved (i.e. it is assumed that the ALH is the same for both modes). In this setup, retrieval studies have been performed for POLDER-3/PARASOL (Hasekamp et al., 2011; Stap et al., 2015), and a global data-set from POLDER-3/PARASOL has been created (Lacagnina et al., 2016, 2017). Also retrievals have been performed from airborne (Wu et al., 2015, 2016; di Noia et al., 2017) and ground based measurements (van Harten et al., 2015; di Noia et al, 2015). In the multi-mode setup, the retrieval state vector is defined based on a larger number of modes (typically 5-10), each with their own fixed effective radius and effective variance. Only the number column of each mode is included in the state vector, in addition to the refractive index for fine (radius < 0.80 micron) and coarse (radius > 0.80 micron) particles. Like for the parametric 2- mode setup, one value for the ALH is retrieved which is assumed to be the same for all modes. In the multi (5-) mode setup, recently aerosol retrievals have been performed from different airborne polarimeters employed during the ACEPOL campaign (Fan et al., 2019; Fu et al., 2020), as well as from a subset of the POLDER-3/PARASOL measurements (Fu and Hasekamp, 2018).

The SRON product evaluated in this WP is generated in 2016 and was used in the study of Lacagnina et 2017). The setup for this global processing corresponds to the parametric 2 mode setup.

Both the GRASP and SRON algorithm have great flexibility in the definition of the retrieval state vector, i.e. the set of aerosol and surface/ocean parameters that are being retrieved. Both algorithms are applied to global processing of POLDER-3/PARASOL multi-spectral multi-angular polarimeter measurements, and generate a set of detailed global aerosol optical and microphysical properties, as well as surface properties. These products are promising and crucial for the community to understand the global pattern of detailed aerosol properties, e.g. size, absorption, etc., and they have been used to estimate global aerosol emission, data assimilation, evaluation of aerosol direct and indirect effects (Chen et al., 2019; Tsikerdekis et al., 2020, Lacagnina et al., 2015, 2017, Hasekamp et al., 2019).

In this report, we aim to understand the two products based on intercomparison and validation against referenced dataset. The overall tasks can be divided into:

- ➔ Validation of existing SRON and GRASP products with AERONET
- ➔ Evaluation of differences between existing SRON and GRASP products AERONET validation
- ➔ Evaluation of differences between existing SRON and GRASP aerosol and surface products globally

2.4 Reference measurements and matchup methodology

2.4.1 AERONET ground-based monitoring network

For the retrieval of aerosol properties the AERONET dataset is the obvious choice for validation (Holben et al., 1998). AERONET provides accurate direct sun AOD products with high reliable accuracy 0.01-0.02. Strict protocols for the calibration and maintenance assure homogeneity among all its instruments. Due to its high data quality, the AERONET AOD products are widely used as “ground truth” to evaluate satellite remote sensing aerosol products. In this report, we use AERONET Version 3 Level direct sun spectral AOD, AE (Giles et al., 2019), fine/coarse mode AOD from spectral deconvolution algorithm (SDA) (O’Neill et al., 2003) and spectral AAOD and SSA from inversion product (Dubovik and King, 2000). All AERONET sites with available Level 2 data in 2006 are adopted.

2.4.2 Matchup methodology

The POLDER/SRON product is at ~18 km spatial resolution, which is retrieved by aggregation of 3x3 POLDER-3 pixels’ measurements. The POLDER/GRASP product is generated at POLDER-3 nativre resolution ~6 km. Due to the differences in product spatial resolution, we firstly re-grid two products into common 0.2 degree resolution, which seems to be the best compromise for 2 products. The validation and intercomparison will be done for the 0.2 degree POLDER/SRON and POLDER/GRASP products. We follow a standard matchup strategy to validate with AERONET as Chen et al. (2020), specifically, the satellite retrievals are averaged in a window (3x3) for the gridded satellite data centered over the AERONET site. The AERONET direct-sun AOD, AE, SDA AODF and AODC data were averaged within ±30 minutes of the PARASOL overpass, while AERONET inverted SSA and AAOD (which have a lower sampling frequency) are averaged within ±180 minutes. In addition, AERONET station elevations greater than 3600 m above mean sea level are omitted from the comparison.

The strategies to select the retrieval product with highest quality to perform AERONET validation are using “Residual Relative” for GRASP and “Chi2” for SRON, which are the errors in fitting the measurements by the algorithms. In this report, we use two versions of GRASP products: (i) GRASP/HP; (ii) GRASP/Models. Because the GRASP/Models product is applied a stricter quality assurance filter while product generation, no additional filter is required for the AERONET validation. For GRASP/HP, we use a general residual threshold (0.05 over land and 0.1 over

ocean) as Chen et al. (2020). For SRON products, the “Chi2” thresholds applied over land and ocean are 2.5 and 10.0 respectively.

2.4.3 Statistical metrics

In order to quantify the validation results, several statistical parameters are considered in this report, e.g. Pearson’s linear correlation coefficient (R), root mean square error (RMSE), bias ($BIAS_{TOTAL}$), and bias for low AOD (<0.2) ($BIAS_{AOD<0.2}$). Besides, the fraction of data within GCOS requirements (GCOS fraction) and within Target requirements (Target fraction) are used to evaluate the AOD products that satisfy the GCOS and Target requirements. The GCOS and Target requirements are defined as:
GCOS: max (0.04 or 10% AOD), Target: max (0.05 or 20% AOD).

General requirements on AOD and SSA are summarized in Table 2-1.

Table 2-1: Requirements on aerosol.

Characteristic	Required Uncertainty	
	Based on GCOS and aerosol CCI	Target: relaxed
AOD	0.04 or 10% (whatever is bigger)	0.05 or 20% (whatever is bigger)
Fine mode AOD (AODf)	0.04 or 10% (whatever is bigger)	0.05 or 20% (whatever is bigger)
SSA	0.02 - 0.03	0.05

2.5 Aerosol validation and intercomparison

2.5.1 AERONET Validation

We validate one year (2006) POLDER-3/SRON, POLDER-3/GRASP Models and POLDER-3/GRASP HP data using all available AERONET L2 data. Figure 2-1 shows the validation of AOD (550 nm) over land. Due to the different filtering strategy, the number of matchups vary from SRON (1414) to GRASP/Models (5224). GRASP/Models seems of better agreement among 3 datasets, with R=0.859, GCOS=47.8%, $BIAS_{TOTAL}$=0.00 (1σ=0.16) and $BIAS_{AOD<0.2}$=0.00 (1σ=0.07). SRON and GRASP/HP show similar performance in general, GCOS around 33% and positive bias for low aerosol loadings $BIAS_{AOD<0.2}$ around 0.06-0.07, which is non-negligible.

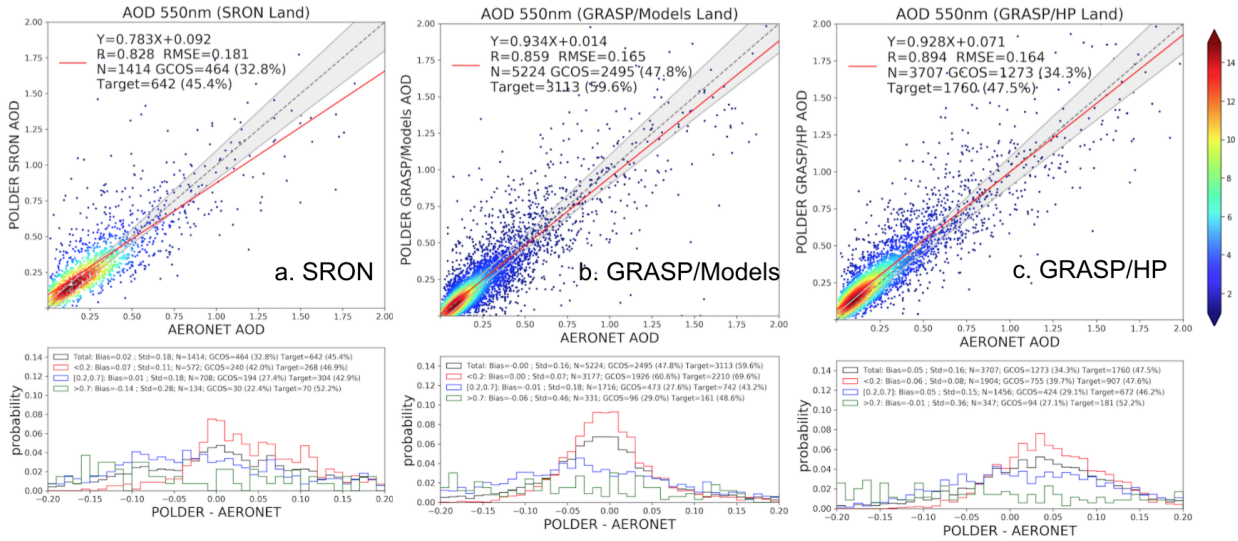

Figure 2-1 Validation of (a) POLDER-3/SRON, (b) POLDER-3/GRASP Models and (c) POLDER-3/GRASP HP AOD at 550 nm over land with AERONET. The gray dashed line and the red solid line are the 1:1 reference line and the linear regression line. The gray envelope indicates GCOS requirement: max (0.04 or 10%AOD). The probability density functions of bias (POLDER-AERONET) and the standard deviation (1σ) of the bias are present in the lower panel. The black, red, blue and green solid lines indicate all AOD conditions: any AOD, AOD<0.2, 0.2≤AOD≤0.7 and AOD>0.7 respectively.

Figure 2-2 shows the validation of AOD (550 nm) over ocean. Similar to results over land, GRASP/Models tends to have better validation metrics, R=0.934, RMSE=0.068, GCOS=63.3% and $BIAS_{TOTAL}$=0.01 (1σ=0.07) and $BIAS_{AOD<0.2}$=0.01 (1σ=0.04). SRON and GRASP/HP show a similar pattern of bias for low aerosol loadings. SRON has a slightly smaller bias than GRASP/HP, 0.03 compared to 0.06. And the GCOS is also better from SRON (46.1%) than GRASP/HP (32.4%).

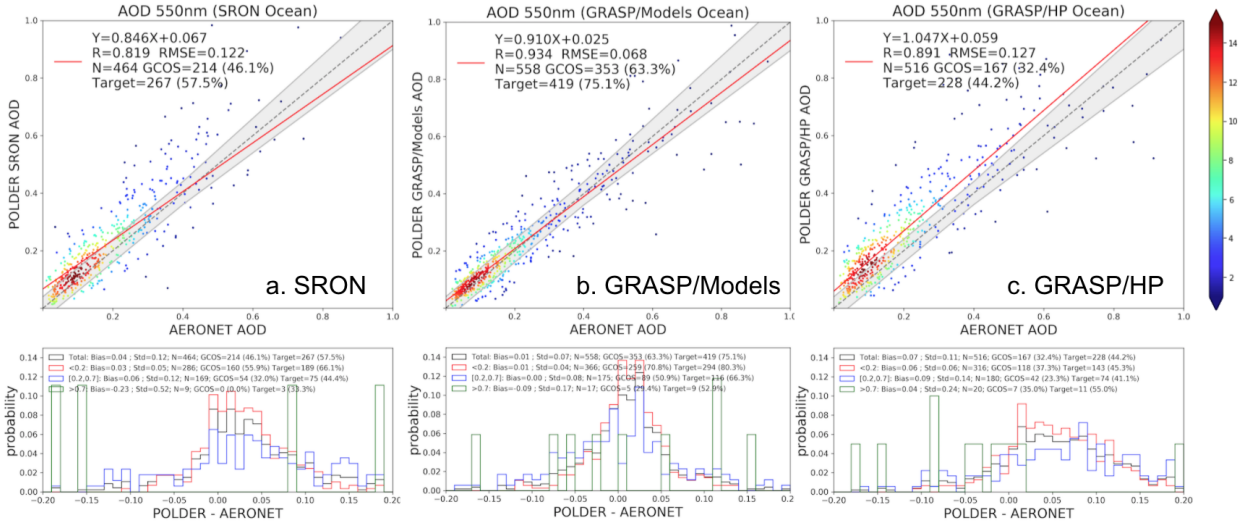

Figure 2-2 Validation of (a) POLDER-3/SRON, (b) POLDER-3/GRASP Models and (c) POLDER-3/GRASP HP AOD at 550 nm over ocean with AERONET.

Table 2-2: Summary of statistics of SRON, GRASP/Models and GRASP/HP spectral POLDER AOD products against AERONET at 440, 550, 670 and 865 nm over land and ocean.

Land/Ocean	WL (nm)	Products	R	RMSE	GCOS (%)	Target (%)	$BIAS_{TOTAL}$	$BIAS_{AOD<0.2}$
Land	440	SRON	0.831	0.210	30.0	46.3	0.04	0.08
		Models	0.867	0.192	**42.8**	**55.3**	**0.00**	**0.00**
		HP	**0.897**	**0.187**	31.8	46.1	0.05	0.06
	550	SRON	0.828	0.181	32.8	45.4	0.02	0.07
		Models	0.859	0.165	**47.8**	**59.6**	**0.00**	**0.00**
		HP	**0.894**	**0.164**	34.3	47.5	0.05	0.06
	670	SRON	0.824	0.168	34.0	44.1	**0.00**	0.05
		Models	0.842	**0.153**	**53.1**	**63.9**	0.01	**0.01**
		HP	**0.889**	**0.153**	35.1	47.4	0.05	0.06
	865	SRON	0.806	0.161	35.9	44.3	-0.02	0.04
		Models	0.804	0.147	**56.0**	**65.3**	**0.01**	**0.02**
		HP	**0.875**	**0.141**	38.8	50.6	0.05	0.06
Ocean	440	SRON	0.833	0.142	36.9	51.5	0.04	0.04
		Models	**0.926**	**0.091**	**51.2**	**67.4**	**0.02**	**0.02**
		HP	0.880	0.144	31.5	43.2	0.07	0.06
	550	SRON	0.819	0.122	46.1	57.4	0.04	0.03
		Models	**0.934**	**0.068**	**63.3**	**75.1**	**0.01**	**0.01**
		HP	0.891	0.127	32.4	44.2	0.07	0.06

	670	SRON	0.792	0.119	43.9	57.1	0.04	0.03
		Models	**0.944**	**0.058**	**68.5**	**79.7**	**0.00**	**0.01**
		HP	0.904	0.125	35.0	43.7	0.07	0.06
	865	SRON	0.776	0.099	60.6	70.4	0.02	0.02
		Models	**0.944**	**0.051**	**71.8**	**82.4**	**0.00**	**0.00**
		HP	0.905	0.111	36.7	45.9	0.07	0.05

Overall ranking of the algorithm AOD product according to the evaluation metrics of Table 2-2 is presented in Table 2-3 and Table 2-4 with green color indicating the best performance, blue and red color corresponding to second and third place in the performance.

Table 2-3: AOD product ranking over land

Land	**Rank**	**Comments**
AOD	1.GRASP/Model	Optimal balance between correlation, RMSE, bias and GCOS
	2.GRASP/HP	Bias at small AOD (0.06)
	2.SRON	All statistical characteristics are similar to GRASP/HP. Bias at small AOD (0.07) There are much less pixels over land than for GRASP/HP and GRASP/Model.

Table 2-4: AOD product ranking over water surfaces

Ocean	**Rank**	**Comments**

AOD	1.GRASP/Model	The best for all statistical characteristics
	2.SRON	Bias at small AOD (0.03)
	3.GRASP/HP	Big bias at small AOD (0.06)

For AE validation, we further filter with satellite AOD (550 nm)>=0.2 to ensure the quality of AE products. Because the accuracy of AE decreases for low AOD because even a small spectral bias the AOD affects AE strongly. Figure 2-3 shows the validation results of (a) POLDER-3/SRON, (b) POLDER-3/GRASP Models and (c) POLDER-3/GRASP HP AE (440/870) over land. All 3 datasets show its strength and weakness to obtain quantitative AE. SRON can capture the cluster of fine mode (AE>1.0), while overestimating the AE for coarse mode dominant (AE<1.0). GRASP/HP shows capability to well capture the cluster of coarse mode, while slightly underestimating AE for fine mode dominant. GRASP/Models AE, however, compensates for overestimation of small AE and underestimation of large AE. Overall, in terms of correlation coefficient and RMSE, GRASP/HP AE over land seems of higher quality (R=0.817, RMSE=0.382).

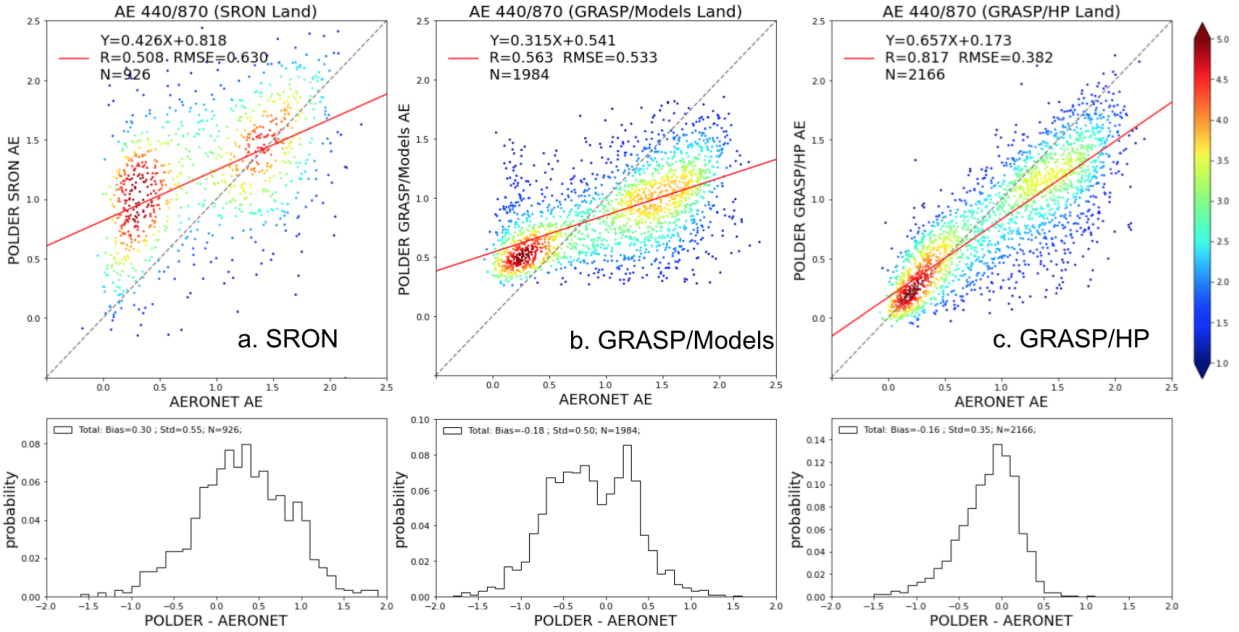

Figure 2-3 Validation of (a) POLDER-3/SRON, (b) POLDER-3/GRASP Models and (c) POLDER-3/GRASP HP AE (440/870) over land with AERONET.

Figure 2-4 shows the validation results of AE over ocean. Due to the filter of AOD<0.2, the number of matchups decreases to ~200-300 over ocean. GRASP/Models and GRASP/HP keep the similar overestimation/underestimation pattern as over land, while the agreement is much better than that over land, for example, R is ~0.9. SRON AE also shows significant improvement over ocean, and the correlation coefficient is ~0.9 and with the smallest RMSE 0.27 among 3 datasets.

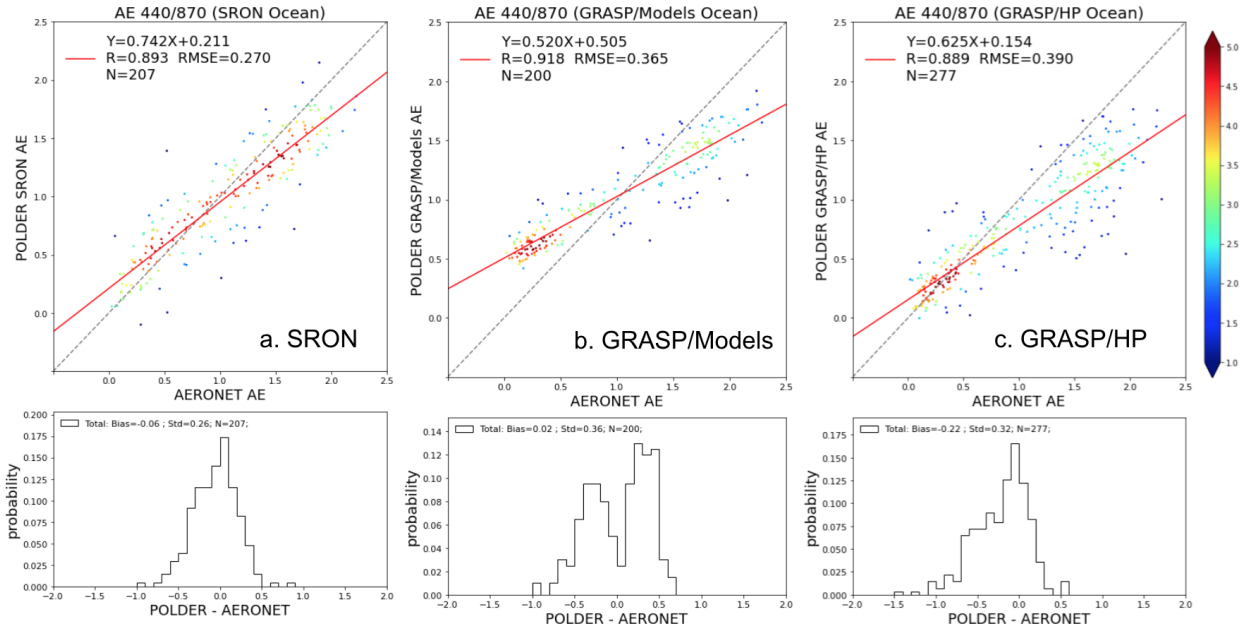

Figure 2-4. Validation of (a) POLDER-3/SRON, (b) POLDER-3/GRASP Models and (c) POLDER-3/GRASP HP AE (440/870) over ocean with AERONET.

Similarly to AOD, the ranking for Angstrom Exponent product is presented in Tables 1.3 and 1.4.

Table 2-5: Angstrom Exponent product ranking over land

Land	**Rank**	**Comments**
AE	1.GRASP/HP	Very good correspondence with AERONET
	2.GRASP/Models	Essential slope in AE
	2.SRON	Essential slope in AE

Table 2-6: Angstrom Exponent product ranking over water surfaces

Ocean	Rank	Comments
AE	1.SRON	Very good correspondence with AERONET
	1.GRASP/HP	Very good correspondence with AERONET
	2.GRASP/Models	Good correspondence with AERONET. Minor slope in AE

The validation results of AODF (550 nm) and AODC (550 nm) over land and ocean with AERONET SDA products are shown in Figure 2-5 to Figure 2-8. It is interesting to note that the validation statistics for AODF seems to be superior to that for AODC over land, and over ocean the situation is reversed for almost all 3 datasets (SRON AODF has similar performance over land and ocean). This can be explained by the fact that the fine mode aerosols have higher abundance over land while coarse mode aerosols are dominant over ocean, i.e. dynamic ranges are different. GRASP/HP AODF seems to have the best agreement with AERONET with R=0.911, RMSE=0.107, BIAS=0.01. GRASP/HP AODC over land seems to have the highest R=0.790, however, the BIAS is 0.04. GRASP/Models total AOD (550) shows nearly zero bias over land, however, splitting it into AODF and AODC, the -0.02 bias is identified for AODF and +0.03 bias is for AODC. SRON AODF and AODC products over land seem not as good as those over ocean in general, for example, over ocean AODF (R=0.775, RMSE=0.097) and AODC (R=0.849, RMSE=0.050), while over land AODF (R=0.759, RMSE=0.153) and AODC (R=0.655, RMSE=0.129). This is probably due to the fact that over dark ocean surface the sensitivity of the observed signal to aerosol is stronger allowing for retrieval of particle size information that is more challenging over land. Overall, the validation results indicate some potential to improve all these retrievals in the following WPs.

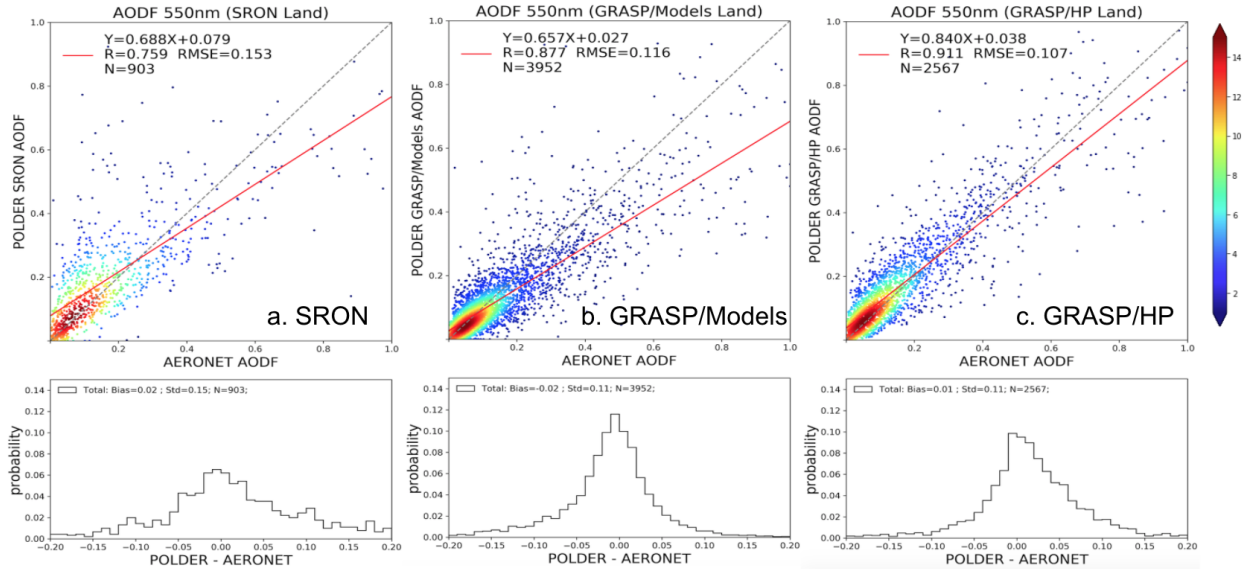

Figure 2-5 Validation of (a) POLDER-3/SRON, (b) POLDER-3/GRASP Models and (c) POLDER-3/GRASP HP AODF at 550 nm over land with AERONET.

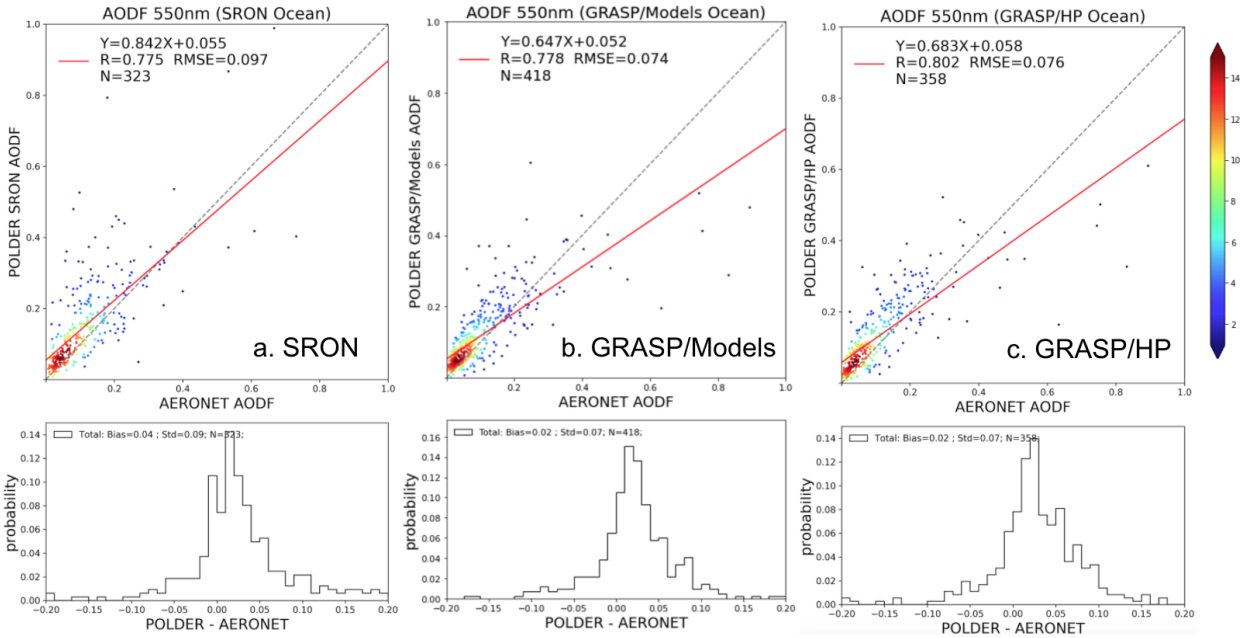

Figure 2-6 Validation of (a) POLDER-3/SRON, (b) POLDER-3/GRASP Models and (c) POLDER-3/GRASP HP AODF at 550 nm over ocean with AERONET.

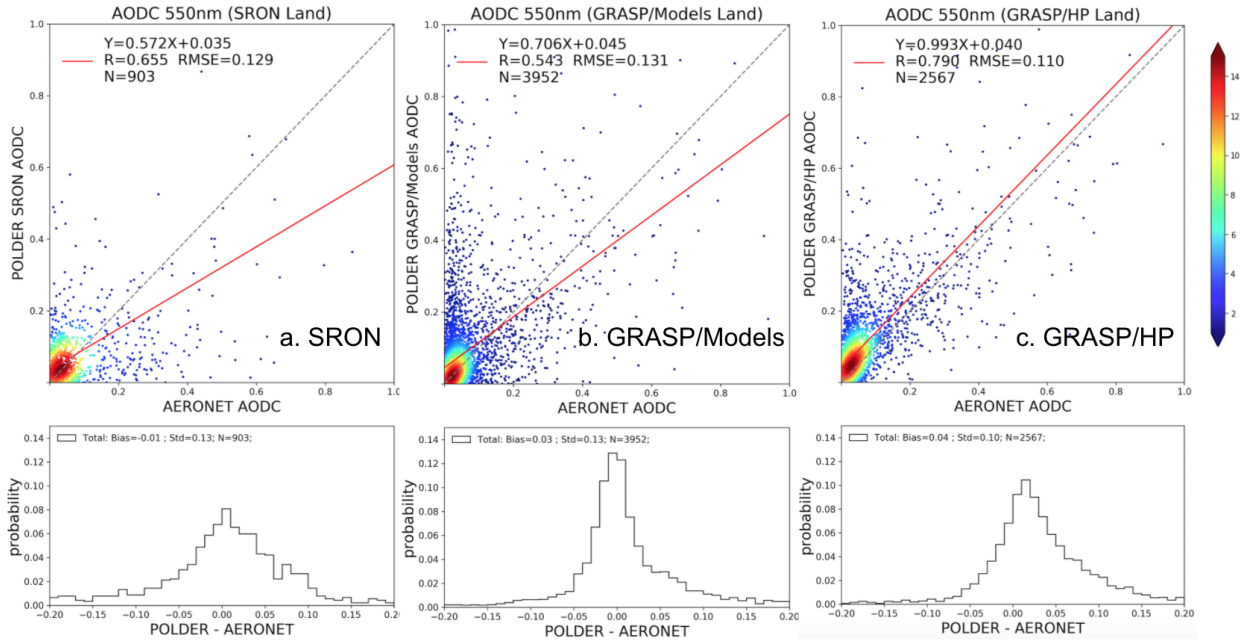

Figure 2-7 The same as Figure 2-5, but for AODC at 550 nm over land.

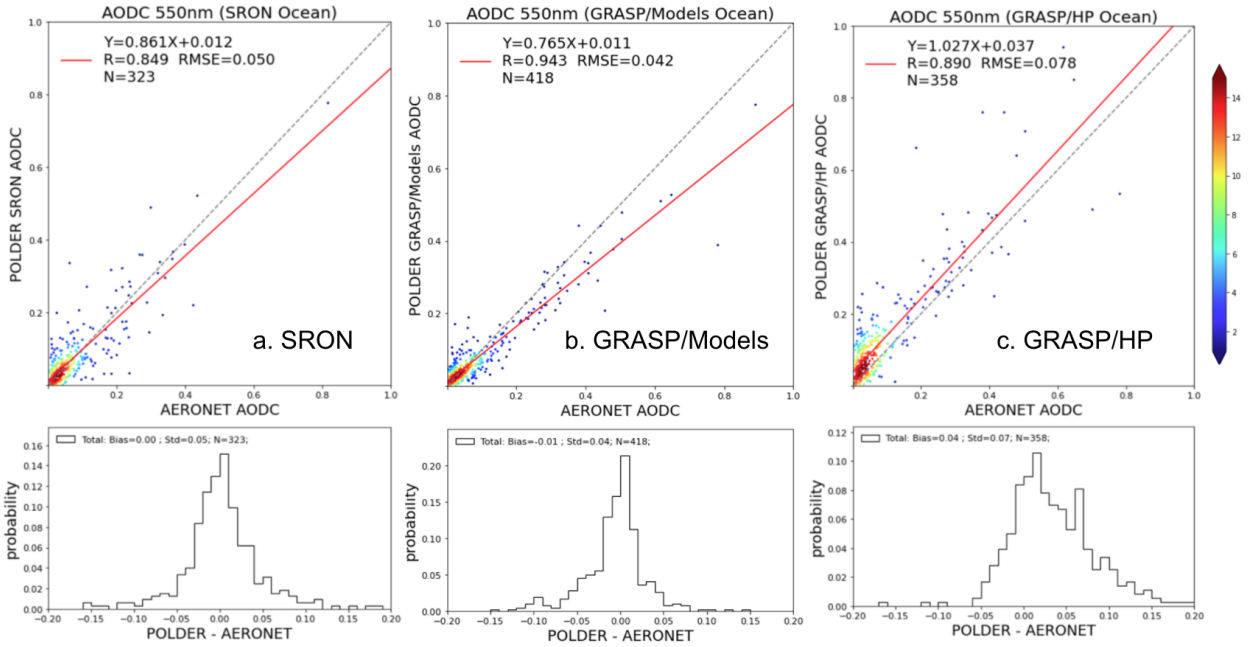

Figure 2-8 The same as Figure 6, but for AODC at 550 nm over ocean.

The validation of POLDER SSA and AAOD at 440 nm with AERONET inversion products are shown in Figure 2-9 and Figure 2-10 respectively. Tables 2 and 3 summarize the RMSE and BIAS of POLDER spectral SSA and AAOD at 440, 550, 670 and 865 nm with respect to AERONET

products. Generally, SRON SSA products outperform the GRASP/Models and GRASP/HP SSA products especially for RMSE and BIAS which are the key parameters for SSA validation (Table 2-7). However, SRON has a smaller number of matchups in comparison to GRASP/Models and GRASP/HP, in general, about 3 times smaller. To meet the requirements of RMSE smaller than 0.05, GRASP/Models and GRASP/HP need further filters using AOD greater than 0.5, which is planned to investigate and address in the following WPs. In terms of AAOD validation results, all 3 datasets show similar performance that the R is relatively low due to the small dynamic of AAOD values, and RMSE ranges from around 0.045 at blue channel to around 0.020 at NIR (Table 2-8).

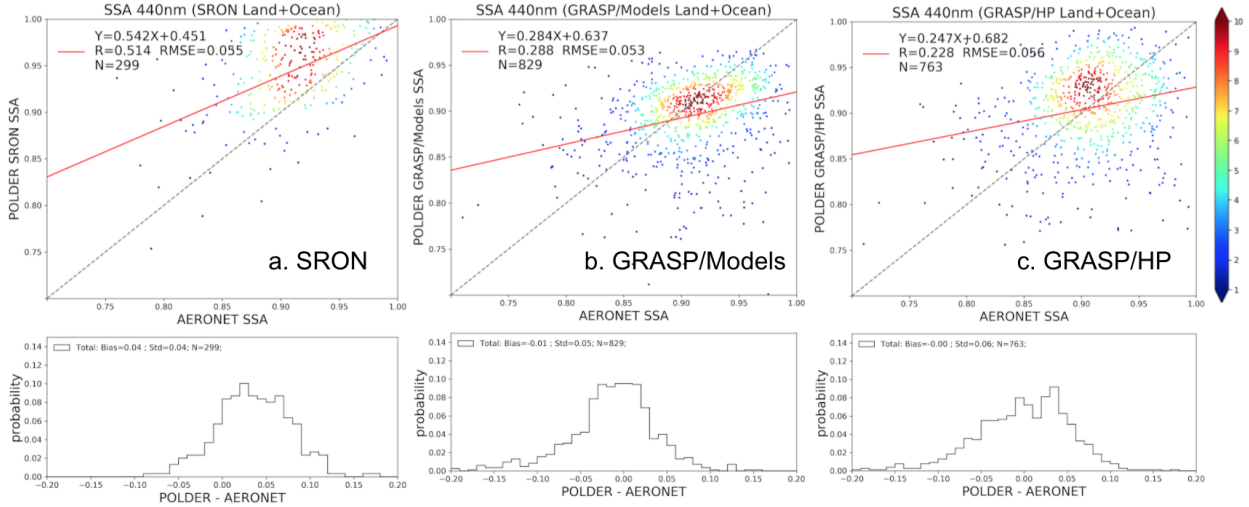

Figure 2-9 Validation for SSA at 440 nm over land and ocean.

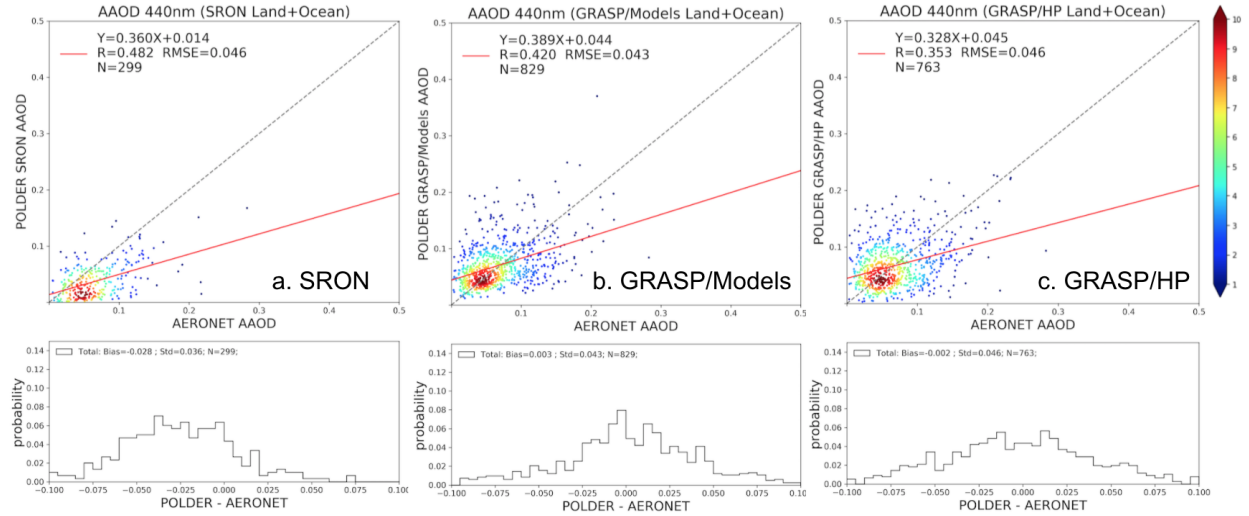

Figure 2-10 validation for AAOD at 440 nm over land and ocean.

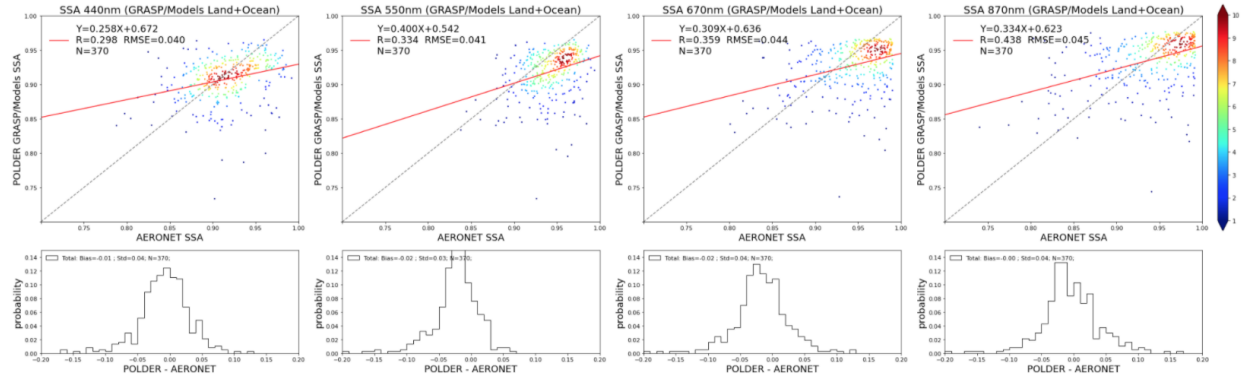

Figure 2-11: Validation of GRASP/Models SSA at 440, 550, 670 and 870 nm over land and ocean for POLDER AOD 550 nm > 0.5

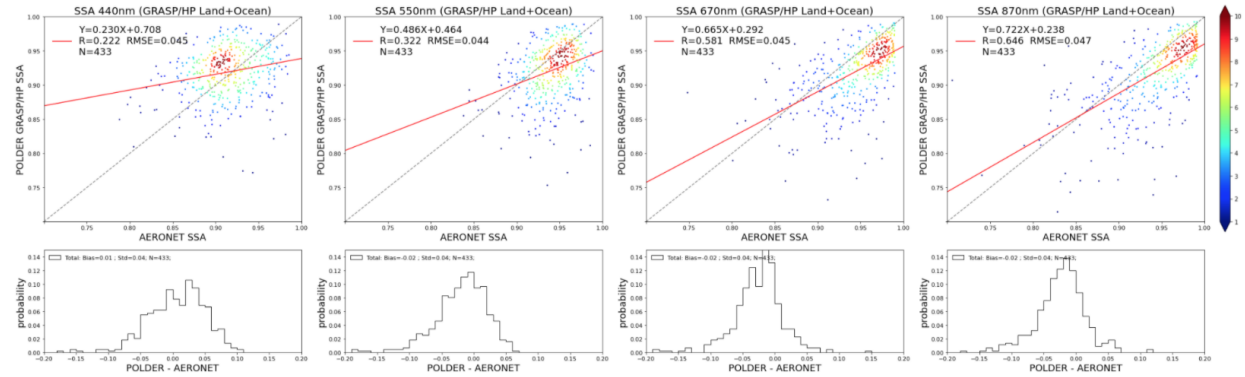

Figure 2-12: The same as Figure 11, but for GRASP/HP.

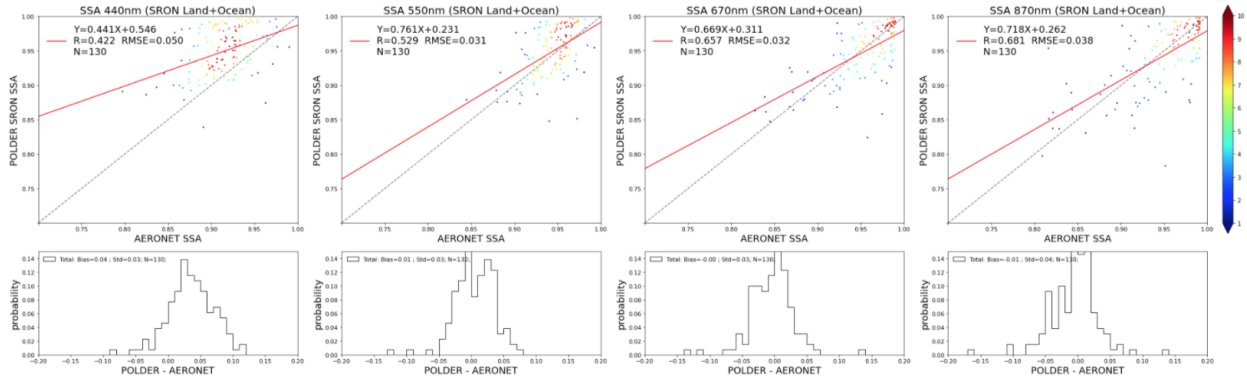

Figure 2-13: The same as Figure 11, but for SRON.

Table 2-7 Summary of RMSE of SRON, GRASP/Models and GRASP/HP spectral POLDER SSA and AAOD products against AERONET at 440, 550, 670 and 865 nm over land and ocean.

Land+Ocean	SSA				AAOD			
	440 nm	550 nm	670 nm	865 nm	440 nm	550 nm	670 nm	865 nm
SRON	0.055	**0.040**	**0.044**	**0.053**	0.046	**0.029**	**0.020**	**0.017**
GRASP/Models	**0.053**	0.059	0.063	0.067	**0.043**	0.033	0.027	0.020
GRASP/HP	0.056	0.061	0.061	0.065	0.046	0.034	0.030	0.024

Table 2-8: Summary of BIAS of SRON, GRASP/Models and GRASP/HP spectral POLDER SSA and AAOD products against AERONET at 440, 550, 670 and 865 nm over land and ocean.

Land+Ocean	SSA				AAOD			
	440 nm	550 nm	670 nm	865 nm	440 nm	550 nm	670 nm	865 nm
SRON	0.04	**0.00**	**0.00**	**-0.01**	-0.028	-0.014	**-0.004**	**-0.003**
GRASP/Models	**-0.01**	-0.03	-0.02	**-0.01**	**0.003**	**0.004**	0.008	0.004
GRASP/HP	0.00	-0.03	-0.03	-0.03	-0.002	0.006	0.015	0.012

Table 2-9: SSA product ranking

Land + Ocean	**Rank**	**Comments**
SSA	1.SRON	Smaller RMSE in comparison to GRASP but the number of pixels is in 3 times less than in GRASP
	2.GRASP/Models	
	2.GRASP/HP	

Table 2-10: AAOD product ranking

Land + Ocean	Rank	Comments
AAOD	1.GRASP/HP	Similar performance for AAOD
	1.GRASP/Models	
	1.SRON	

2.5.2 POLDER/SRON and POLDER/GRASP global aerosol intercomparison

This section presents the inter-comparison of POLDER/SRON aerosol products with PODER/GRASP Models and HP aerosol products for the year 2006 data on global scale, i.e. not only over AERONET sites. Specifically, we want to know if the consistency of the products remains the same in the areas where no AERONET observations are available. The 3 datasets are pixel-to-pixel intercompared in a spatial resolution of 0.2° x 0.2°.

To begin, we investigate the number of available AOD retrievals for the year 2006 of 3 aerosol products. Figure 2-14 shows the number of available AOD retrievals for the year 2006 of GRASP/Models, SRON and their differences. GRASP/HP is not presented due to its high similarity with GRASP/Models. We see a similar pattern for SRON and GRASP in that a higher number of retrievals over deserts where the cloud free possibility is higher than anywhere else. However, SRON products have a much smaller amount of retrievals than GRASP, specifically, the total number of 0.2 degree AOD retrievals is 15 442 708 for SRON, 47 374 037 for GRASP/Models and GRASP/HP 47 608 024 for entire year 2006. This is unexpected because the 3 products are generated using the same POLDER L1 measurements. One possible reason is that SRON algorithms perform retrieval on aggregation of 3x3 native pixels, while GRASP performs retrieval on native pixels. The further investigation will be in the following WPs.

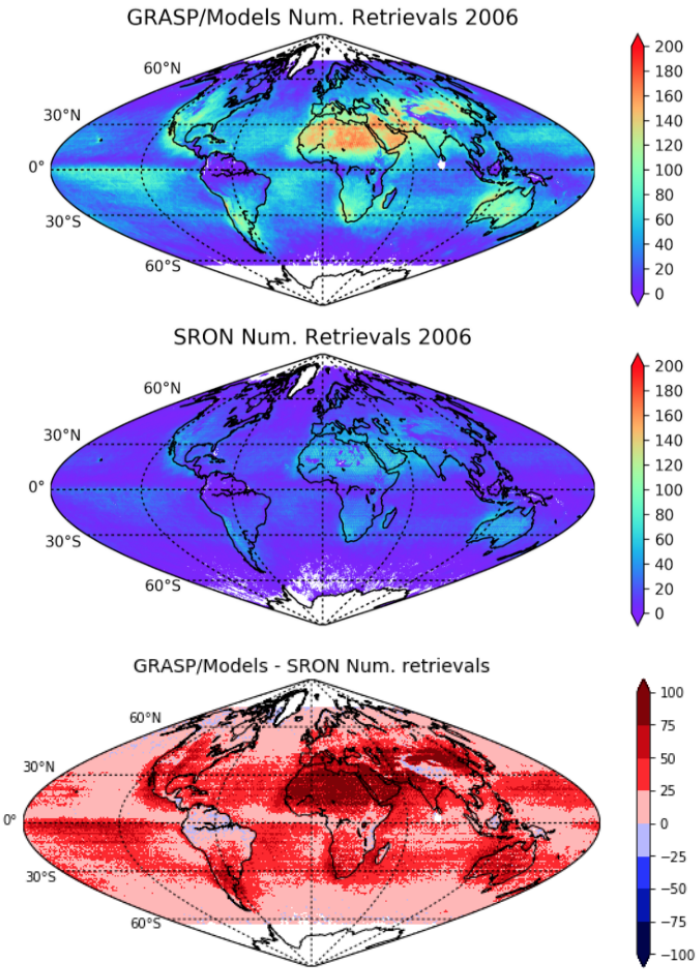

Figure 2-14 The number of available AOD retrievals for the year 2006. Upper panel: GRASP/Models; Middle panel: SRON; Lower panel: GRASP/Models - SRON.

In order to clarify the level of consistency of POLDER/SRON aerosol products with PODER/GRASP Models and HP aerosol products, Figure 2-15 shows the annual pattern of AOD (550 nm) from GRASP (GRASP/HP and GRASP/Models) and SRON products, as well as the differences of (SRON - GRASP/Models) and (SRON - GRASP/HP) AOD. Note the differences are not based on the annual mean, instead of an accumulation of daily differences and averaged over a year. A positive value indicates that the SRON product had a higher value. As one can see, SRON AOD is comparable with GRASP/HP, while generally higher than GRASP/Models everywhere. This is consistent with the AERONET validation results that GRASP/HP and SRON AOD 550 nm are higher than AERONET ~0.02-0.07, while GRASP/Models AOD 550 nm seems unbiased with AERONET. Over ocean, SRON AOD 550 nm tends to be smaller than GRASP/HP, and over land, SRON AOD seems higher than GRASP/HP over desert.

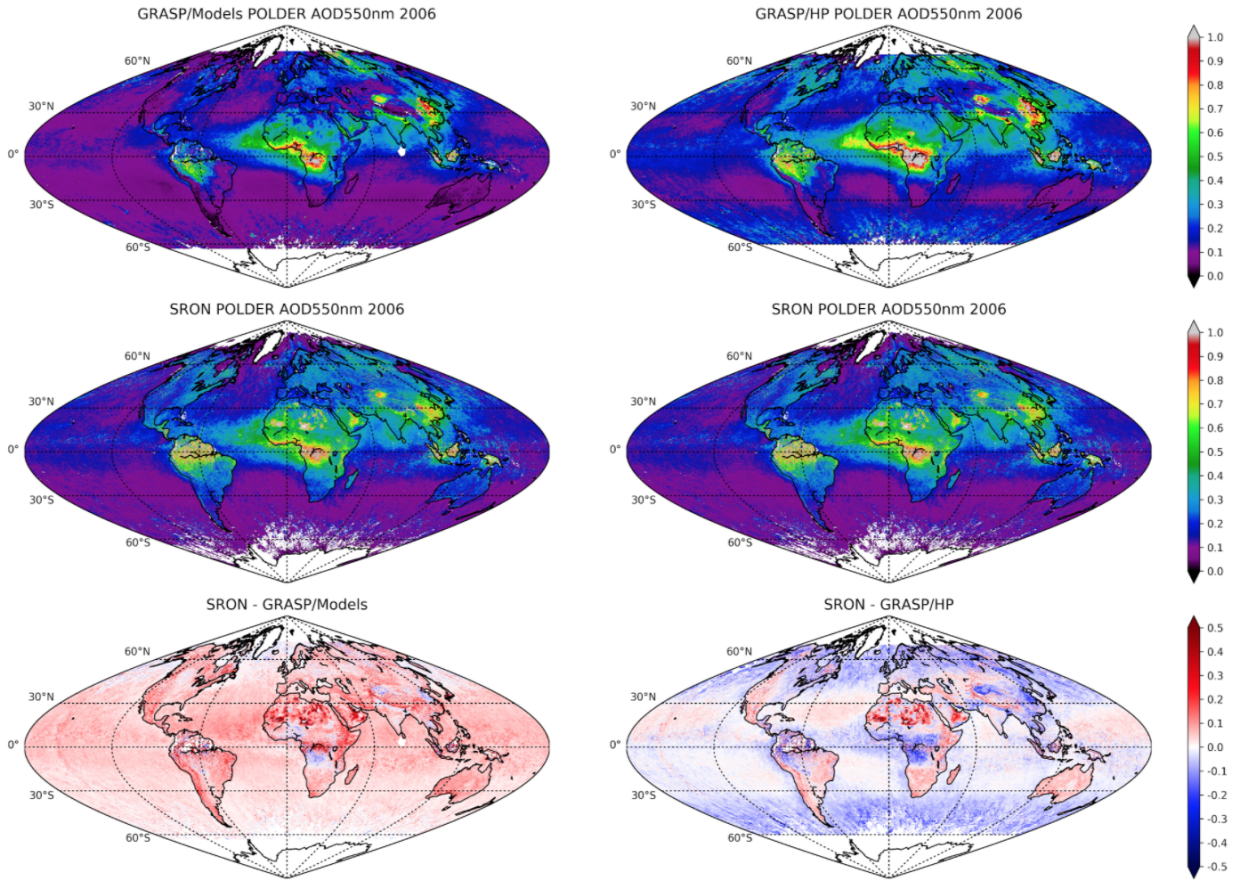

Figure 2-15 Inter-comparison of GRASP/Models, GRASP/HP and SRON AOD at 550 nm for the year 2006. The differences (SRON - GRASP/Models) and (SRON - GRASP/HP) are also presented.

The pixel-to-pixel intercomparison of SRON AOD 550 nm with GRASP/Models and GRASP/HP is shown in Figure 2-16. The statistics are calculated over land and ocean respectively. All AOD products are in close agreement over ocean, with the correlation coefficients above 0.87, RMSE around 0.075 and >50% pixels satisfy the GOCS requirements. Statistics over the ocean rely on ~7 million pairs. Also, in line with the validation over AERONET sites, SRON and GRASP/HP AOD (550 nm) has a positive offset ~0.04-0.07 with respect to GRASP/Models. And the difference between SRON and GRASP/HP AOD is ~0.02 (GRASP/HP is higher than SRON). However, over land surfaces the situation is quite different. The correlations between SRON and GRASP/Models or GRASP/HP are decreased to ~0.7, RMSEs are around 0.21-0.23, and ~30% pixels satisfy the GCOS requirements. Generally, SRON AOD 550 nm over land is higher than GRASP/Models (0.08) and GRASP/HP (0.01). Statistics over the land rely on ~5.5 million pairs.

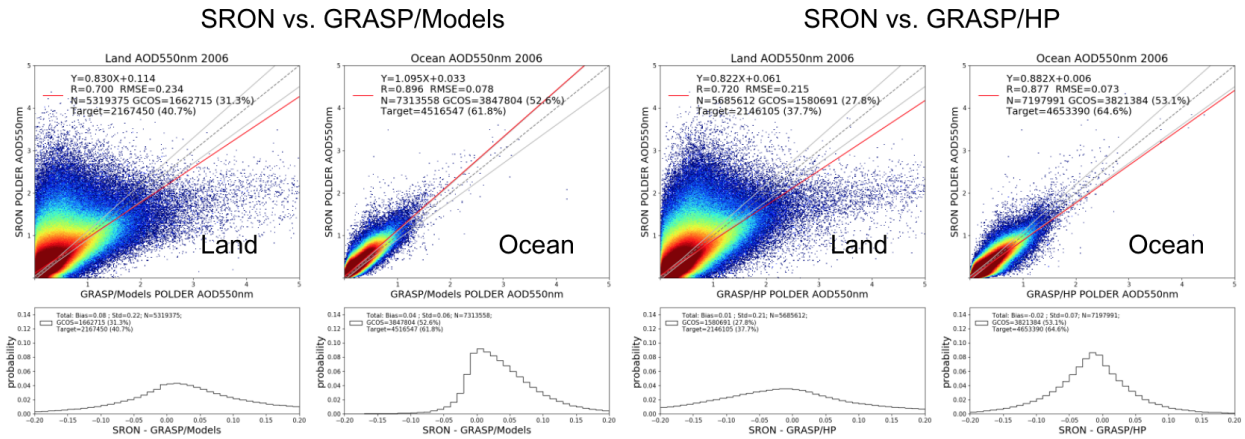

Figure 2-16 Pixel-to-pixel intercomparison of SRON AOD 550 nm with GRASP/Models and GRASP/HP over land and ocean respectively.

The pixel-to-pixel statistics of SRON and GRASP (Models and HP) spectral AOD products at 440, 550, 670 and 865 nm over land and ocean are summarized in Table 2-11. Over ocean, SRON and GRASP/Models, GRASP/HP AOD agree well, while in general SRON AOD is constantly higher than GRASP/Models ~0.04 and lower than GRASP/HP ~0.02. Over land, the agreement declines to R ~0.7 and RMSE greater than 0.19. SRON AOD is higher than GRASP/Models 0.09-0.04 from blue to NIR channels, and the differences between SRON and GRASP/HP vary from 0.03 (blue) to -0.02 (NIR). Even though the land surface is much more complicated than the ocean surface. Nevertheless, the seen differences are huge therefore the efforts to understand and harmonize are therefore crucial.

Table 2-11 Summary of pixel-to-pixel statistics of SRON and GRASP (Models and HP) spectral AOD products at 440, 550, 670 and 865 nm over land and ocean.

Land/Ocean	Products	WL (nm)	R	RMSE	GCOS (%)	Target (%)	Diff. (SRON-GRASP)
Land	SRON vs. Models	440 nm	0.726	0.264	28.0	38.3	0.09
		490 nm	0.715	0.248	29.5	39.6	0.08
		550 nm	0.700	0.234	31.3	40.7	0.08
		670 nm	0.668	0.213	33.4	42.3	0.06
		865 nm	0.623	0.195	35.4	43.7	0.04
	SRON vs. HP	440 nm	0.735	0.244	25.4	36.2	0.03

		490 nm	0.728	0.230	26.4	36.8	0.01
		550 nm	0.720	0.215	27.8	37.7	0.01
		670 nm	0.696	0.200	28.5	37.5	-0.01
		865 nm	0.658	0.189	29.4	37.7	-0.02
Ocean	SRON vs. Models	440 nm	0.914	0.077	55.0	65.8	0.04
		490 nm	0.906	0.075	54.7	64.8	0.04
		550 nm	0.896	0.078	52.6	61.8	0.04
		670 nm	0.874	0.075	54.2	62.7	0.04
		865 nm	0.852	0.072	57.4	65.4	0.04
	SRON vs. HP	440 nm	0.891	0.083	49.9	62.3	-0.02
		490 nm	0.885	0.079	50.8	62.9	-0.02
		550 nm	0.877	0.073	53.1	64.6	-0.02
		670 nm	0.862	0.068	54.4	65.4	-0.02
		865 nm	0.844	0.063	57.2	67.5	-0.02

The annual pattern of AE(440/870) from POLDER/GRASP (Models and HP) and POLDER/SRON products is presented in Figure 2-17, as well as, AE differences (SRON - GRASP/Models) and (SRON - GRASP/HP) are also presented. Figure 2-18 shows the global pixel-to-pixel statistic metrics between AE products over land and ocean respectively. The 3 datasets show qualitatively similar patterns of AE, however they are quantitatively different. For example, 3 products all show fine mode dominant over South Africa biomass burning region with AE higher than 1.0, however, the GRASP/Models reports AE ~1.2-1.4, in contrast with GRASP/HP and SRON AE higher than 1.5. Over ocean, GRASP/Models AE are generally higher than GRASP/HP and SRON, which means smaller particles. The findings are consistent with the AERONET validation results indicating the overestimation of small AE and underestimation of large AE for GRASP/Models. The agreement between GRASP/HP and SRON AE is better than any of them with

GRASP/Models. While, there are still some clear differences, such as over Sahara desert GRASP/HP reports lower AE than SRON, which means larger particles. GRASP/HP shows domination of big particles over land as well as over ocean in polar and mid-altitude regions also in comparison to SRON (AE(GRASP/HP) < AE(SRON)). GRASP/HP shows domination of small particles over the ocean in equatorial regions (AE(GRASP/HP) > AE(SRON)). In terms of pixel-to-pixel comparison, GRASP/HP and SRON AE show quite good agreement over ocean, with R=0.899, RMSE=0.219 and the diff. (SRON-GRASP/HP) is 0.01. Over land, the agreement between 3 products is generally lower than over ocean, especially the dispersion is high for coarse mode (AE<1.0).

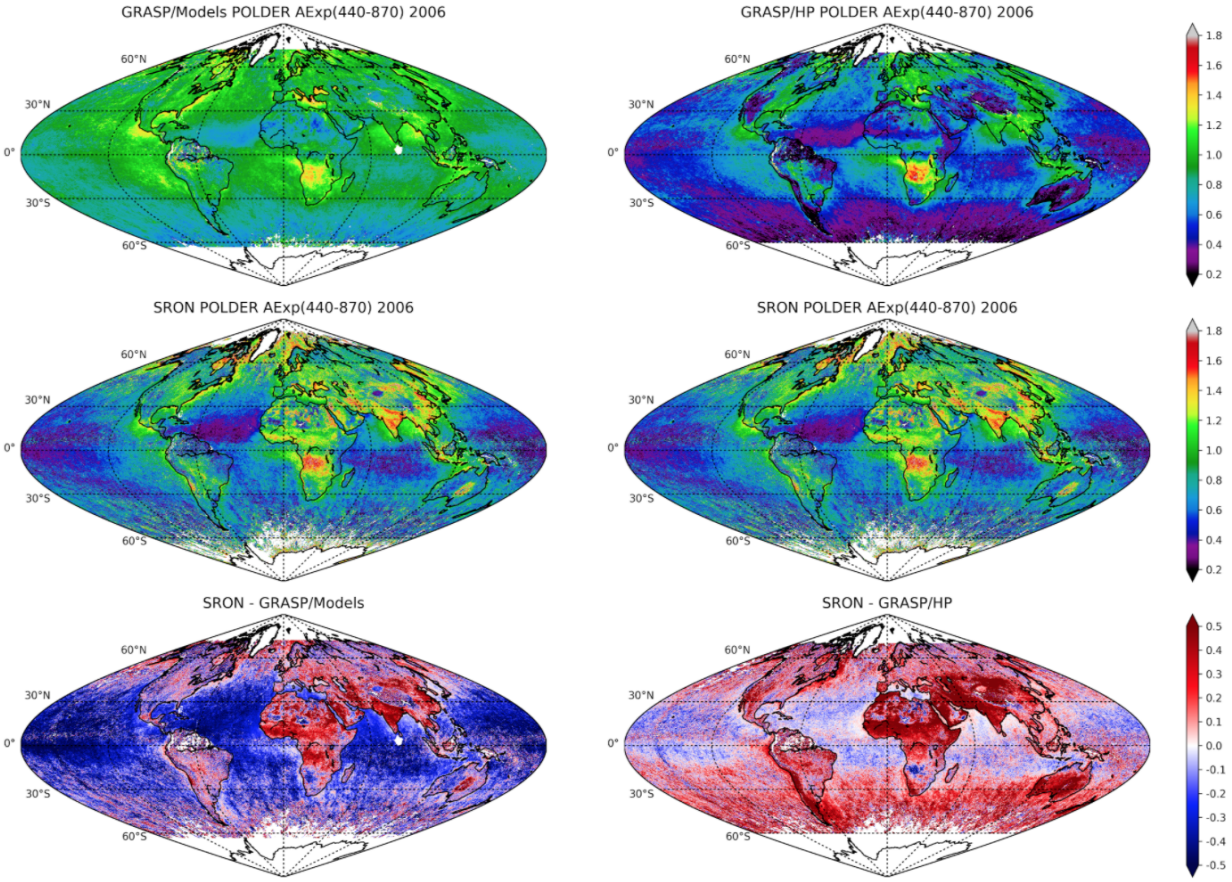

Figure 2-17 Inter-comparison of GRASP/Models, GRASP/HP and SRON AE(440/870) for the year 2006. The differences (SRON - GRASP/Models) and (SRON - GRASP/HP) are also presented.

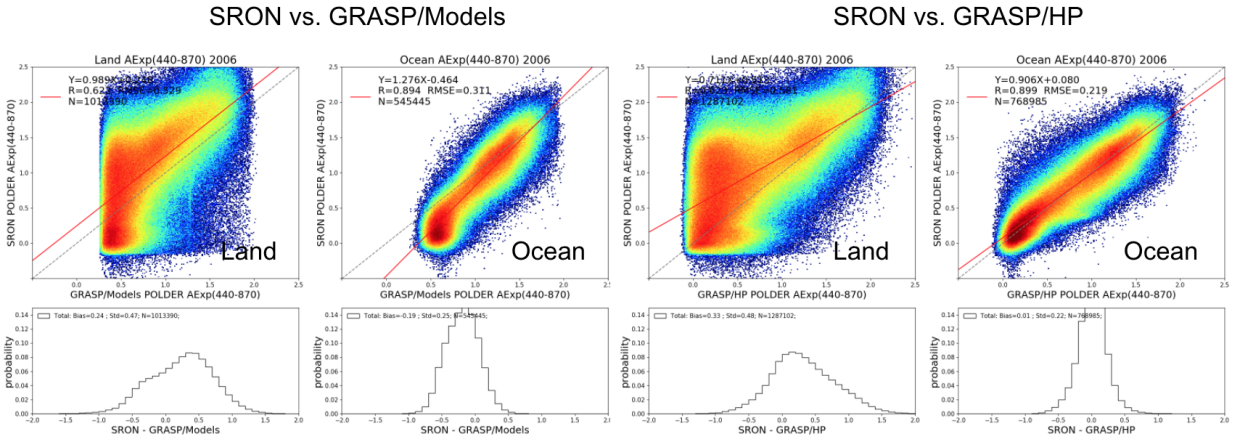

Figure 2-18 Pixel-to-pixel intercomparison of SRON AE(440/870) with GRASP/Models and GRASP/HP over land and ocean respectively.

We further compare spectral SSA from SRON, GRASP/Models and GRASP/HP. The annual distribution of SSA (440 nm) from POLDER/GRASP (Models and HP) and POLDER/SRON products is presented in Figure 2-19, as well as, SSA differences (SRON - GRASP/Models) and (SRON - GRASP/HP) are also presented. Figure 2-20 shows the global pixel-to-pixel statistic metrics between SSA (440 nm) products over land and ocean respectively. The pixel-to-pixel statistics of SRON and GRASP (Models and HP) spectral SSA products at 440, 550, 670 and 865 nm over land and ocean are summarized in Table 2-12. Generally, GRASP/Models and GRASP/HP show stronger absorption (lower SSA) than SRON. Specifically, GRASP/Model shows stronger absorption over land and GRASP/HP show stronger absorption both over land and ocean. This is in line with the AERONET validation results that GRASP/Models and GRASP/HP SSA tend to be smaller than AERONET inversion products, and SRON SSA shows smaller bias with AERONET especially from 550 to 870 nm where the bias is within 0.01. Since the global aerosol absorption is key information to understand aerosol climate effects, the harmonizing of the SRON and GRASP SSA products is therefore crucial for the project. In addition, the SRON and GRASP SSA products have been included in the intercomparison with other available satellite products in the study by Schutgens et al. (2021).

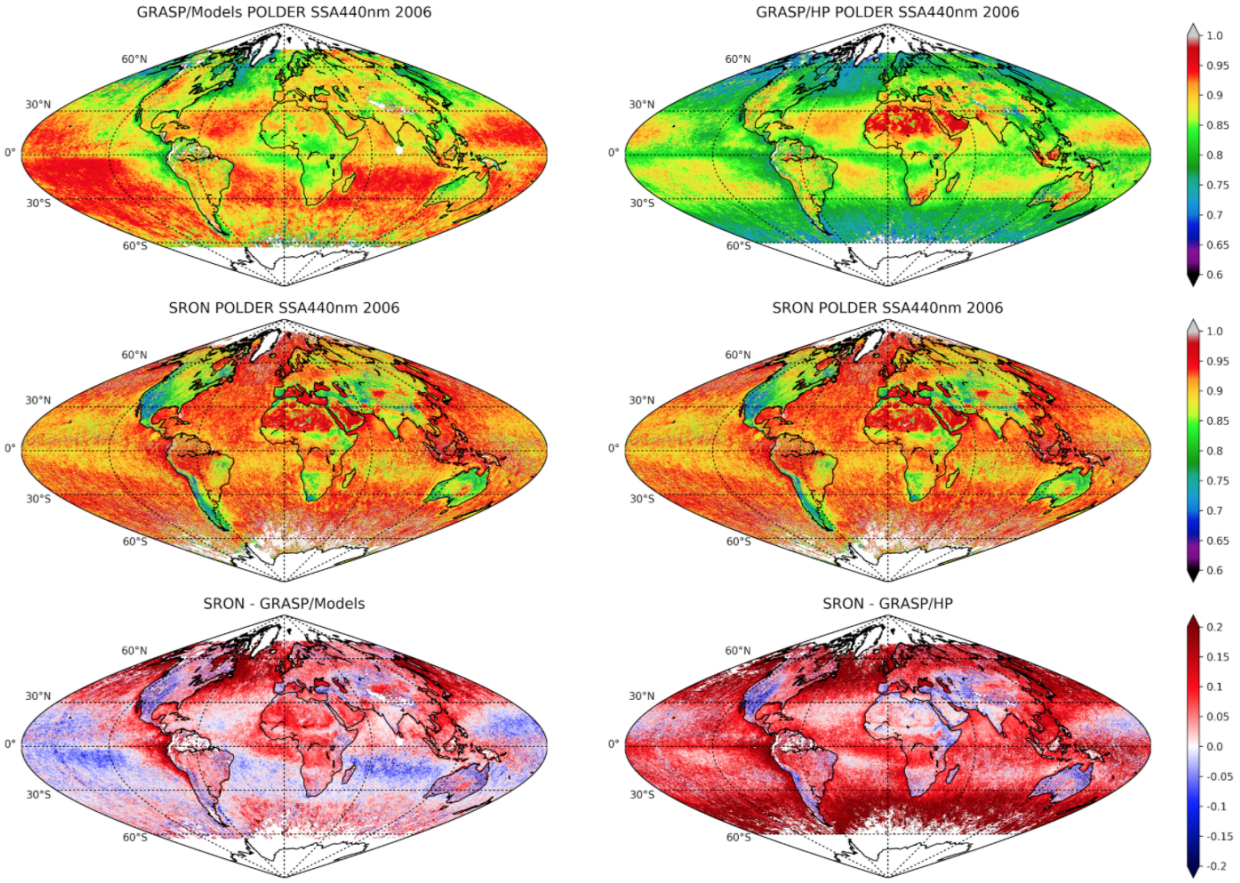

Figure 2-19. Inter-comparison of GRASP/Models, GRASP/HP and SRON SSA (440 nm) for the year 2006. The differences (SRON - GRASP/Models) and (SRON - GRASP/HP) are also presented.

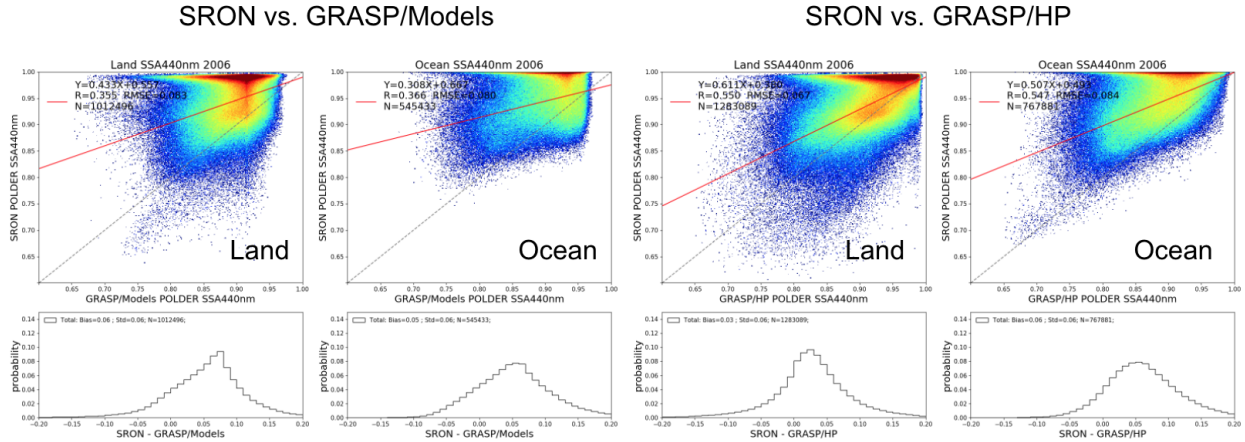

Figure 2-20. Pixel-to-pixel intercomparison of SRON SSA (440 nm) with GRASP/Models and GRASP/HP over land and ocean respectively.

Table 2-12: Summary of pixel-to-pixel statistics of SRON and GRASP (Models and HP) spectral SSA products at 440, 550, 670 and 865 nm over land and ocean.

Land/Ocean	Products	WL (nm)	R	RMSE	Diff. (SRON-GRASP)
Land	SRON vs. Models	440	0.355	0.083	0.06
		490	0.383	0.080	0.05
		550	0.422	0.077	0.04
		670	0.469	0.074	0.03
		865	0.510	0.071	0.01
	SRON vs. HP	440	0.550	0.067	0.03
		490	0.576	0.066	0.02
		550	0.597	0.066	0.02
		670	0.624	0.068	0.02
		865	0.650	0.073	0.01
Ocean	SRON vs. Models	440	0.366	0.080	0.05
		490	0.393	0.080	0.05
		550	0.433	0.079	0.05
		670	0.483	0.078	0.04
		865	0.535	0.078	0.04
	SRON vs. HP	440	0.547	0.084	0.06
		490	0.572	0.080	0.06

		550	0.602	0.079	0.06
		670	0.638	0.070	0.05
		865	0.669	0.081	0.05

In addition, we also looked into detail of the regional pixel-to-pixel intercomparison between SRON and GRASP AOD and SSA at 670 nm. The differences presented as a function of chi2, minimal scattering angle, AOD, as well as surface reflectance. Figure 2-21 shows an example over the Australia and New Zealand region. In general, the results are in line with the global comparison. The difference between to GRASP and SRON seems to correlate with the difference in retrieved surface reflectance.

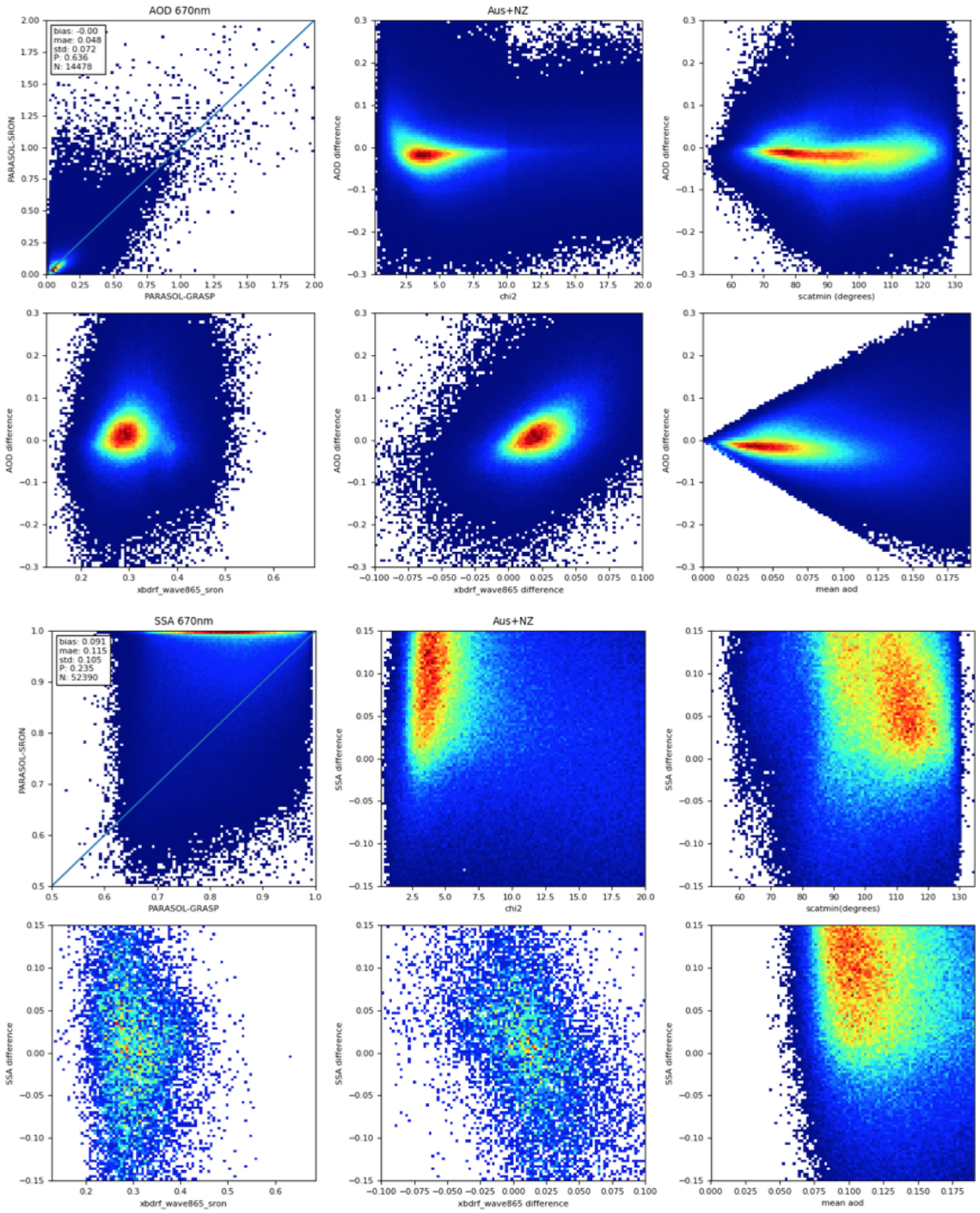

Figure 2-21 Pixel-to-pixel intercomparison of an example of regional (oceanic: Australia and New Zealand) AOD (top 2 panels) and SSA (lower 2 panels) at 670 nm. The differences are presented as a function of chi2, minimal scattering angle, AOD, as well as surface reflectance.

2.6 Surface intercomparison

One of the advantages of SRON and GRASP algorithms is that both of them retrieve aerosol and surface simultaneously. The evaluation of surface products will give extra information about the overall performance of the aerosol-surface decoupling. However, there is no surface reference dataset that can be used for validation as AERONET aerosol measurements, therefore, we will conduct the intercomparison of SRON and GRASP surface retrievals to identify the major differences. We also include the MODIS surface product (MCD43C1) (Schaaf and Wang, 2015) as an independent dataset to make some intercomparisons.

SRON and GRASP algorithms are using similar treatment of surface modeling, for example, Ross-Li BRDF model (Ross, 1981; Li and Strahler, 1992) and BPDF (Bidirectional Polarization Distribution Function) (Maignan et al., 2009) models under assumption that the retrieved parameters are spectrally smooth (the strength of smoothness is different for each parameter) (Litvinov et al., 2011a, 2011b). Figure 2-22 shows the spatial distribution of SRON, GRASP/Models and GRASP/HP derived Ross-Li BRDF1 isotropic terms for the year 2006, and the differences (SRON - GRASP/Models) and (SRON - GRASP/HP) are presented as well. The pixel-to-pixel statistical matrix of Ross-Li spectral BRDF1 at 490, 670, 865 and 1020 nm for the year 2006 is shown in Table 2-14, and the statistics for BRDF2 and BPDF are presented in Table 2-15. The global statistics are based on ~6 millions pixels. In general, the SRON and GRASP surface retrieval products show reasonable agreement, with ~30% pixels satisfying the surface "Optimal" requirements (if albedo<0.03, threshold=0.02, else: threshold = max (0.01 or 5%)) and >60% pixels satisfying the surface "Target" requirements (if albedo<0.03, threshold=0.04, else: threshold = max (0.03 or 10%)).

Table 2-13 Requirements on the surface

Requirements BRDF/albedo	**Uncertainties**	
	Albedo <= 0.03	Albedo > 0.03
Target	0.04	0.03 or 10%
Optimal	0.02	0.01 or 5%

For 440-670 nm SRON shows bigger values of BRDF1 than GRASP, and for 870, 1020 nm GRASP shows bigger values of the region where it gives smaller value in shorter channels. In general, globally SRON BRDF1 is around 0.01-0.02 higher at all wavelengths than GRASP/Models and GRASP/HP. The biggest differences are found for BRDF2 and BPDF, where the RMSE is ~0.24 for BRDF2 and ~1.4-1.7 for BPDF. This can explain both by uncertainties in

the algorithms but also by differences in BRDF/ BPDF models implementations which should be considered at the next stage of the project.

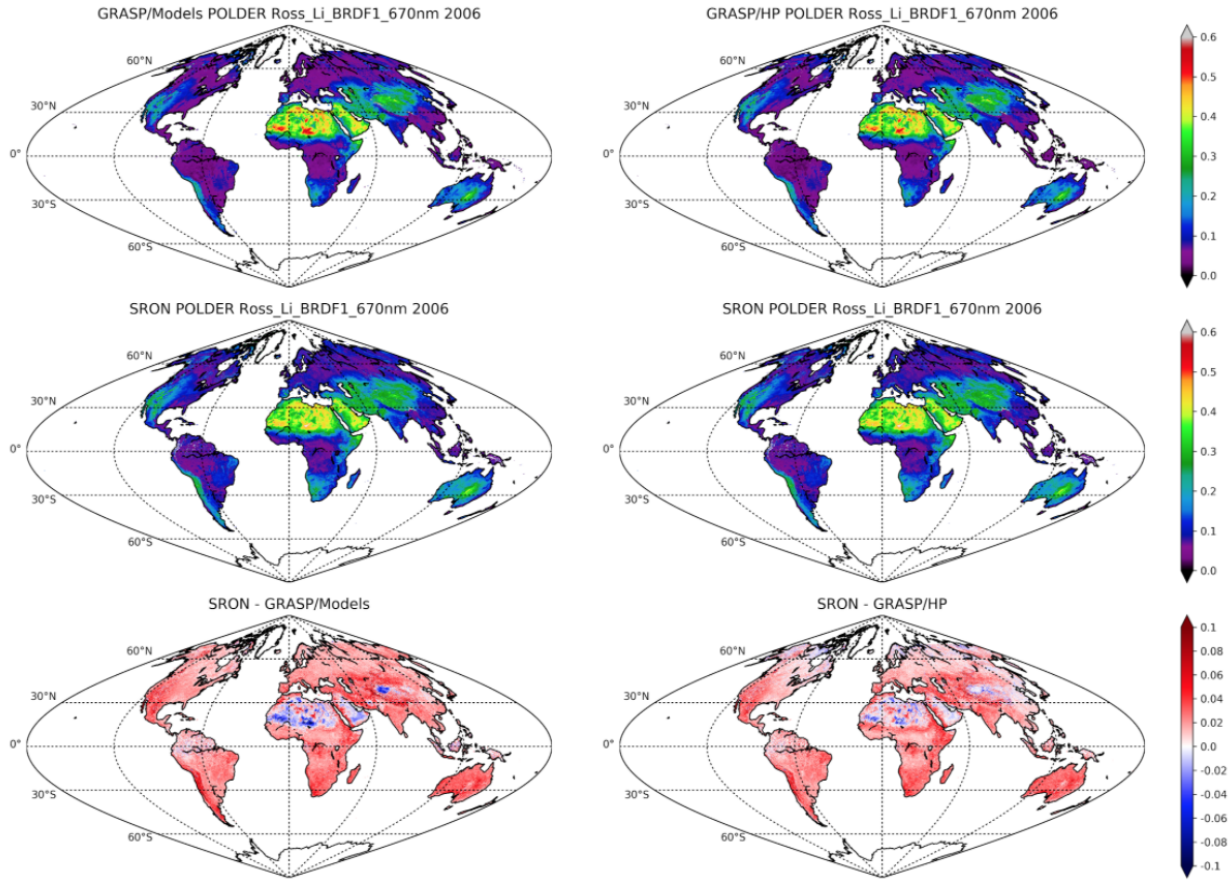

Figure 2-22 The spatial distribution of SRON, GRASP/Models and GRASP/HP derived Ross-Li BRDF1 isotropic terms for the year 2006. The differences (SRON - GRASP/Models) and (SRON - GRASP/HP) are also presented.

Table 2-14 Summary of pixel-to-pixel statistics of SRON and GRASP (Models and HP) spectral BRDF1 at 490, 670, 865 and 1020 nm.

Products	WL (nm)	R	RMSE	Optimal (%)	Target (%)	Diff. (SRON-GRASP) (1 σ)
SRON vs. Models	490	0.846	0.033	28.6	72.9	0.02 (0.03)
	670	0.963	0.038	26.6	63.8	0.02 (0.03)
	865	0.886	0.042	31.9	62.5	0.01 (0.04)
	1020	0.888	0.043	34.8	64.5	0.01 (0.04)

SRON vs. HP	490	0.866	0.032	26.2	70.2	0.02 (0.03)
	670	0.965	0.036	30.3	65.8	0.02 (0.03)
	865	0.875	0.042	33.1	62.9	0.01 (0.04)
	1020	0.881	0.042	36.1	65.2	0.01 (0.04)

Table 2-15 Summary of pixel-to-pixel statistics of SRON and GRASP (Models and HP) BRDF2, BRDF3 and BPDF.

Parameters	Products	R	RMSE	Diff. (SRON-GRASP) (1 σ)
BRDF2	SRON vs. Models	0.591	0.238	0.10 (0.22)
	SRON vs. HP	0.619	0.239	0.06 (0.23)
BRDF3	SRON vs. Models	0.791	0.052	-0.03 (0.05)
	SRON vs. HP	0.813	0.047	-0.02 (0.04)
BPDF	SRON vs. Models	0.776	1.412	-0.98 (1.01)
	SRON vs. HP	0.792	1.782	-1.35 (1.16)

To compare with independent MODIS surface product, it was analyzed one month (September 2006) of data of SRON, GRASP/Models, GRASP/HP and MODIS MCD43C1 BRDF products at 670 nm, which is the common wavelength available for all products. Figure 2-23 shows the spatial distribution of monthly 4 BRDF1 products for September 2006. The differences between POLDER SRON, GRASP/Models, GRASP/HP and MODIS are presented as well. Figure 2-25 and Figure 2-27 show the monthly spatial distribution of BRDF2 and BRDF3 for the 4 datasets. The pixel-to-pixel statistics of BRDF1, BRDF2 and BRDF3 are shown in Figure 2-24, Figure 2-26 and Figure 2-28 respectively. In general, the very good correspondence is found between POLDER and MODIS products, for example, >40% pixels satisfying Optimal requirement and >80% pixels for Target requirement, and the RMSE does not exceed 0.03. The global difference between SRON and MODIS is 0.01 (SRON>MODIS), in contrast that GRASP/HP is 0.01 smaller than MODIS, and GRASP/Models is nearly zero difference with MODIS global mean.

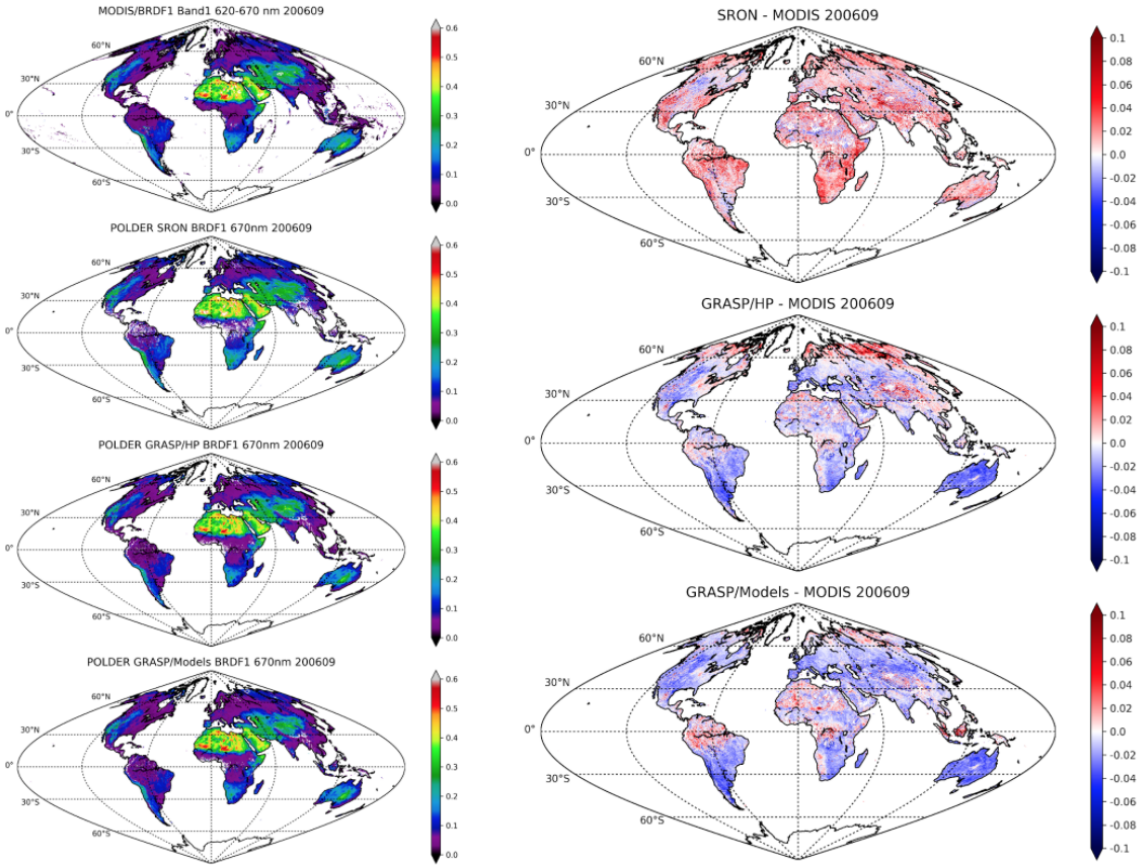

Figure 2-23. Spatial distribution of monthly Ross-Li BRDF1 at 670 nm for POLDER products from SRON, GRASP/Models, and GRASP/HP and MODIS MCD43C1. The differences between POLDER and MODIS products are presented in the right panel.

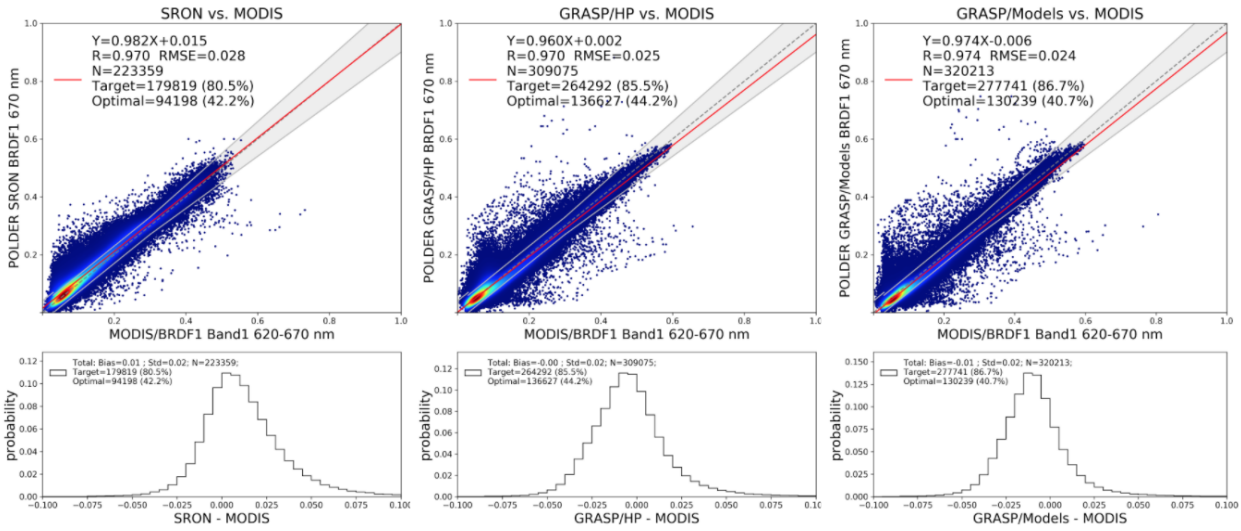

Figure 2-24. The pixel-to-pixel comparison of SRON, GRASP/Models and GRASP/HP POLDER BRDF1 with MODIS product at 670 nm.

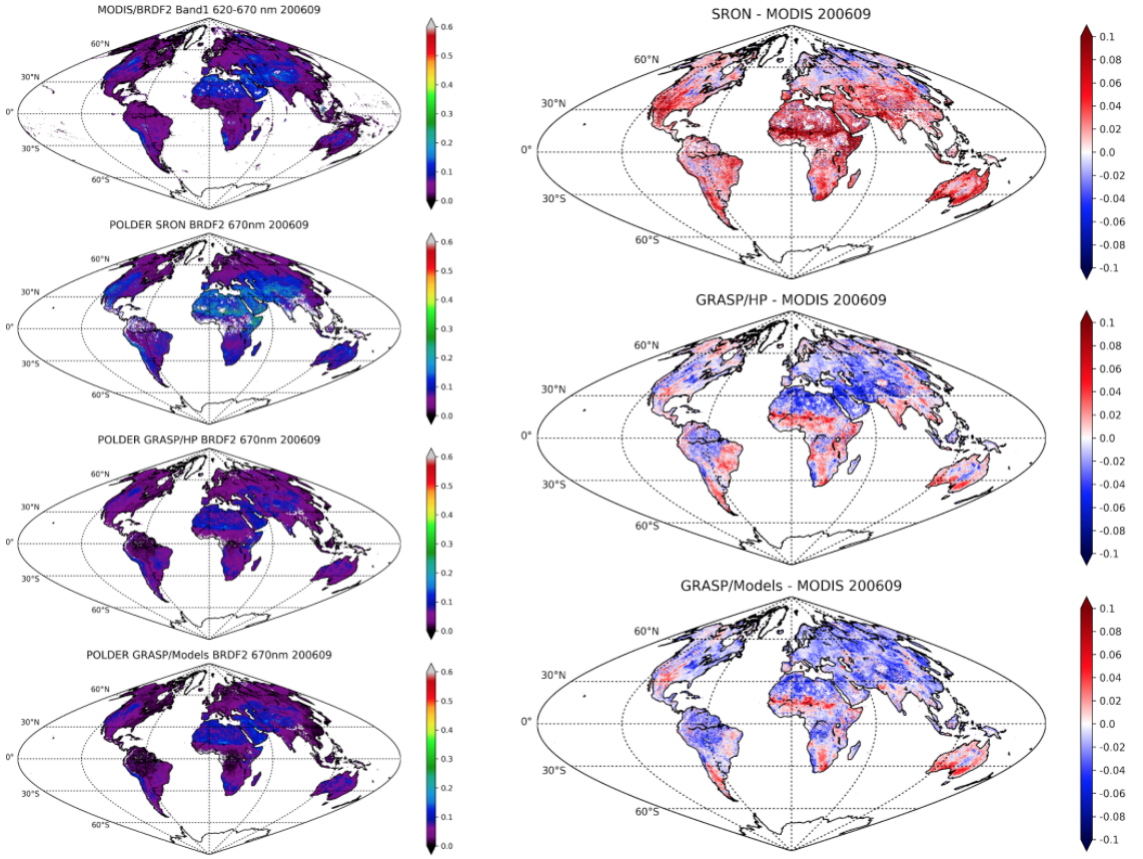

Figure 2-25. Spatial distribution of monthly Ross-Li BRDF2 at 670 nm for POLDER products from SRON, GRASP/Models, and GRASP/HP and MODIS MCD43C1. The differences between POLDER and MODIS products are presented in the right panel.

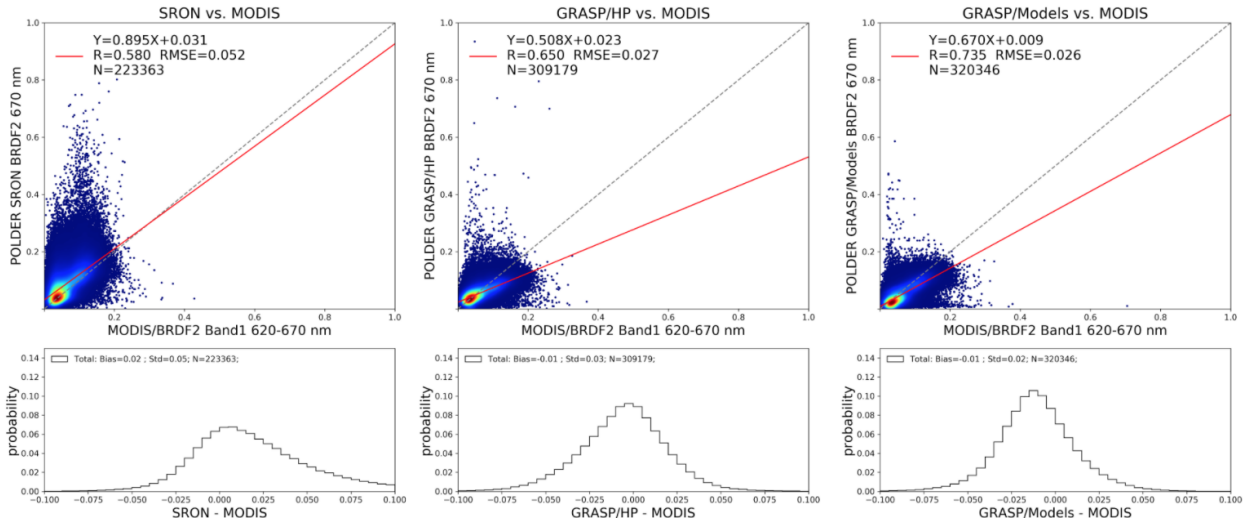

Figure 2-26. The pixel-to-pixel comparison of SRON, GRASP/Models and GRASP/HP POLDER BRDF2 with MODIS product at 670 nm.

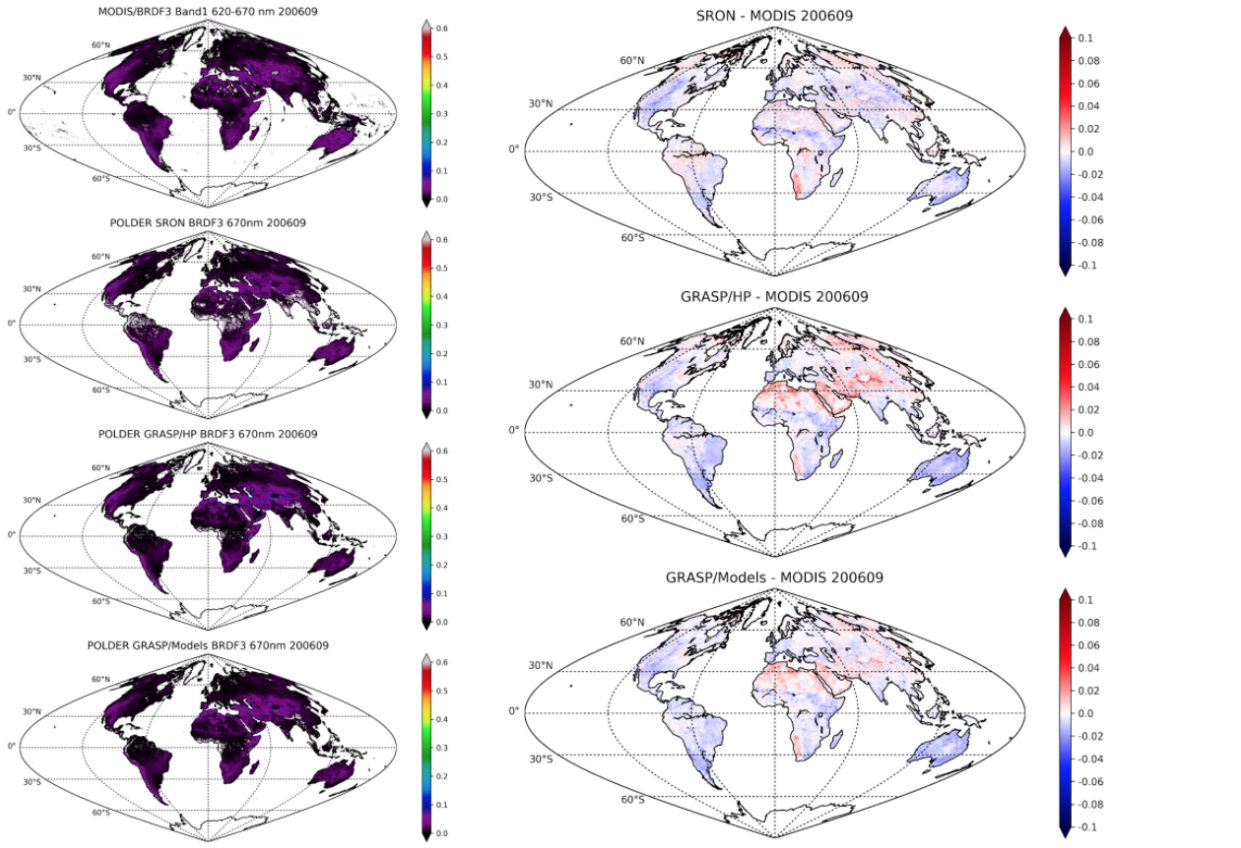

Figure 2-27. Spatial distribution of monthly Ross-Li BRDF2 at 670 nm for POLDER products from SRON, GRASP/Models, and GRASP/HP and MODIS MCD43C1. The differences between POLDER and MODIS products are presented in the right panel.

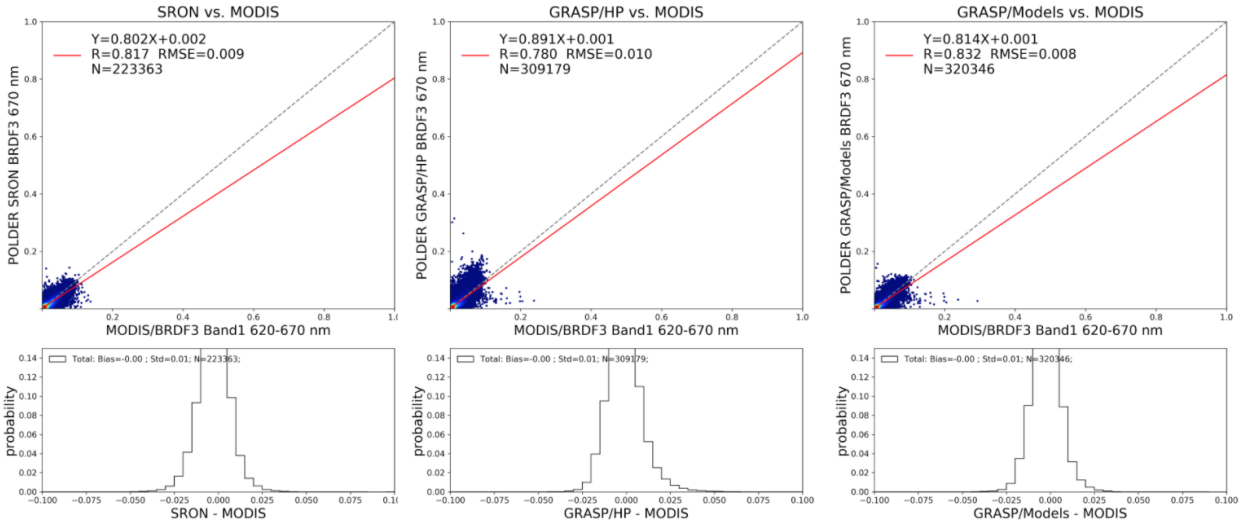

Figure 2-28. The pixel-to-pixel comparison of SRON, GRASP/Models and GRASP/HP POLDER BRDF3 with MODIS product at 670 nm.

Overall, the reasonable correspondence is found between GRASP and SRON surface retrievals. The biggest differences are in BRDF2 and BPDF. For 440-670 nm SRON shows bigger values of BRDF1 than GRASP, and for 870, 1020 nm GRASP shows bigger values of the region where it gives smaller value in shorter channels. On the other hand, both GRASP and SRON show reasonable correspondence with MODIS BRDF.

2.7 Conclusion

In this WP1 report, the existent aerosol/surface products from POLDER based on the SRON and GRASP algorithms are validated using ground-based AERONET measurements and the validation results are compared. In addition, the global pixel-to-pixel intercomparison is made for POLDER/SRON, POLDER/GRASP Models and POLDER/GRASP HP products. The MODIS surface product (MCD43C1) is also included in the intercomparison. The activities in WP1 can be summarized by the following conclusions:

- Aerosol products validation using AERONET measurements:
  - The AOD validation using AERONET direct sun product shows that GRASP/Models AOD present the optimal balance between correlation, GCOS fraction and bias over land with R ~0.86, GCOS fraction ~48% and nearly zero bias for total and low aerosol loading cases for AOD at 550 nm. GRASP/HP and SRON also show good agreement with AERONET, and all statistical metrics are similar between them, while the bias for small AOD is non-negligible ~0.06-0.07 for both GRASP/HP and SRON AOD products over land. Over ocean,

GRASP/Models AOD still shows the best for all statistical metrics. The biases at small AOD still exist for SRON (0.03) and GRASP (0.06).

- The AE validation with AERONET product shows that GRASP/HP AE over land is in very good correspondence with AERONET. GRASP/Models and SRON also have good agreement with AERONET, while SRON AE is overestimated for coarse mode and GRASP/Models also tends to overestimate coase mode AE, in addition, GRASP/Models AE for fine model seems to underestimate. Over ocean, both SRON and GRASP/HP AE are in good correspondence with AERONET measurements. The GRASP/Models overestimation/ underestimation issue seems to persist over ocean.
- The SSA validation with AERONET inversion product shows that SRON SSA is with smaller RMSE and smaller biases with AERONET than 2 GRASP products. Nevertheless, GRASP SSA was evaluated for much bigger number pixels. The additional filter (satellite AOD>=0.5) helps GRASP products to obtain RMSE smaller than 0.05, which is a target requirement for SSA products.
- AAOD validation shows similar performance of GRASP and SRON products relatively AERONET, which indicates the fact that the observed GRASP dispersion in SSA (RMSE>0.05 without additional AOD>0.5 filtering) is greatly affected by uncertainties of SSA retrieval at small AOD cases.

➢ POLDER/SRON and POLDER/GRASP aerosol products intercomparison:

- SRON and GRASP/HP AOD show overestimation with respect to GRASP/Models AOD over both land and ocean surface. The global mean differences (SRON-GRASP/Models) are ~0.06 over land and ~0.04 over ocean for AOD at 550 nm. Good correlations are found between SRON and GRASP/Models, GRASP/HP over ocean, with the R>0.87, RMSE around 0.075 and >50% pixels satisfy the GOCS requirements. Over land, the correlation coefficients decrease to ~0.7, RMSEs are ~0.21-0.23, and ~30% pixels satisfy the GCOS requirements. Some variations in AOD can be observed between SRON and GRASP products over land regions, for example, Sahara.
- Good correspondence of AE is found over ocean for both GRASP/Models, GRASP/HP with SRON products. The 3 datasets show qualitatively similar patterns of AE, however they are quantitatively different. For example, GRASP/HP shows domination of big particles over land as well as over ocean in polar and mid-altitude regions also in comparison to SRON (AE(GRASP/HP) < AE(SRON)). GRASP/HP shows domination of small particles over the ocean in equatorial regions (AE(GRASP/HP) > AE(SRON)).
- For SSA global comparison, 2 GRASP products (Models and HP) generally show stronger global absorption than SRON, which is in line with AERONET validation that GRASP products tend to have lower SSA than AERONET. Specifically,

GRASP/Models show stronger absorption over land and GRASP/HP show stronger absorption both over land and ocean than SRON.

- POLDER/SRON, POLDER/GRASP and MODIS surface products intercomparison:
  - The reasonable correspondence is found between GRASP and SRON surface retrievals. For example, ~30% pixels satisfying the surface Optimal requirements and >60% pixels satisfying the surface Target requirements. In general, SRON BRDF1 is around 0.01-0.02 higher than GRASP/Models and GRASP/HP for all wavelengths. The biggest differences are in BRDF2 and BPDF where the RMSE is ~0.24 for BRDF2 and ~1.4-1.7 for BPDF. Together with uncertainties of the retrieval this indicates the existent differences in BRDF/BPDF modeling in SRON and GRASP algorithm which should be considered at the next stage of the project.
  - Both GRASP and SRON show reasonable correspondence with MODIS BRDF. >40% pixels satisfy the Optimal requirement and >80% pixels satisfy the Target requirement. The RMSE does not exceed 0.03. The global difference between SRON and MODIS is 0.01 (SRON>MODIS), in contrast that GRASP/HP is 0.01 smaller than MODIS, and GRASP/Models is nearly zero difference with MODIS from the point of global mean.

3 Work Package 2: Synthetic comparison

3.1 Scope & Objective

In HARPOL WP2, we performed a comparison between the GRASP and RemoTAP (SRON) forward models, and their main components (optical properties, surface reflection, radiative transfer code). Also, we compared retrievals performed on synthetic measurements by both GRASP and SRON/RemoTAP. Here, we considered 2 different experiments: i) Consistent retrievals where each algorithm creates its own synthetic measurements using the same assumptions as used in the retrieval. ii) Inconsistent retrievals, where a more complex and realistic representation is used for the creation of the synthetic measurements than is used in the retrieval and where SRON/RemoTAP performs retrievals on synthetic measurements created by the GRASP forward model and GRASP performs retrievals on the synthetic measurements created by the SRON/RemoTAP forward model. The objective of the synthetic experiments is to investigate the importance of differences between the GRASP and SRON/RemoTAP forward models and retrieval assumptions, and to test the 'robustness' of the algorithms against inconsistencies between the measurement and retrieval assumptions.

3.2 Chapter overview

This chapter starts (section 2.3) with a description of the setup of both SRON/RemoTAP and GRASP for the different experiments in WP2, and then in section 2.4 we provide a description of the scenarios for which the forward model comparisons and synthetic retrievals have been performed. Then, section 2.4 describes the comparison of forward models, with the comparison of the Mie/T-matrix codes in section 2.4.1, the comparison of the surface reflection models in section 2.4.2, and comparison of the radiative transfer coded in section 2.4.3. Then, section 2.5 describes the synthetic retrieval experiments, with the consistent retrievals in section 2.5.1, and the inconsistent retrievals in section 2.5.2.

3.3 Setup of SRON/RemoTAP and GRASP Algorithms

3.3.1 SRON/RemoTAP

For the forward model comparisons and creation of synthetic measurements in WP2, SRON/RemoTAP used 32 streams in the Radiative Transfer (RT) model, combined with the delta-M method for phase matrix truncation. In the retrieval, SRON/RemoTAP uses 8 streams with delta-M truncation. Overall, the differences between 32 and 8 streams are very minor. For the vertical discretization of the atmosphere, SRON/RemoTAP used 15 homogeneous layers, with 2

km spacing between 0-20 km and 4 km spacing up to 36 km. Further, the temperature vertical profile is taken from the AFGL US standard atmosphere. The surface pressure was fixed at 1013 hPa and the pressure profile is computed using the hydrostatic equation. Absorption by trace gases has not been taken into account.
The surface reflection matrix $\mathbf{R}_s$ as function of wavelength λ, incoming zenith angle θ_{in}, outgoing zenith angle θ_{out}, and relative azimuth angle Δϕ, is described as:

$$\mathbf{R}_s(\lambda, \theta_{\text{in}}, \theta_{\text{out}}, \Delta\varphi) = r_{11}(\lambda, \theta_{\text{in}}, \theta_{\text{out}}, \Delta\varphi)\ \mathbf{D} + \mathbf{R}_{\text{pol}},$$

Where **D** is the null matrix except D_{11}=1, and

$$r_{11}(\lambda, \theta_{\text{in}}, \theta_{\text{out}}, \Delta\varphi) = A(\lambda)\ \ (1 + k_{\text{geo}} f_{\text{geo}}(\theta_{\text{in}}, \theta_{\text{out}}, \Delta\varphi) + k_{\text{vol}} f_{\text{vol}}(\theta_{\text{in}}, \theta_{\text{out}}, \Delta\varphi))$$

where f_{geo} and f_{vol} are respectively the geometric (Li-Sparse) and volumetric (Ross-Thick) kernel with corresponding coefficients k_{geo} and k_{vol}, assumed wavelength independent, and A(λ) is referred to as the Isotropic BRDF parameter. Further,

$$\mathbf{R}_{\text{pol}}(\theta_{\text{in}}, \theta_{\text{out}}, \phi_v - \phi_0) = B_{\text{pol}} \left(\frac{\exp\left(-\tan(\frac{\pi-\Theta}{2})\right)\ \exp(-\nu)\ \mathbf{F}_p(m, \Theta)}{4(\mu_{\text{in}} + \mu_{\text{out}})} \right)$$

where B_{pol} is a wavelength independent scaling parameter, F_p is the Fresnel matrix as function of scattering angle Θ and surface refractive index m (assumed to be 1.5), and ν=0.1.

For the state vector with retrieved parameters, we use a bi-modal aerosol description for the consistent retrievals of section 2.6.1 and a 3 mode aerosol description for the more realistic retrievals of section 2.6.2. In both cases we describe the wavelength dependent refractive index as

$$m(\lambda) = \sum_{k=1}^{n_\alpha} \alpha_k\ m^k(\lambda)$$

where $m_k(\lambda)$ are prescribed functions of wavelength, for which we use standard refractive index spectra (d'Almedida et al., 1990) for different aerosol components, i.e. Dust (DU) ,Inorganic / Sulphate (INORG) and Black Carbon (BC), and Organic Carbon (OC).

For the bi-modal aerosol description, we consider the following size modes and state vector parameters:

- A fine mode for which the state vector includes effective radius r_{eff}, effective variance v_{eff}, column number N_{aer}, as well as the refractive index coefficients that correspond to a refractive index spectra with spectrally constant value of 1.53-0.005i.
- A coarse mode for which the state vector includes r_{eff}, v_{eff}, N_{aer}, the fraction of sphere f_{sph}, as well as the refractive index coefficients that correspond to a refractive index spectra with spectrally constant value of 1.53-0.005i.

For the 3-mode aerosol description, we consider the following size modes and state vector parameters:

1) A fine mode for which the state vector includes r_{eff}, v_{eff}, N_{aer}, the fraction of sphere f_{sph}, as well as the refractive index coefficient α_k that correspond to the standard refractive index spectra INORG, BC, OC.
2) A coarse insoluble mode that consists of non-spherical dust. For this mode the state vector includes r_{eff} , N_{aer}, and a coefficient for the imaginary part of the DU refractive index. The fixed parameters are f_{sph} = 0, v_{eff} = 0.6, a_k = 1 for the DU real part refractive index. One value for the Aerosol Layer Height (ALH) is included which is assumed to be the same for modes 1 and 2. w_0 is fixed at 2000 m.
3) A coarse soluble mode. For this mode the state vector includes r_{eff}, N_{aer}, and coefficient a_k of the INORG refractive index spectrum. The fixed parameters are f_{sph} = 1, v_{eff} = 0.6, and ALH=500 m.

For all retrievals SRON/RemoTAP includes for the surface reflection the parameters A(l), k_{geo}, k_{vol}, and B_{pol} in the state vector.

3.3.2 GRASP

For the forward model comparisons and creation of synthetic measurements in WP2, GRASP used 20 streams in the Radiative Transfer (RT) model. The truncation method is described in (Waquet and Heman, 2019). In the retrieval, GRASP uses 10 streams with truncation. Similarly to SRON/RemoTAP, overall, the differences between 20 and 10 streams are very minor. Vertical discretization in GRASP is dynamically adjustable to the optical thickness. The maximum number of layers is 50 with the same optical thickness in the layers. Absorption by trace gases has not been taken into account as well.

Both GRASP and SRON/RemoTAP use the same BRDF and BPDF model with some minor difference of combining BRDF and BPDF and scaling factor for BPDF.

In GRASP the element "11" of the surface reflection matrix $\mathbf{R}_s$ is a combination of r_{11} and R_{11pol}: $R_{11s}=r_{11}+R_{11pol}$

All other elements of $\mathbf{R}_s$ in GRASP are defined similarly to SRON/RemoTAP.

The scaling BPDF parameter B_{GRASP} in GRASP is related to the SRON/RemoTAP as following: $B_{GRASP}=B_{pol}$ * exp (-v).

Similarly to SRON/RemoTAP, GRASP results in the section 2.6.1 are presented for the bi-modal aerosol description. GRASP retrieval results in the Section 3.6 are presented for two approaches: Chemical Component approach, and 5 Log-Normal bins approaches.

In the Chemical Component approach aerosols are assumed to be mixtures of hydrated soluble particles embedded with black carbon, brown carbon, iron oxide, and other (non-absorbing) insoluble inclusions. The complex refractive indices of the dry components are fixed a priori. The refractive index of the soluble host is allowed to vary with hydration. The complex refractive indices of the mixture are computed using mixing rules (Li et al., 2019). The volume fractions of these components are derived along with the size distribution and the fraction of spherical particles. Two modes of aerosol are considered in this approach. The fine mode aerosol is described by 3 lognormal bins and include such chemical components as 'black_carbon', 'brown_carbon', 'quartz'. The coarse mode size distribution is described by 3 log-normal bins and consists of 'iron_oxide' and 'quartz' components. The vertical profile is considered the same for fine and coarse mode and is described by exponential function with retrieved scale height parameter.

The vector of aerosol retrieved parameters in the 5 log-normal bins approach consists of such microphysical properties as: complex refractive index, aerosol concentration, nonsphericity parameter, 5 log-normal particle size distribution characteristics. The complex refractive index is retrieved for each wavelength with applied spectral constraints. The results presented in section 3.6 are obtained for the case when the same refractive index and the same exponential vertical profile were used for fine and coarse mode. The results with different refractive indices and log-normal bins retrieval for the two modes have not shown essential improvement and were omitted from this report.

3.4 Description of synthetic cases

3.4.1 Consistent Scenario

Table 3-1: Aerosol properties used for forward model comparisons and generic synthetic retrievals

	mode 1 (log-normal)	mode 2 (log normal)
r_eff (μm)	0.15	1.5
v_eff	0.2	0.6
RRI	1.53	1.53
IRI	0.005	0.005
f_sphere	1.0	0.5
AOD	0.3, 1.0	0, 0.1, 0.5, 1.0, 2.0
Altitude distribution	homogeneously 0-2 km	homogeneously 0-2 km

Table 3-2: Surface properties used for forward model comparisons and generic synthetic retrievals.

	440 nm	490 nm	563 nm	670 nm	865 nm	1020 nm
Ross-Li scaling	0.03	0.03	0.05	0.07	0.40	0.5
Ross Thick	0.6	0.6	0.6	0.6	0.6	0.6
Li Sparse	0.1	0.1	0.1	0.1	0.1	0.1
Maignan scaling	1	1	1	1	1	1
Maignan ν	0.1	0.1	0.1	0.1	0.1	0.1

We first defined a setup for forward model comparisons and for generic synthetic aerosol retievals where the assumptions in the retrieval are the same as those used to create synthetic measurements. The corresponding aerosol properties are shown in Table 3-1. We have chosen a typical bi-modal size distribution where we vary the AOD of fine and coarse mode respectively. The surface properties are shown in Table 3-2. Here we use the Ross-Li Bi-directional Reflection Distribution Function (BRDF) model combined with the Maignan model for polarized surface reflection.

For the geometries, we use POLDER-3 geometries from overpasses over the AERONET stations of Table 3-3.

Table 3-3: *AERONET stations for which the geometries of POLDER-3 overpasses have been used for forward model comparisons and generic retrieval experiments. Also, aerosol and surface data from these stations have been used to create synthetic measurements for more realistic conditions.*

AERONET station	lon, lat
Mongu	23.15,-15.25
Ilorin	4.34, 8.32
Kanpur	80.23, 26.51
Banizoumbou	2.66, 13.54
Beijing	116.38, 39.98

3.4.2 Inconsistent Realistic Conditions

To compare the SRON/RemoTAP and GRASP retrievals for more realistic conditions, we also created 2 additional sets of synthetic measurements:

- **'ECHAM'**. Based on aerosol microphysical properties from simulations by the ECHAM-HAM aerosol climate model. ECHAM-HAM provides mass-mixing ratio in different vertical layers of the atmosphere of different aerosol species (Sulfate, Organic Carbon, Black Carbon, Dust, Sea Salt) in seven different size modes: Nucleation Soluble (NS), Aitken Soluble (KS), Accumulation Soluble (AS), Coarse Soluble (CS), Aitken Insoluble (KI), Accumulation Insoluble (AI), Coarse Insoluble (CI). Based on the composition we can compute the refractive index for each mode. The 7 modes aerosol description is different from the standard setup of the SRON/RemoTAP algorithm (3 modes with different refractive index) and also from the standard GRASP algorithm (5 modes with same refractive index, mixture of aerosol models, or a mixture of models with different chemical components). For surface BRDF / BPDF properties and AOD we use POLDER-3 retrieved values over the AERONET sites of Table 3. The solar and viewing geometries are based on POLDER-3 geometries for overpasses over these AERONET stations. The corresponding measurements are generated by the SRON/RemoTAP forward model.
- **'22-Bin'**. Based on AERONET retrievals for the 5 stations of Table 3. AERONET retrieves the aerosol size distribution in 22 bins, and one size independent, wavelength dependent complex refractive index. The 22-bin size distribution is inconsistent with the assumptions in both SRON/RemoTAP and GRASP. For surface BRDF/BPDF and geometry we use the values from POLDER-3 overpasses as above. The corresponding measurements are generated by the GRASP forward model.

3.5 Comparison of Forward Models

3.5.1 Mie / T-Matrix calculations

Figure 3-1 shows the difference between SRON/RemoTAP and GRASP in the most important elements of the scattering phase matrix. It can be seen that differences in element F11 are up to 3%, with larger errors in the fine mode than coarse mode. For the ratio F21/F21, representative for the Degree of Linear Polarization (DoLP) of single scattering, the differences are up to 0.016 for the fine mode and 0.02 for the coarse mode, but for the coarse mode the differences are largest in a more restricted range of scattering angles around 150 degrees. For POLDER-3 measurements, the measurement uncertainty is around 3% for radiance and 0.02 for DoLP which means that for POLDER-3 the difference shown in Figure 3-1 may be just acceptable. However, future instruments will have smaller uncertainty on DoLP (e.g. ~0.003 for SPEXone/PACE and MAP-CO2M). Also, the differences are larger than expected because both GRASP and SRON/RemoTAP use the same tables with pre-calculated Mie and T-Matrix / geometrical optics calculations from Dubovik et al. (2006). So, the difference comes from further processing of the tabulated values. Here, the tables contain computed values of optical properties for different size

bins and a wavelength of 340 nm. To do calculations for an arbitrary wavelength, SRON/RemoTAP uses a fixed grid of the size parameter (2 π r / lambda) so that the tabulated values do not have to be interpolated (but the size distribution has to be computed for a different radius grid for different wavelengths). GRASP on the other hand uses a fixed radius grid of the size distribution which means that the tabulated optical properties have to be interpolated for each different wavelength. For the calculations in Figure 3-1 GRASP used linear interpolation which mostly explains the differences between GRASP and SRON/RemoTAP. The differences can be reduced by using spline interpolation with increased computation time. For the radiative transfer and retrieval comparisons in this section GRASP has used spline interpolation.

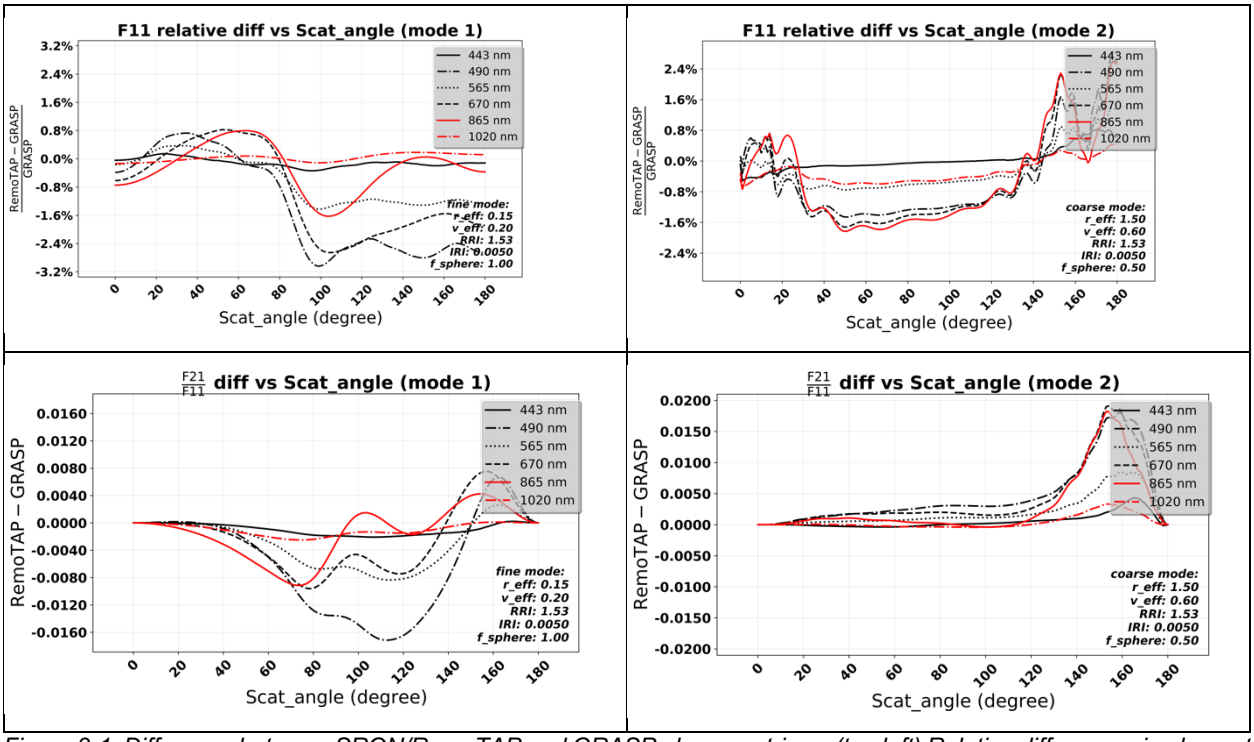

Figure 3-1: Difference between SRON/RemoTAP and GRASP phase matrices. (top left) Relative differences in element F11 for the fine mode, (top right) and for the coarse mode, (bottom left) absolute differences in F21/F11 for the fine mode, (bottom right) and coarse mode. Fine and coarse mode are specified in Table 1.

3.5.2 Surface Reflection Models

A comparison of the surface reflection models for r_{11} (BRDF) and $R_{pol,21}$ (polarized BRDF or BPDF) is shown in Figure 3-2. Both GRASP and SRON/RemoTAP use the Ross-Li kernel model for radiance and the Maignan parameteric model for polarized surface reflection. The comparison for the original setup of the SRON/RemoTAP surface BRDF model (left) shows a difference in radiance reflectance close to backscattering angle. This difference can be traced back to a different application of the hotspot correction in the Ross-Li model, which was applied to both the volumetric ('Ross') and geometric ('Li') kernels in SRON/RemoTAP. It is more common to apply it only to the volumetric kernel so SRON/RemoTAP has been adjusted accordingly. After this

adjustment GRASP and SRON/RemoTAP are in perfect agreement. For the polarized BRDF the comparison revealed an error in the SRON/RemoTAP implementation which has now been corrected, leading also to perfect agreement between SRON/RemoTAP and GRASP.

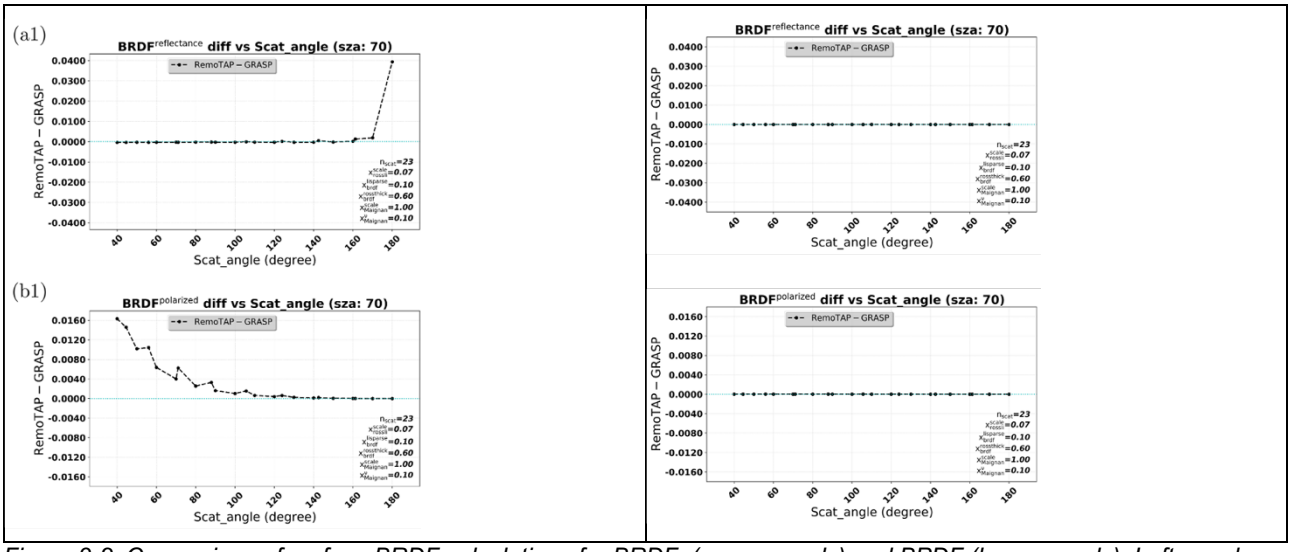

Figure 3-2: Comparison of surface BRDF calculations for BRDF (upper panels) and BPDF (lower panels). Left panels show comparison with original SRON/RemoTAP version and right panel with updated version (harmonized hotspot correction and corrected the polarized surface reflection model).

3.5.3 Radiative Transfer Calculations

Figure 3-3 shows the forward model comparisons between SRON/RemoTAP and GRASP. The bias and standard deviation of the differences in radiance are mostly below 2% and for DoLP mostly below 0.005. There is a dependence on wavelength of the differences: For radiance the differences are somewhat larger at 490 and 565 nm, and for DoLP the differences are larger at 670 nm (up to 0.01 for some angles). The wavelength dependence of the differences can most likely be explained by differences in the optical input parameters, as for the accuracy of the radiative transfer model itself we do not expect it can show such wavelength dependent features. Overall, the comparison between the GRASP and SRON/RemoTAP forward models look reasonably good, and the differences are in general smaller than the measurement uncertainty for POLDER-3. In section 2.5.3 we will investigate the importance of the forward model differences by performing SRON/RemoTAP retrievals on synthetic measurements created by the GRASP forward model and vice-versa.

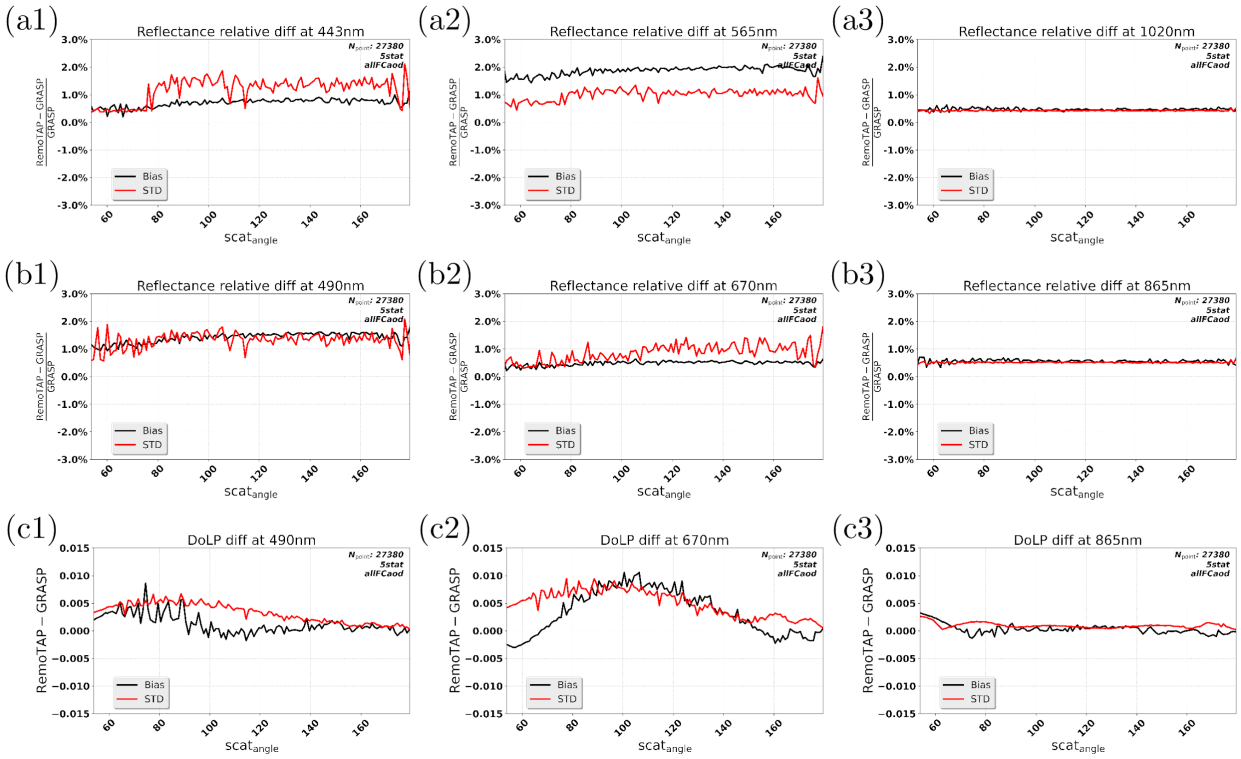

Figure 3-3: Comparison of forward model calculations (SRON/RemoTAP-GRASP) for the aerosol and surface properties of Table 1, surface properties of Table 2, and geometries of PARASOL overpasses for the AERONET stations of Table 3. Shown are the bias and standard deviation of the differences.

3.6 Retrieval on Synthetic Measurements

3.6.1 Retrieval on Consistent Synthetic Measurement

Figure 3-4 shows the results of the consistent synthetic retrieval experiment where both GRASP and SRON/RemoTAP have performed retrievals on synthetic measurements created by their own forward models using a consistent aerosol description (bi-modal) both in the synthetic measurement and forward model. For GRASP both multi-pixel (MP) and single-pixel (SP) retrievals have been performed. It can be seen from Figure 3-4 that for none of the algorithms the retrieval is perfect, despite the consistent setup of the experiment. This shows a principal limitation in information content of satellite remote sensing of aerosol properties, especially at larger AOD, where it is hard to separate the surface properties from aerosol.

If we look at AOD, the GRASP MP retrievals clearly perform better than the GRASP SP retrievals. GRASP MP and SRON/RemoTAP show quite similar performance where SRON/RemoTAP has

a smaller bias and slightly smaller MAE and RMSE. For both, the fraction of retrievals within the GCOS requirements is very high (~97%). Looking at the other aerosol properties, the difference between GRASP-MP and GRASP-SP is less obvious, although GRASP-MP still performs better also for these properties. Overall, SRON/RemoTAP has somewhat better performance on all properties but it should be noted that both GRASP and SRON/RemoTAP perform well. It should also be noted that the results correspond to a bi-modal retrieval which has been much less exploited in GRASP than in SRON/RemoTAP, which may explain the somewhat better performance of SRON/RemoTAP for these retrievals.

3.6.2 Retrieval on Inconsistent Synthetic Measurement

In real life, the assumed aerosol description in the retrieval will typically be different from the real aerosol properties. Therefore, it is important to investigate the performance of the algorithms for synthetic measurements created with a more extended and realistic set of aerosol properties than assumed in the retrieval. At the same time, it is important to evaluate the effect of differences due to differences in the forward models of GRASP and SRON/RemoTAP. Therefore, the 'ECHAM' measurements have been created with the SRON/RemoTAP forward model and the '22-bin' measurements have been created with the GRASP forward model.

Figure 3-5 shows the results for the 'ECHAM' synthetic measurements created by the SRON/RemoTAP forward model. For GRASP, both results for the 'Chemical Component (CC)' setup and the regular 5-mode setup are shown. For AOD, GRASP-CC and GRASP-5-mode show similar performance with MAE 0.05-0.06 (69.1% and 51.3% within GCOS, respectively), whereas SRON/RemoTAP has better performance with MAE of 0.033 (79.6% within GCOS) . For SSA, GRASP-CC shows the best performance with a MAE of 0.024 (77.6% within GCOS) while SRON/RemoTAP has a somewhat larger MAE of 0.029 (65.4% within GCOS). The GRASP-5-mode results have the largest MAE of 0.051 (43.6% within GCOS). Finally, for the fine mode effective radius (not provided by GRASP-CC), GRASP-5-mode has an MAE of 0.024 micron and SRON/RemoTAP of 0.012 micron. Overall, for most properties SRON/RemoTAP performs better on the 'ECHAM' synthetic measurements but it should be noted again that these synthetic measurements were created by the SRON/RemoTAP forward model which should be an 'advantage' for SRON/RemoTAP retrievals.

Figure 3-6 shows the results for the '22 bin' synthetic measurements created by the GRASP forward model. For AOD, the GRASP-5-mode retrieval shows the best performance with an MAE of 0.045 and 80.9% of the pixels within the GCOS requirements. GRASP-CC and SRON/RemoTAP show similar performance, where GRASP-CC has an MAE of 0.077 and 54.1% within GCOS requirements, whereas SRON/RemoTAP has an MAE of 0.083 and 56.1% within GCOS requirements. For SSA, GRASP-CC and GRASP-5 mode show similar performance, where GRASP-5-mode has a slightly better MAE than GRASP-CC (0.018 vs 0.02) and more retrievals within GCOS requirements (85.7% vs 73.1%) but GRASP-CC has a smaller bias (-0.006 vs -0.015). SRON/RemoTAP shows a larger MAE (0.024) and smaller fraction of retrievals

within GCOS requirements (69.7%) but on the other hand shows the smallest bias (-0.004). For the fine mode effective radius GRASP-5-mode shows a somewhat better performance than SRON/RemoTAP (MAE 0.012 vs 0.018 micron). Overall, for most properties, GRASP-5 mode performs better than SRON/RemoTAP for the ’22 bin’ synthetic measurements created by the GRASP forward model whereas GRASP-CC and SRON/RemoTAP show similar performance. Here it should be noted again that the synthetic measurements were created by the GRASP forward model which should be an ‘advantage’ for GRASP retrievals.

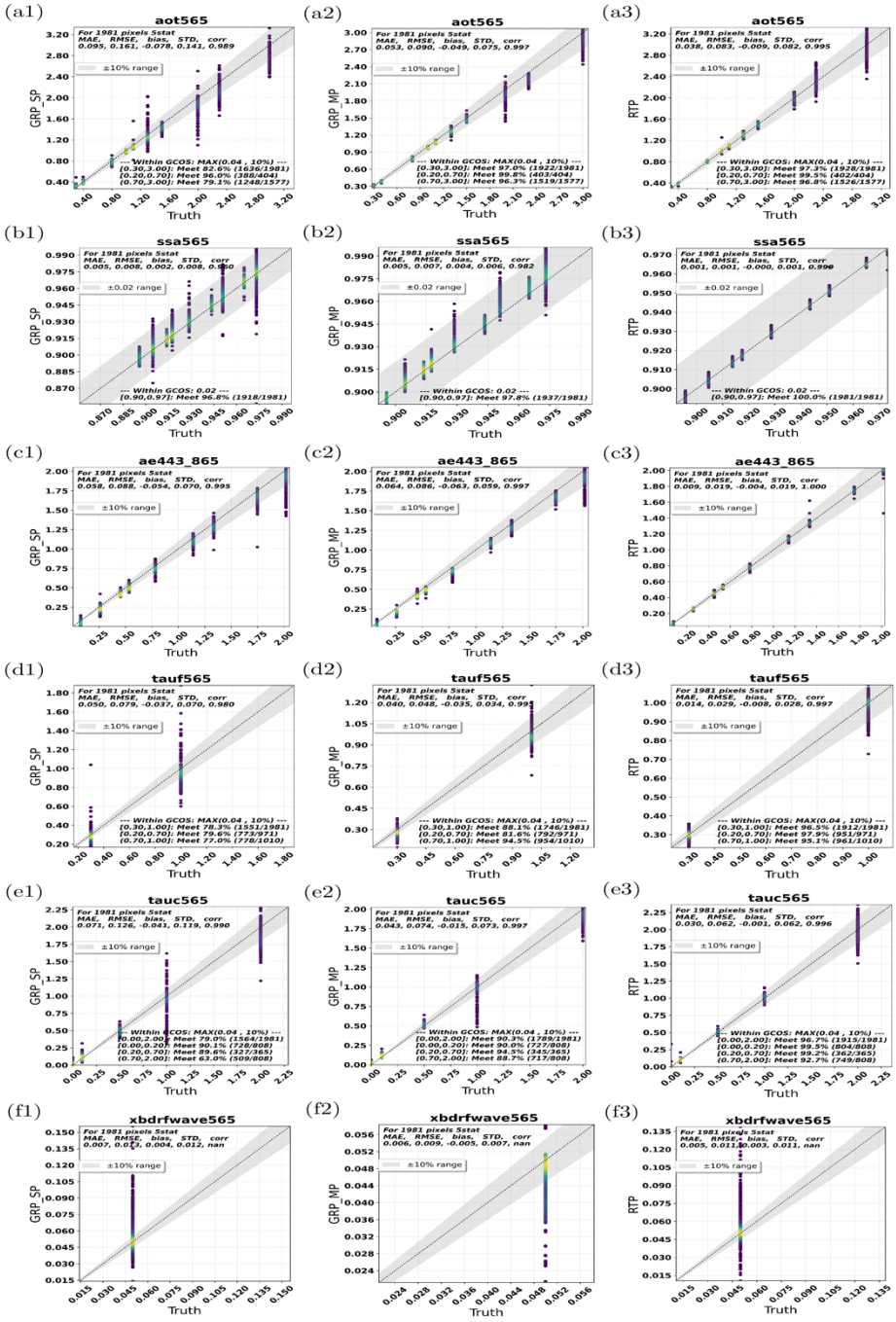

Figure 3-4: Results of consistent synthetic retrievals for GRASP Single Pixel (SP) retrievals (left columns), GRASP Multi-Pixel (MP) retrievals (middle columns), and SRON/RemoTAP retrievals (right columns). Each algorithm has performed retrievals on synthetic measurements created by the same forward model as used in the retrieval with the same assumptions on aerosol properties (e.g. number of modes etc.). Results are show for AOT, SSA, Angstrom Exponent between 443 and 865 nm (AE443_865), fine mode aot at 565 nm (tauf565), coarse mode AOT at 565nm (tauc565), and the wavelength dependent Isotropic BRDF factor at 565 nm (xbdrfwave_565).

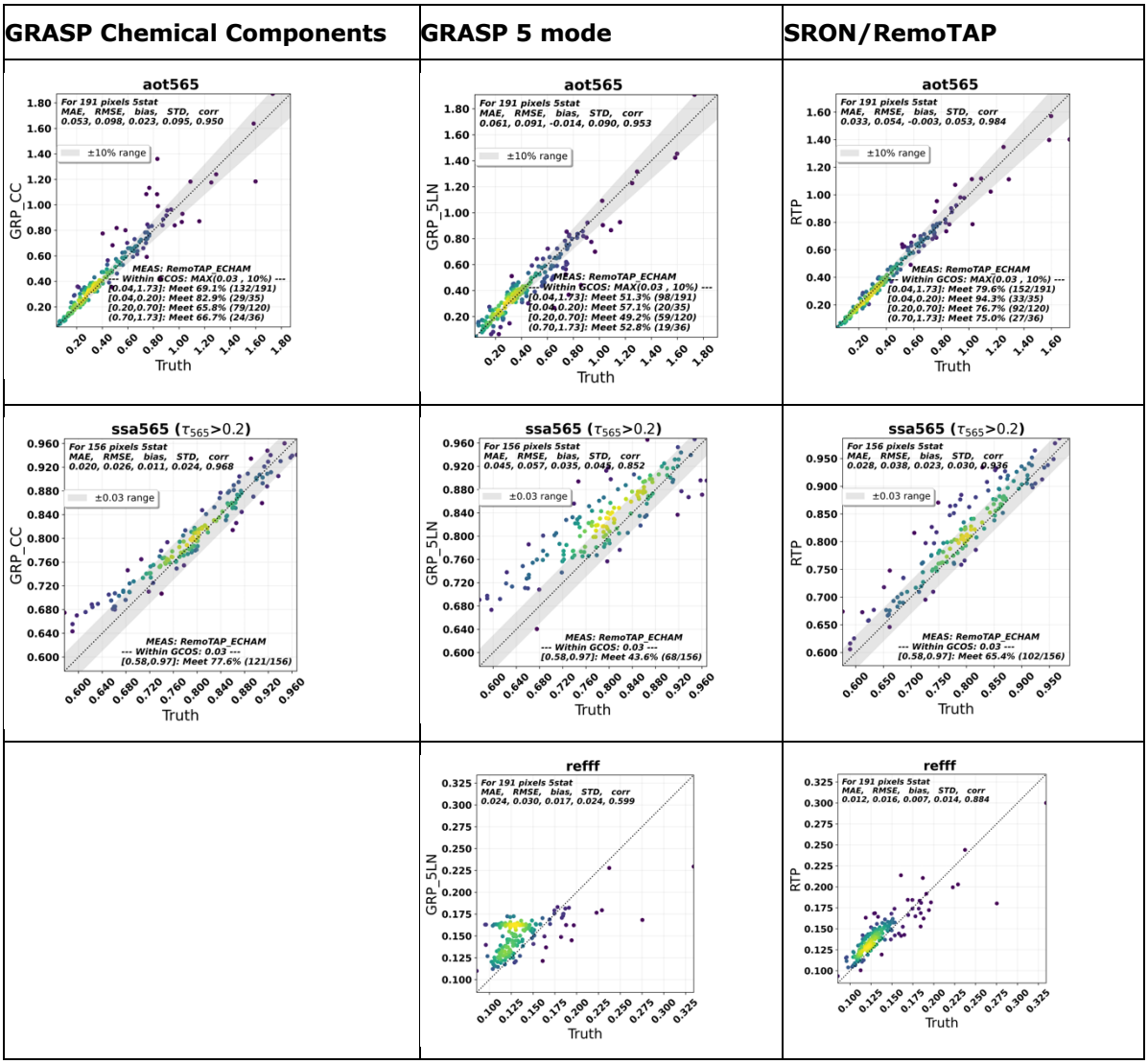

Figure 3-5: Synthetic retrieval results for the 'ECHAM' synthetic measurements created by the SRON/RemoTAP forward model. Shown are the results GRASP 'Chemical Components' setup (left), the GRASP regular 5 mode setup (middle), and the SRON/RemoTAP algorithm (right). Properties shown (from top to bottom) are the AOT, SSA, fine mode effective radius reff. Results have been filtered for SRON/RemoTAP chi2 < 1 (keeping 191 out of 202 retrievals).

GRASP Chemical Components	**GRASP 5 mode**	**SRON/RemoTAP**
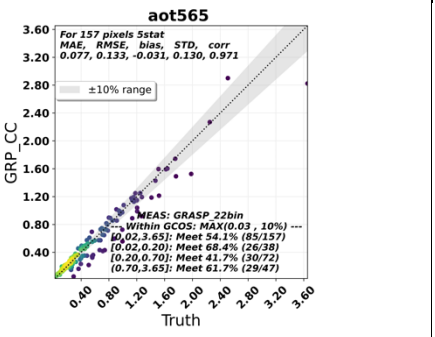	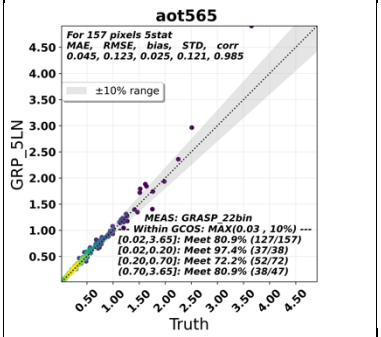	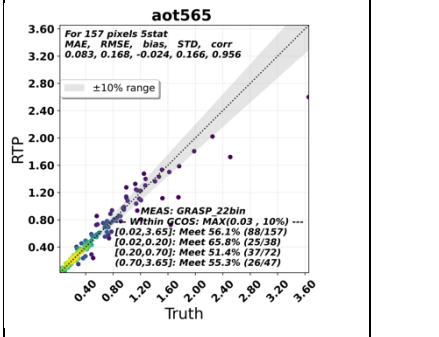
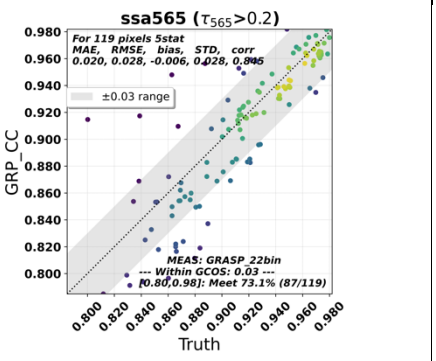	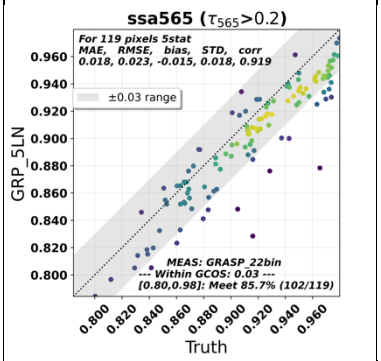	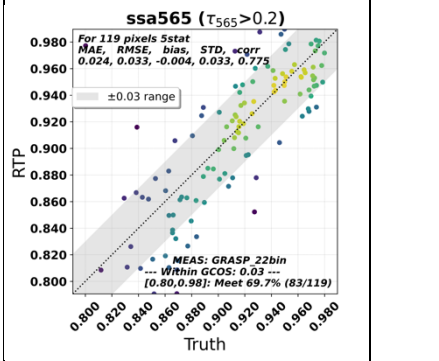
	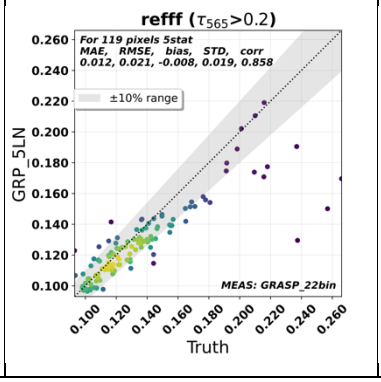	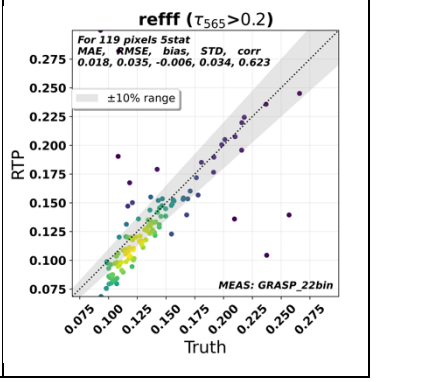

Figure 3-6: Synthetic retrieval results for the '22-bin' synthetic measurements created by the GRASP forward model. Shown are the results GRASP 'Chemical Components' setup (left), the GRASP regular 5 mode setup (middle), and the SRON/RemoTAP algorithm (right). Properties shown (from top to bottom) are the AOT, SSA, fine mode effective radius reff. Results have been filtered for SRON/RemoTAP chi2 < 1 (keeping 157 out of 202 retrievals).

chi2 < 0.5	chi2 < 5	all retrievals

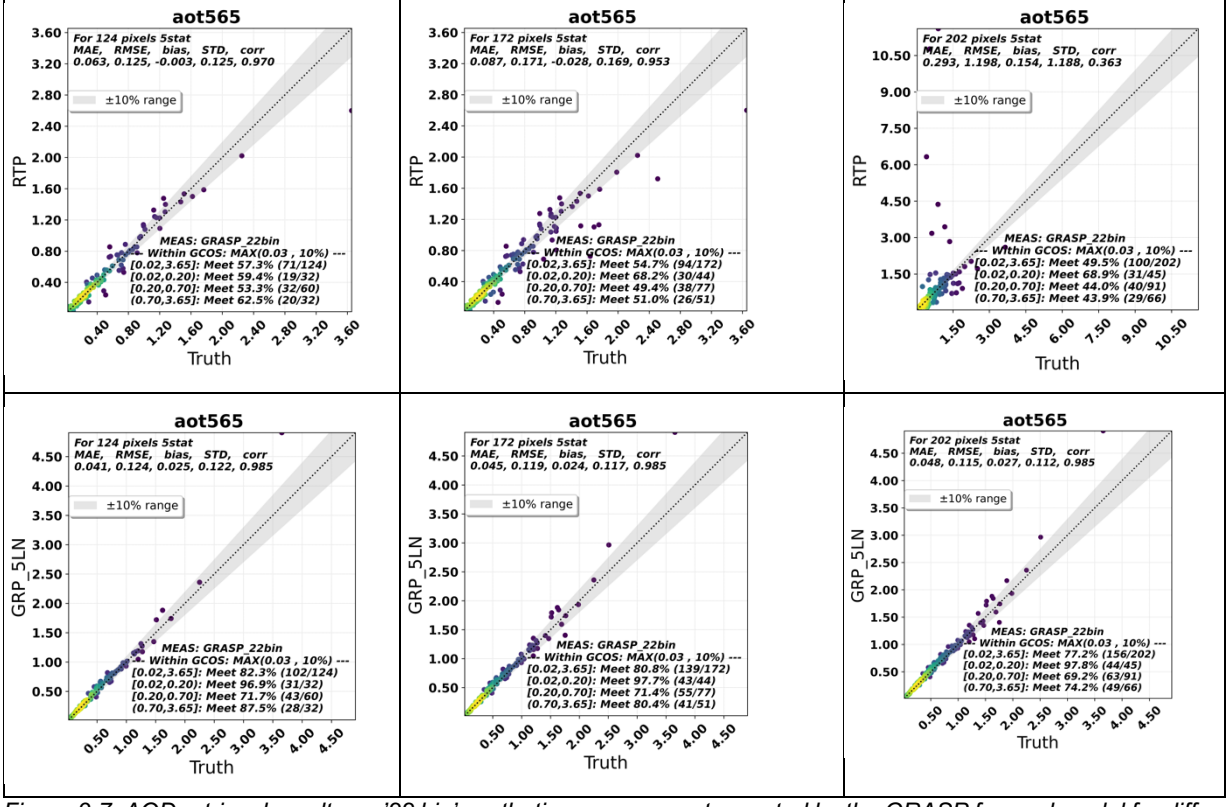

Figure 3-7: AOD retrieval results on '22 bin' synthetic measurements created by the GRASP forward model for different SRON/RemoTAP chi2 thresholds for data filtering: chi2 < 0.5 (left), chi2 < 5 (middle), and no filtering (right).

For the results of Figure 3-5 and Figure 3-6, data have been screened out based on the goodness-of-fit of SRON/RemoTAP retrievals, keeping only pixels with chi2 < 1. High values of chi2 indicate non-convergence of the retrieval and/or an inconsistency between the measurement and the forward model used in the retrieval. To investigate the effect of this data filtering, Figure 3-7 shows the AOD retrieval results for SRON/RemoTAP and GRASP-5-mode for different chi2 thresholds of SRON/RemoTAP, with one stricter value (chi2 < 0.5) than in Figure 3-6, one less strict value (chi2 < 5), and also for the case of no filtering at all. It can be seen that for the stricter filtering (chi2 < 0.5) the MAE of the SRON/RemoTAP can be improved from 0.083 to 0.063 while excluding 33 retrievals compared to Figure 3-6. By applying a less strict filtering (chi2 < 5) the

effect on MAE is minor but on the other hand only 15 extra retrievals can be obtained compared to Figure 3-6. However, when applying no data filtering at all, the SRON/RemoTAP retrievals show some very strong outliers with very large retrieved AOD. So, it is obvious that for SRON/RemoTAP some filtering based on chi2 is essential. The actual threshold value has to be determined empirically. On the other hand, the GRASP results show comparable performance for the different chi2 filter values, which suggests that GRASP can provide valid retrievals for a larger fraction of the data.

3.7 Conclusions

In HARPOL WP2 we performed a detailed comparison of the GRASP and SRON/RemoTAP forward models and retrieval performance on synthetic measurements. Based on the comparison of aerosol scattering matrices, we found considerable differences that were caused by the use of linear interpolation by GRASP of the tabulated optical properties as function of size parameter. This was mostly remedied by the use of spline interpolation in the further retrieval comparisons. Also, the comparison revealed an error in the implementation of the surface polarization in SRON/RemoTAP which was corrected. After these corrections, the forward models of GRASP and SRON/RemoTAP agree better than 2% (better than 1% for most wavelengths and angles) for radiance and better than 0.01 (better than 0.005 for most wavelengths and angles) for Degree of Linear Polarization (DoLP).

For comparison of retrievals, we performed first retrievals on consistent synthetic measurements created by the forward model of each algorithm with consistent assumptions about the aerosol description in the forward model and the measurements. Both GRASP and SRON/RemoTAP perform well for these cases but the retrievals are not perfect despite the ideal settings. This shows a limitation in the information content of satellite remote sensing of aerosol, in particular at high AOD (> ~2). Next, 2 sets of synthetic measurements were created: 1) By the SRON/RemoTAP forward model using aerosol properties of the ECHAM aerosol climate model as input, and 2) by the GRASP forward model using AERONET aerosol properties as input. The assumptions on aerosol properties in both these sets of measurements are different (and more realistic) than what is assumed in both SRON/RemoTAP and GRASP, which allows to give an indication of the performance under more realistic conditions. Also, by performing SRON/RemoTAP retrievals on GRASP synthetic measurements and vice versa, we get an indication to what extend the retrievals are limited by differences in the respective forward models. Both SRON/RemoTAP and GRASP are able to provide accurate aerosol retrievals also for inconsistent synthetic measurements and also for synthetic measurements created by a different forward model. Here, as expected, SRON/RemoTAP performs somewhat better on on the SRON/RemoTAP measurements and GRASP performs somewhat better on the GRASP measurements. For SRON/RemoTAP, it is important to filter out retrievals with a large chi2 difference between forward model and measurements (indication of non-convergence or large inconsistency between retrieval assumptions and measurements) while GRASP is hardly sensitive to such filtering. Overall, both SRON/RemoTAP and GRASP have demonstrated

robustness against aerosol assumptions and forward model differences and are capable of performing accurate retrievals under different circumstances.

4 Work Package 3: Real measurements

4.1 Scope & Objective

In HARPOL WP3, we performed inversion of POLDER real measurements. First we optimized the GRASP and RemoTAP (SRON) algorithms, individually. Then, for the optimized setups of both algorithms, the retrieval results were validated and intercompared. Specifically, we retrieved 3x3 pixels over all available AERONET sites in 2008 (Figure 4-1). Only comparisons were performed if AERONET, GRASP and RemoTAP data were available. and then regional processing was done over some selected regions. The purpose of this chapter is to present the evaluation of the SRON/SRON/RemoTAP and GRASP POLDER-3/PARASOL aerosol and surface retrievals based on the processing of pixels over AERONET stations and selected regions.

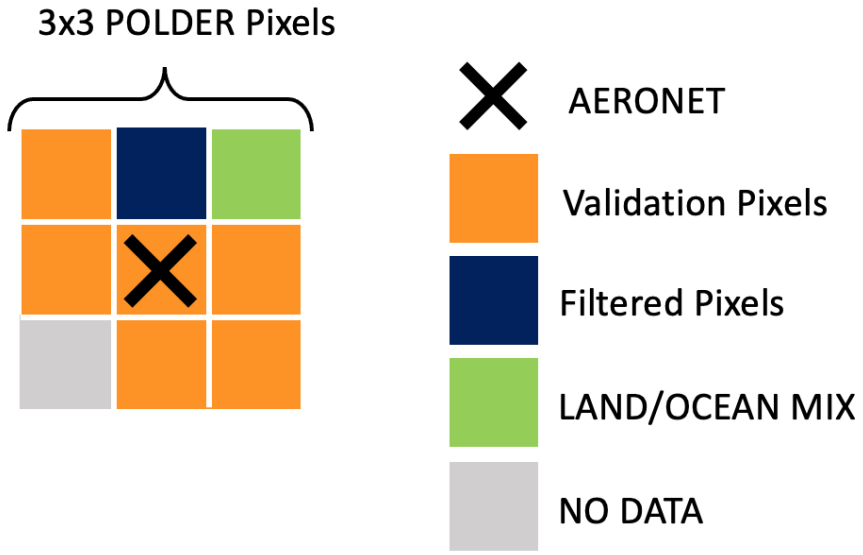

Figure 4-1. Schematic diagram of the validation of 3x3 POLDER pixels over AERONET. The pure land or ocean pixels satisfying filter scheme ("Validation Pixels") are averaged and validated against AERONET measurements.

4.2 Chapter overview

The structure of this WP3 report is as follows. The optimized SRON/RemoTAP and GRASP methods used in the real measurements processing are described in Section 4.3, followed by validation and intercomparison of the results over AERONET stations in Section 4.4. Section 4.5 describes the intercomparison of SRON/RemoTAP and GRASP/Component regional processing over some selected regions. Section 4.6 concludes the activities conducted in WP3.

4.3 Description of SRON and GRASP methods

From both SRON and GRASP sides, there are different methods to perform aerosol retrievals from real measurements. The main differences between these methods are the way of modeling aerosols. The detailed description of these methods are presented in Section 3.3. Here we give a summary.

SRON/RemoTAP

For SRON RemoTAP we investigated the following 2 setups

- SRON/RemoTAP 3 modes where the size distribution is described by 3 log-normal modes (i.e. Nmodes = 3), with one fine mode and 2 coarse modes (soluble and insoluble). For the fine mode the state vector includes effective radius r_{eff} , effective variance v_{eff} , number column N_{aer} and fraction of spheres f_{sph} and the refractive index coefficients k that correspond to the standard refractive index spectra inorganic (INORG),Black Carbon (BC), and Organic Carbon (OC). The coarse insoluble mode consists of non-spherical dust (DU). For this mode the state vector includes r_{eff} , N_{aer}, and a coefficient for the imaginary part of the DU refractive index. The fixed parameters are f_{sph} = 0, v_{eff} = 0.6, k = 1 for the DU real part refractive index. One value for aerosol layer height z_{aer} is included which is assumed to be the same for modes 1 and 2. The width is fixed at 2000 m. The 3rd mode is a coarse soluble mode. For this mode the state vector includes r_{eff} , N_{aer}, and coefficient k of the INORG refractive index spectrum. The fixed parameters are f_{sph} = 1, v_{eff} = 0.6, and z_{aer}=0.5 km.
- SRON/RemoTAP 5modes where the size distribution is described by a combination of 5 log-normal modes. For each mode Naer is included in the state vector while r_{eff} , v_{eff} are fixed to the same values as the GRASP algorithm. The state vector includes one value for f_{sph} for all fine modes and one value for all coarse modes and for the fine mode refractive index (i.e. assumed the same for all fine modes) it includes the coefficients k that correspond to the standard refractive index spectra INORG, BC, OC, and for the coarse mode refractive index (i.e. assumed the same for all coarse modes) the coefficients corresponding to INORG and DU. Further, one value for z_{aer} is included which is assumed to be the same for all modes, i.e. all modes have the same vertical distribution. The width is fixed at 2000 m.

Compared to WP1 of the HARPOL project, SRON/RemoTAP has improved on different aspects. First of all, we investigated different aerosol state vector definitions (3-mode and 5-mode) that provide improved retrieval accuracy compared to the 2-mode retrieval of WP1. Further, we now take into account spectral dependent refractive indices based on pre-defined spectra for different chemical components while in WP1 we assumed a spectrally neutral refractive index. Here, we investigated the use of the same refractive indices as used by the GRASP team. This leads to slightly worse RMSE for the AOD (by 0.015) and for AE (by 0.02) and for very similar performance for SSA. Because of the slightly worse overall performance when using GRASP refractive indices we decided to keep the original set of refractive indices. We also optimized the side constraint

(prior and weight in the inversion) for different fit parameters. Here, we found it is important to give more freedom in the fit for the coarse mode. This mostly affects the Angstrom Exponent. For improving the retrieval of SSA, we optimized the side constraint for Black Carbon and Organic Carbon. For the surface BRDF description, in addition to the bug fixes of WP2, we now add the Fresnel reflection term (previously only used for the BPDF) to the BRDF to improve consistency between polarized and non-polarized reflectance. For the ocean reflectance, we now fit an additional wavelength dependent Lambertian albedo term to correct for an imperfect ocean model (ocean body and foam). Concerning input data, we now use atmospheric information from MERRA2-asm for vertical information on pressure, temperature, and O3 mass mixing ratio. Previously, they were from NCEP and climatology for O3. The final retrieval result also depends substantially on the 1st guess that we obtain from a LUT retrieval. We improved the LUT in terms of the grid (spacing and range) and and improved the approach for combining different modes in the LUT.

GRASP

For GRASP side, 2 approaches are investigated in this project:

- GRASP/LN5Bins

GRASP/LN5Bins approach assumes one aerosol component with 5 Log-Normal bins size distribution and spectrally dependent complex refractive index, and the aerosol vertical distribution is modeled using exponential profile and scale height is retrieved (Dubovik et al., 2011). Meanwhile, spectral surface BRDF and BPDF parameters are retrieved together with aerosol. This approach is known as “High-Precision” (HP) and “Optimized” in WP1. The HP and Optimized are different only by the adopted precision of the RT calculation. Compared to WP1, the LN5Bins approach has been adjusted and improved in the following aspect: the aerosol concentration is treated separately from the size distribution, where only the relative ratios of each size bin are present. Therefore, we could apply different multi-pixel constraints on aerosol concentration and size distribution, for example, strong constraint on size distribution in space and small constraint on aerosol concentration in time.

- GRASP/Component

GRASP/Component approach inherits from GRASP/LN5Bins approach with adjustments for the treatment of aerosol size distribution complex refractive index. It assumes a similar 5 Log-Normal bins size distribution, while size-resolved (fine mode - first 3 bins; coarse mode - 4th and 5th bins) chemical components are mixed based on Maxwell-Gernett (MG) effective approximation to derive spectral dependent complex refractive index for fine and coarse modes. Each chemical component is defined with a prescribed spectral complex refractive index (Li et al., 2019). For fine mode, hydrated soluble particles are embedded with black carbon, brown carbon and quartz, while iron oxide and quartz are present in the coarse mode. This approach is newly developed and it was not included in the WP1 intercomparison, while based on some preliminary analysis it shows overall stable and encouraging performance.

4.4 Validation and intercomparison over AERONET

In this section, the SRON/RemoTAP and GRASP methods are used to perform retrievals on 3x3 pixels of real POLDER measurements over all available AERONET stations in 2008. Then the retrieval results of aerosol are validated with AERONET datasets. We follow the similar matchup strategy as in WP1. Specifically, the 3x3 pixel retrieval results are averaged. Figure 4-1 shows the schematic diagram of the validation of 3x3 POLDER pixels over AERONET sites. We select the pure land or ocean pixels' retrievals within the 3x3 window that satisfy the filter scheme ("Validation Pixels") to validate against AERONET measurements. The AERONET direct-sun AOD, AE, SDA AODF and AODC data are averaged within ±60 minutes of the POLDER overpass, while AERONET inverted SSA and AAOD (which have a lower sampling frequency) are averaged within ±180 minutes. The strategies to select the retrieval product with highest quality to perform AERONET validation are using "Residual Relative" for GRASP and "Chi2" for SRON, which are the errors in fitting the measurements by the algorithms. The thresholds are the "relative residual" smaller than minimal+3% and 10% for GRASP over land and ocean, and the "Chi2" smaller than 5 for SRON over land and ocean. The filter is applied before 3x3 retrieval aggregation.

In order to select the optimal methods to process real measurements, we perform the retrievals using 2 SRON methods (RemoTAP/3modes and RemoTAP/5modes) and 2 GRASP methods (GRASP/LN5Bins and GRASP/Component). Based on the performance of AERONET validation, the methods used for further processing will be selected. Figure 4-2 shows the validation of 2 SRON methods (RemoTAP/3modes and RemoTAP/5modes) and 2 GRASP methods (GRASP/LN5Bins and GRASP/Component) AOD at 550 nm over land with AERONET. In comparison with the validation of current products in WP1 (Figure 2-1), we observed significant improvement from both SRON and GRASP sides. For SRON/RemoTAP, the bias of low AOD decreases from ~+0.07 (WP1) to ~+0.02, meanwhile the GCOS fraction improves from ~32% to ~52%. From the GRASP side, the improvement is mainly for the LN5Bins approach that the bias decreases to ~+0.01, which is previously of non-negligible positive bias (+0.06). In addition, we processed with a newly developed method GRASP/Component (Li et al., 2019) that shows overall stable and encouraging performance. Notably, SRON/RemoTAP and GRASP algorithms obtained quite similar results for AOD over AERONET. Besides, we plot the validation metrics over spatial distributed AERONET sites in Figure 4-3. The AOD validation is conducted over all sites that have at least 10 matchup points in 2008, and the circle size indicates the number of points used to generate the statistics. Overall, the tendency is similar between SRON and GRASP algorithms, for example, we obtained good correlation coefficients over Africa, Europe and East Asia, while over Australia all retrievals seem to have slightly weaker correlation than over other continents. The observed biases are reversed over central Africa, where SRON tends to overestimate a bit while GRASP tends to underestimate slightly.

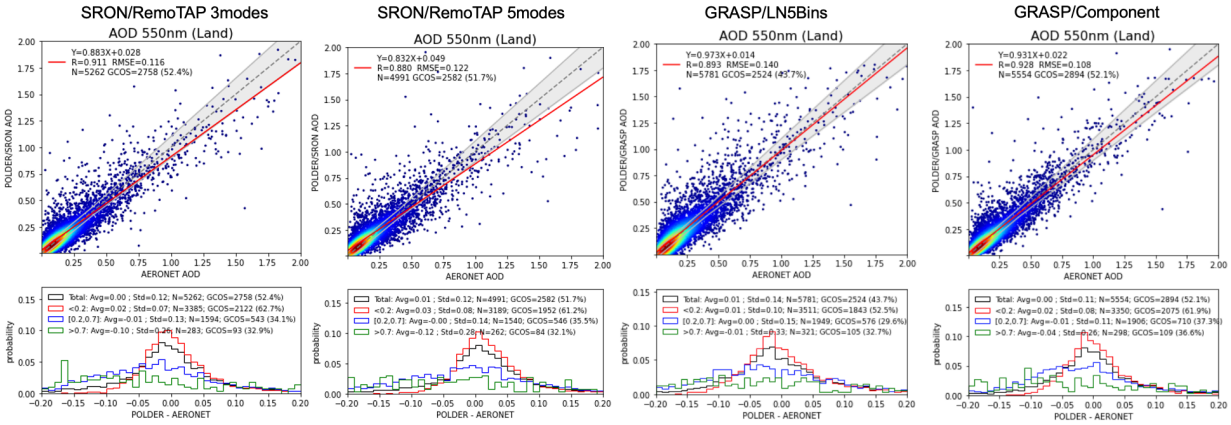

Figure 4-2. Validation of 2 SRON methods (RemoTAP/3modes and RemoTAP/5modes) and 2 GRASP methods (GRASP/LN5Bins and GRASP/Component) AOD at 550 nm over land with AERONET.

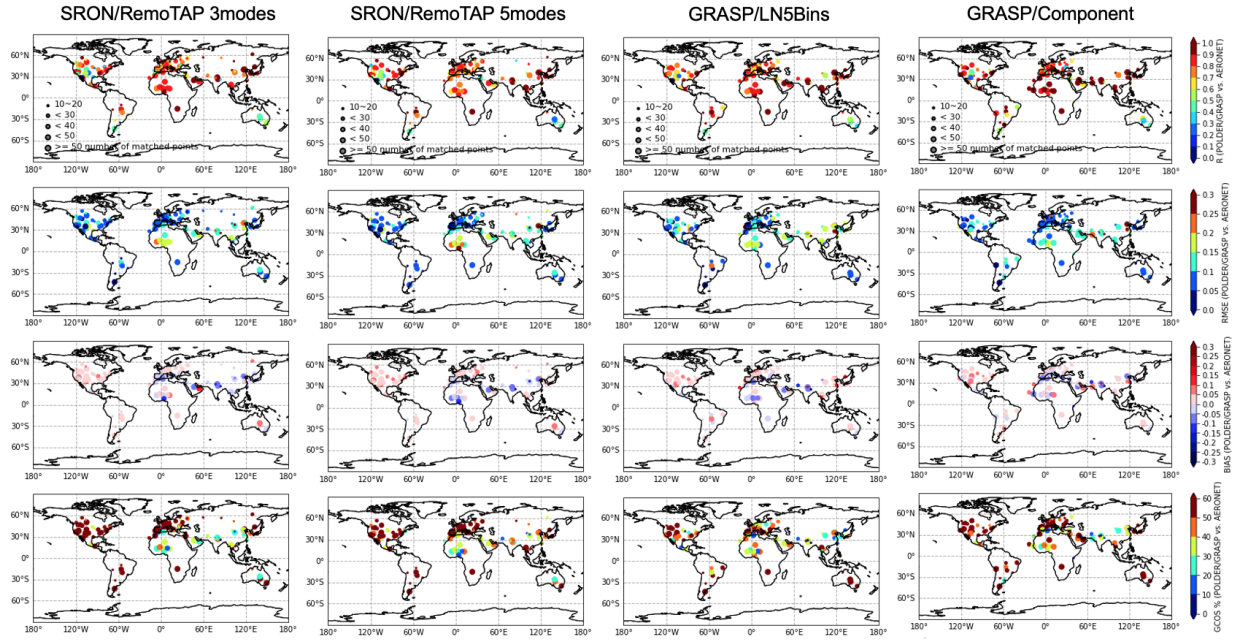

Figure 4-3. Maps showing statistical metrics (R, RMSE, BIAS and GCOS) for the AOD (550 nm) products of 2 SRON methods (RemoTAP/3modes and RemoTAP/5modes) and 2 GRASP methods (GRASP/LN5Bins and GRASP/Component).

In addition to AOD, we also observe the improvements with respect to the WP1 for more detailed properties, such as AExp in Figure 4-4 and SSA in Figure 4-5. We follow the same validation strategy as Chen et al. (2020) that we require POLDER AOD (550 nm) higher than 0.2 for AExp validation and POLDER AOD (550 nm) higher than 0.3 for SSA validation. Even though we see the results of AExp and SSA are dependent on the methods used. Both SRON/RemoTAP 3modes and 5modes overestimate AExp for coarse particles especially for 5modes, and GRASP/LN5Bins underestimates AExp for small particles. GRASP/Components obtained overall the optimal AExp. For SSA at mid-visible, SRON/RemoTAP 3modes and 5modes show very good performance;

GRASP/Components, SRON/RemoTAP 3modes and 5modes show overall similar statistics that RMSE around 0.035 and fractions within confidence region (+/- 0.03) around 66%.

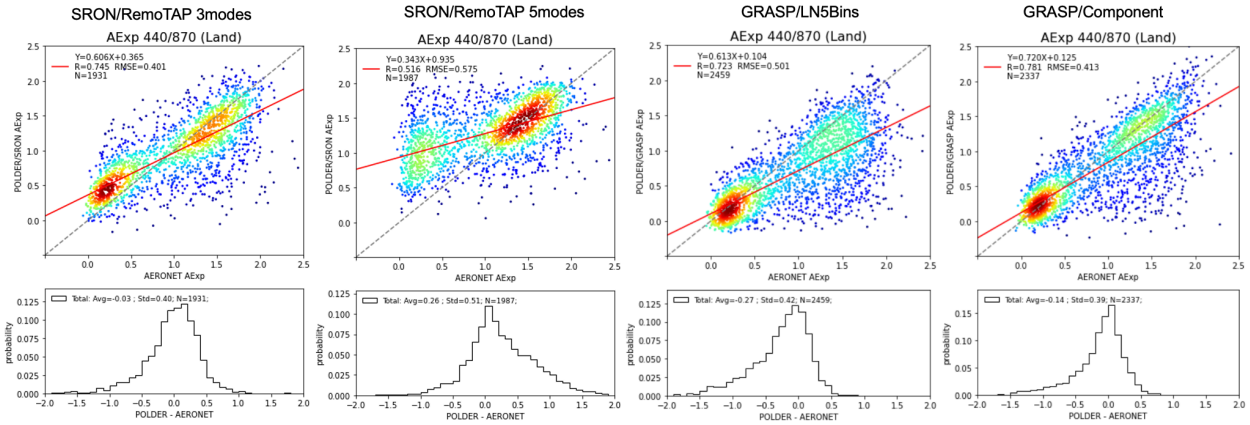

Figure 4-4. Validation of 2 SRON methods (SRON/RemoTAP/3modes and SRON/RemoTAP/5modes) and 3 GRASP methods (GRASP/LN5Bins and GRASP/Component) AExp (440/870) over land with AERONET.

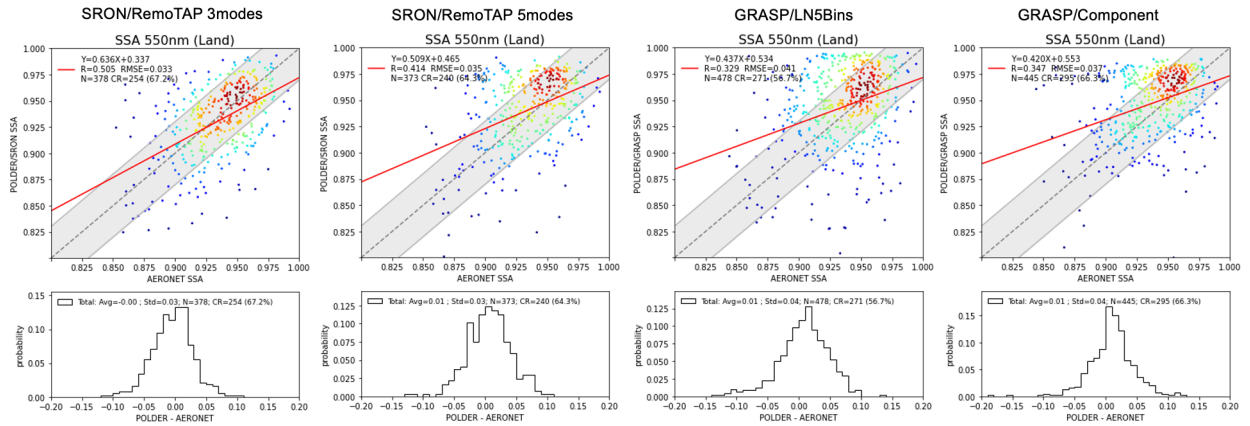

Figure 4-5. Validation of 2 SRON methods (SRON/RemoTAP/3modes and SRON/RemoTAP/5modes) and 3 GRASP methods (GRASP/LN5Bins, GRASP/Component and GRASP/Models) SSA (550 nm) over land with AERONET.

The 2 GRASP approaches (GRASP/LN5Bins and GRASP/Component) use the same LN5Bins size distribution, while GRASP/Component approach adopts prescribed spectral complex refractive index for aerosol components which reduces the number of directly retrieved parameters. Meanwhile, both synthetic tests and the validation over AERONET stations show overall better and more balanced performance of the derived spectral AOD, AE and SSA from GRASP/Component approach. In addition, the GRASP/Component approach can provide information of columnar concentration and complex refractive index separately for fine and coarse modes of aerosol. Therefore the GRASP/Component approach is selected for the further tests and global processing.

For the selection of the best SRON/RemoTAP setup, we base it on the comparison to AERONET for AOD, SSA, and AE. For the final selection, we incorporated all SRON/RemoTAP algorithm improvements listed in the previous subsection to both the 3-mode and 5-mode

retrievals. For all properties the RemoTAP/3-mode outperforms the RemoTAP/5-mode retrievals. For AOD the improvement of the 3-mode retrieval is only marginal (0.006 in RMSE). For SSA, RMSE is similar but the 3-mode retrievals have no bias while 5-mode retrievals have an 0.01 bias. The largest difference between the 3-mode and 5-mode retrievals we found for AE, where the 3-modes has a clearly better RMSE (0.40 vs 0.58) and the overestimation at small AE is significantly reduced.

In the following, we will continue to perform intercomparison of the results of these 2 selected approaches. In order to make the comparison sophisticated, we firstly select the common pixels that satisfy the filtering used for both RemoTAP/3modes and GRASP/Component then validate and compare these pixels over land and ocean. Figures 4-6 - 4-12 show the RemoTAP/3modes and GRASP/Component validation results of AOD, AExp, AODF, AODC and SSA for common pixels over land and ocean. The summary of SRON RemoTAP/3modes and GRASP/Component validation metrics for common pixels of AOD, AExp, AODF, AODC and SSA over land and ocean are present in Tables 4-1 - 4-4. Overall, the performance of 2 approaches is very close. Specifically, GRASP/Component tends to slightly obtain better Angstrom Exponent and separation of fine/coarse mode AOD, and RemoTAP/3modes obtain slightly better SSA.

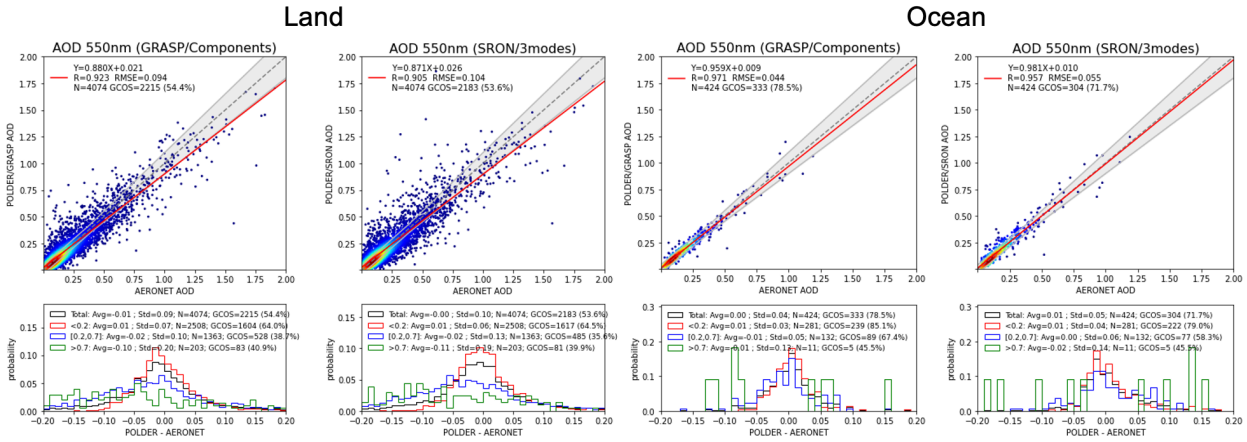

Figure 4-6. Validation of RemoTAP/3modes and GRASP/Component AOD at 550 nm over land and ocean with AERONET for common pixels that pass the GRASP residual and SRON Chi2 filter.

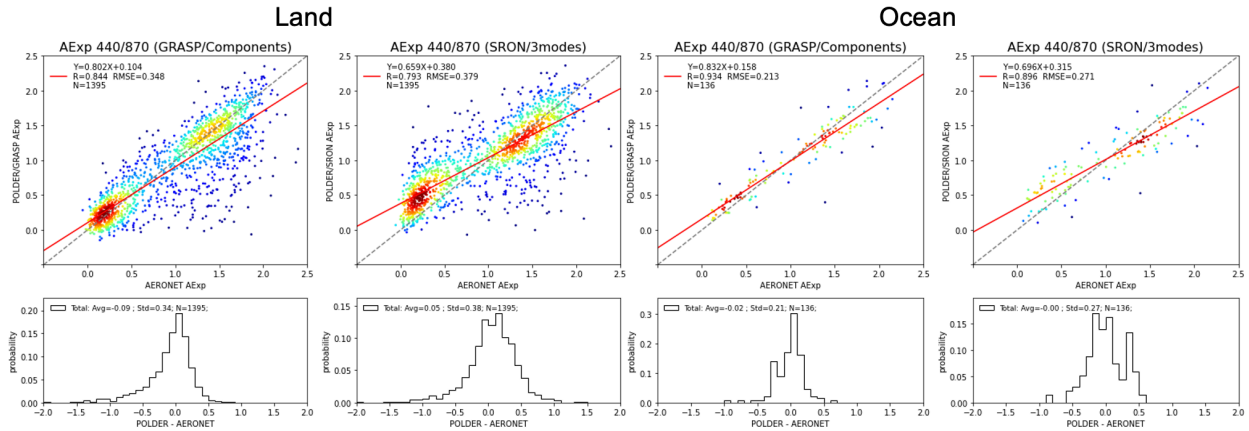

Figure 4-7. The same as Figure 4-6, but for AExp (440/870).

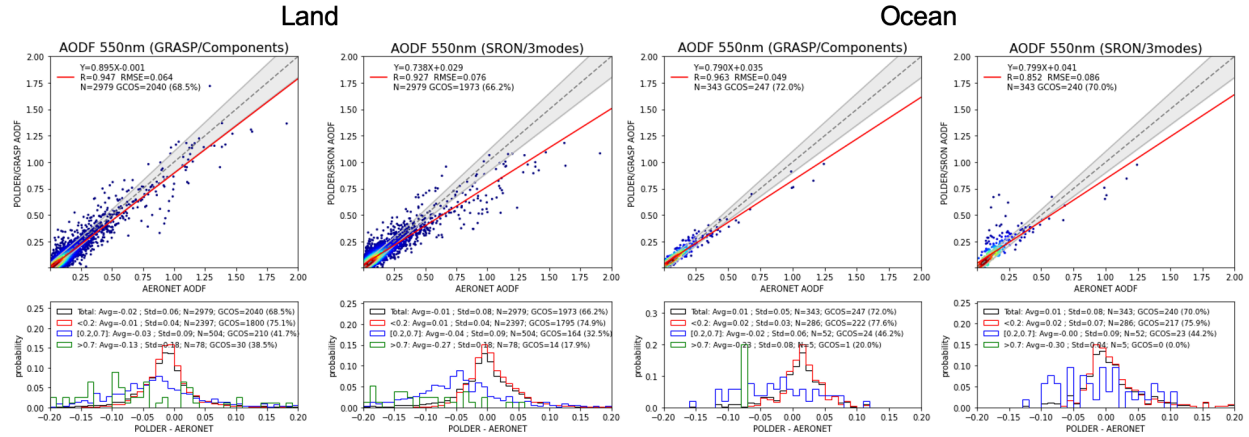

Figure 4-8. The same as Figure 4-6, but for AODF (550 nm).

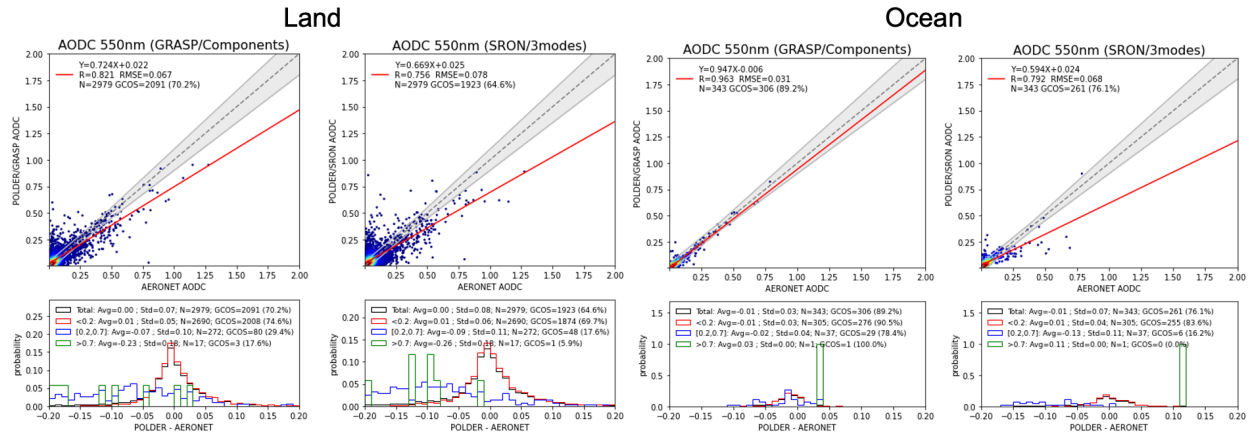

Figure 4-9. The same as Figure 4-6, but for AODF (550 nm).

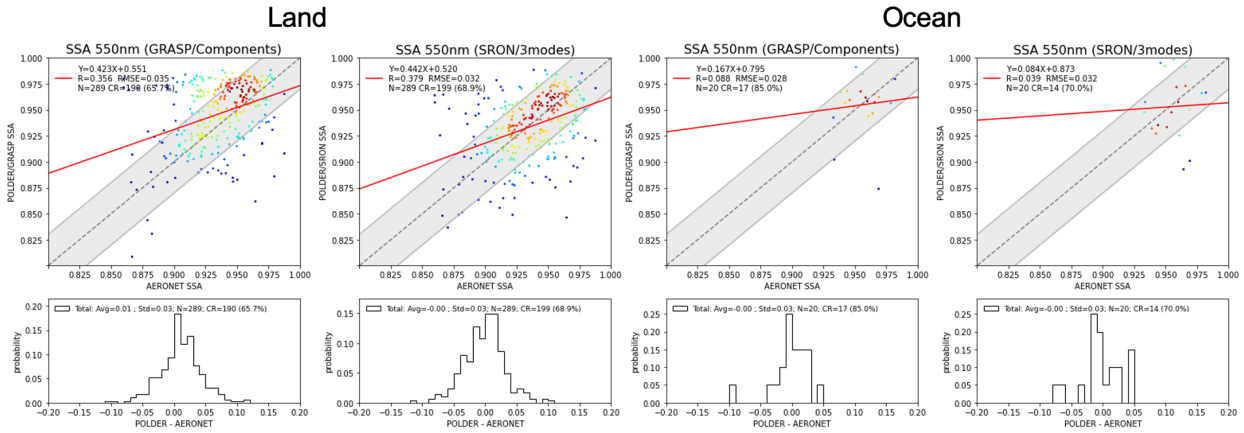

Figure 4-10. The same as Figure 4-6, but for SSA (550 nm).

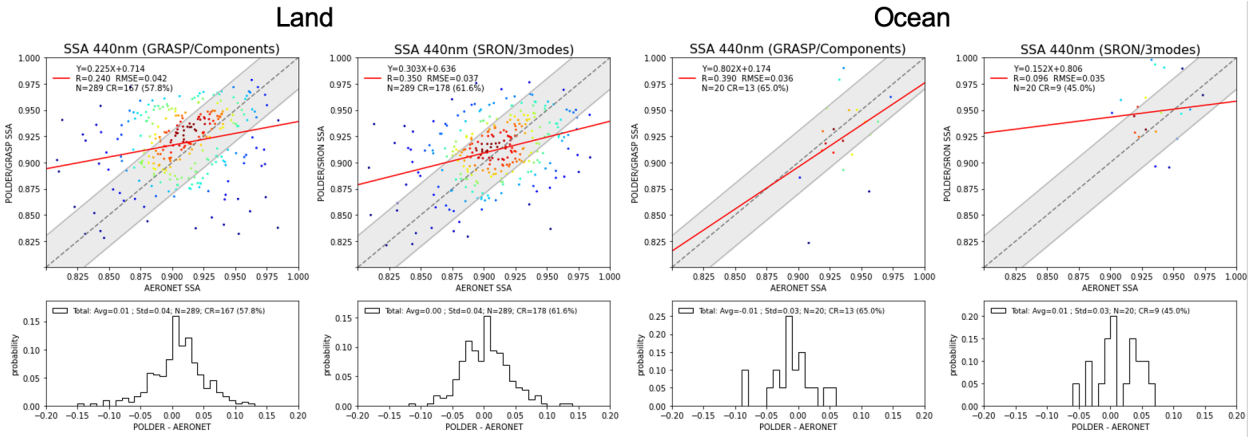

Figure 4-11. The same as Figure 4-10, but for SSA (440 nm).

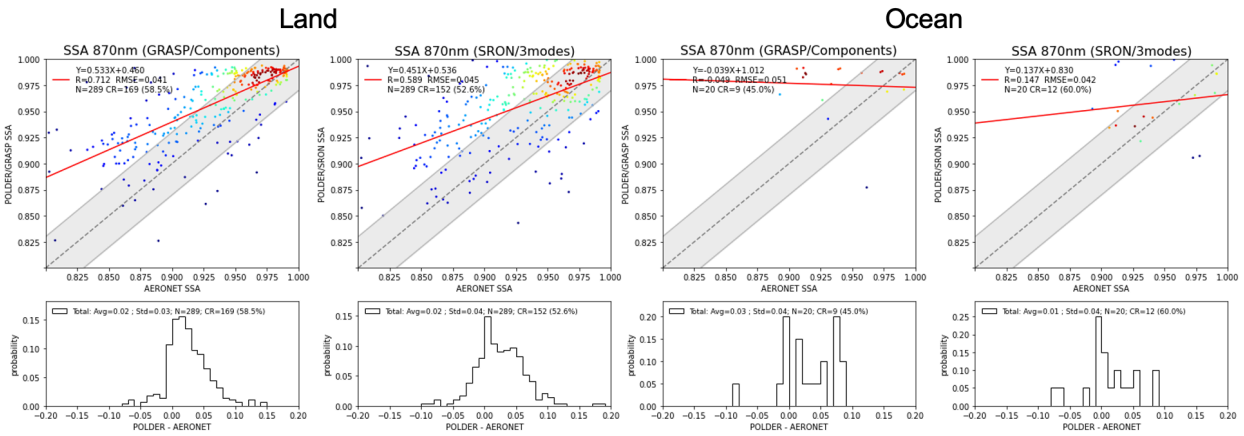

Figure 4-12. The same as Figure 4-10, but for SSA (870 nm).

Table 4-1: Summary of SRON RemoTAP/3modes and GRASP/Component spectral AOD (443, 550 and 865 nm) common pixel validation metrics over land and ocean. In brackets, the corresponding statistics obtained from WP1 are listed, and we use the GRASP/HP results from WP1.

Land/ Ocean	Band (nm)	Products	R	Slope	Offset	RMSE	GCOS (%)	MAE	BIAS	Bias (AOD<0.2)	Bias (0.2<=AOD<=0.7)	Bias (AOD>0.7)
Land	443	SRON/3modes	0.915 (0.831)	0.869 (0.802)	0.035 (0.118)	0.121 (0.210)	46.9 (30.0)	0.075 (0.135)	0.00 (0.04)	0.02 (0.08)	-0.01 (0.05)	-0.09 (-0.10)
		GRASP/Components	0.932 (0.897)	0.871 (0.914)	0.017 (0.081)	0.110 (0.187)	47.9 (31.8)	0.071 (0.117)	-0.02 (0.05)	0.00 (0.06)	-0.03 (0.06)	-0.11 (-0.01)
	550	SRON/3modes	0.905 (0.828)	0.871 (0.783)	0.026 (0.092)	0.104 (0.181)	53.6 (32.8)	0.064 (0.116)	0.00 (0.02)	0.01 (0.07)	-0.02 (0.01)	-0.11 (-0.14)
		GRASP/Components	0.923 (0.894)	0.880 (0.928)	0.021 (0.071)	0.094 (0.164)	54.4 (34.3)	0.059 (0.103)	-0.01 (0.05)	0.01 (0.06)	-0.02 (0.05)	-0.10 (-0.01)
	865	SRON/3modes	0.870 (0.806)	0.824 (0.651)	0.022 (0.062)	0.093 (0.161)	59.7 (35.9)	0.055 (0.105)	-0.01 (0.02)	0.01 (0.04)	-0.04 (-0.07)	-0.14 (-0.30)
		GRASP/Components	0.894 (0.875)	0.800 (0.926)	0.032 (0.065)	0.083 (0.141)	62.5 (38.8)	0.050 (0.088)	0.00 (0.05)	0.02 (0.06)	-0.03 (0.06)	-0.20 (-0.06)
Ocean	443	SRON/3modes	0.958 (0.833)	0.876 (0.833)	0.022 (0.079)	0.074 (0.142)	64.1 (36.9)	0.047 (0.087)	-0.01 (0.04)	0.00 (0.04)	-0.01 (0.05)	-0.12 (-0.13)
		GRASP/Components	0.962 (0.880)	0.851 (1.001)	0.024 (0.071)	0.073 (0.144)	67.3 (31.5)	0.045 (0.100)	-0.01 (0.07)	0.01 (0.06)	-0.03 (0.09)	-0.13 (0.02)
	550	SRON/3modes	0.957 (0.819)	0.981 (0.846)	0.010 (0.067)	0.055 (0.122)	71.7 (46.1)	0.037 (0.070)	0.01 (0.04)	0.01 (0.03)	0.00 (0.06)	-0.02 (-0.23)
		GRASP/Components	0.971 (0.891)	0.959 (1.047)	0.009 (0.059)	0.044 (0.127)	78.5 (52.4)	0.029 (0.089)	0.00 (0.07)	0.01 (0.06)	-0.01 (0.09)	-0.01 (0.04)
	865	SRON/3modes	0.938 (0.776)	0.906 (0.756)	0.016 (0.053)	0.046 (0.099)	77.6 (60.6)	0.029 (0.049)	0.00 (0.02)	0.01 (0.02)	-0.02 (0.05)	-0.09 (-0.54)
		GRASP/Components	0.968 (0.905)	0.962 (1.124)	0.000 (0.046)	0.034 (0.111)	87.5 (38.7)	0.021 (0.077)	0.00 (0.07)	0.00 (0.05)	-0.02 (0.10)	0.01 (0.11)

Table 4-2: Summary of SRON RemoTAP/3modes and GRASP/Component AExp (443/865) common pixel validation metrics over land and ocean. In brackets, the corresponding statistics obtained from WP1 are listed, and we use the GRASP/HP results from WP1.

Land/ Ocean	Band (nm)	Products	R	Slope	Offset	RMSE	MAE	BIAS
Land	443-865	SRON/3modes	0.793 (0.508)	0.659 (0.426)	0.380 (0.818)	0.379 (0.630)	0.283 (0.504)	0.05 (0.30)
		GRASP/Components	0.844 (0.817)	0.802 (0.657)	0.104 (0.173)	0.348 (0.382)	0.237 (0.284)	-0.09 (-0.16)
Ocean	443-865	SRON/3modes	0.896 (0.893)	0.696 (0.742)	0.315 (0.211)	0.271 (0.270)	0.216 (0.211)	0.00 (-0.06)
		GRASP/Components	0.934 (0.889)	0.832 (0.625)	0.158 (0.154)	0.213 (0.390)	0.150 (0.288)	-0.02 (-0.22)

Table 4-3: Summary of SRON RemoTAP/3modes and GRASP/Component AODF and AODC (550 nm) common pixel validation metrics over land and ocean. In brackets, the corresponding statistics obtained from WP1 are listed, and we use the GRASP/HP results from WP1.

Land/ Ocean	Band (nm)	Products	R	Slope	Offset	RMSE	GCOS (%)	MAE	BIAS	Bias (AODf/c<0.2)	Bias (0.2<=AODf/c<=0.7)	Bias (AODf/c>0.7)
Land	AODF 550	SRON/3modes	0.927 (0.759)	0.738 (0.688)	0.029 (0.079)	0.076 (0.153)	66.2 (42.0)	0.044 (0.089)	-0.01 (0.02)	0.01 (0.05)	-0.04 (-0.02)	-0.27 (-0.30)
		GRASP/Components	0.947 (0.911)	0.895 (0.840)	-0.001 (0.038)	0.064 (0.107)	68.5 (57.8)	0.040 (0.058)	-0.02 (0.01)	-0.01 (0.02)	-0.03 (0.00)	-0.13 (-0.16)
	AODC 550	SRON/3modes	0.756 (0.655)	0.669 (0.572)	0.025 (0.035)	0.078 (0.129)	64.6 (47.8)	0.047 (0.077)	0.00 (-0.01)	0.01 (0.02)	-0.09 (-0.17)	-0.26 (-0.36)
		GRASP/Components	0.821 (0.790)	0.724 (0.993)	0.022 (0.040)	0.070 (0.110)	70.2 (54.2)	0.040 (0.063)	0.00 (0.04)	0.01 (0.04)	-0.07 (0.00)	-0.23 (0.15)
Ocean	AODF 550	SRON/3modes	0.852 (0.775)	0.799 (0.842)	0.041 (0.055)	0.086 (0.097)	70.0 (58.2)	0.046 (0.059)	0.01 (0.04)	0.02 (0.04)	0.00 (0.01)	-0.30 (-0.27)
		GRASP/Components	0.963 (0.802)	0.790 (0.683)	0.035 (0.058)	0.049 (0.076)	72.0 (55.0)	0.033 (0.051)	0.01 (0.02)	0.02 (0.03)	-0.02 (-0.01)	-0.23 (-0.34)
	AODC 550	SRON/3modes	0.792 (0.849)	0.594 (0.861)	0.024 (0.012)	0.068 (0.050)	76.1 (74.3)	0.037 (0.033)	-0.01 (0.00)	0.01 (0.00)	-0.13 (-0.02)	0.11 (-0.04)
		GRASP/Components	0.963 (0.890)	0.947 (1.027)	-0.006 (0.037)	0.031 (0.078)	89.2 (54.7)	0.021 (0.052)	-0.01 (0.04)	-0.01 (0.04)	-0.02 (0.06)	0.03 (-0.10)

Table 4-4: Summary of SRON RemoTAP/3modes and GRASP/Component spectral SSA (443, 550 and 865 nm) common pixel validation metrics over land and ocean. In brackets, the corresponding statistics obtained from WP1 are listed, and we use the GRASP/HP results from WP1.

Land/ Ocean	Band (nm)	Products	R	Slope	Offset	RMSE	CR +/- 0.03 (%)	MAE	BIAS
Land	443	SRON/3modes	0.350 (0.583)	0.303 (0.659)	0.636 (0.345)	0.037 (0.054)	61.6 (39.7)	0.028 (0.044)	0.00 (0.04)
		GRASP/Components	0.240 (0.242)	0.225 (0.254)	0.714 (0.681)	0.042 (0.051)	57.8 (40.7)	0.032 (0.041)	0.01 (0.00)
	550	SRON/3modes	0.379 (0.645)	0.442 (0.991)	0.520 (0.012)	0.032 (0.038)	68.9 (60.3)	0.025 (0.029)	0.00 (0.00)
		GRASP/Components	0.356 (0.327)	0.423 (0.507)	0.551 (0.436)	0.035 (0.054)	65.7 (50.1)	0.026 (0.040)	0.01 (-0.02)
	865	SRON/3modes	0.589 (0.678)	0.451 (0.801)	0.536 (0.178)	0.045 (0.051)	52.6 (55.1)	0.035 (0.037)	0.02 (-0.01)
		GRASP/Components	0.712 (0.634)	0.533 (0.760)	0.460 (0.197)	0.041 (0.056)	58.5 (50.2)	0.031 (0.041)	0.02 (-0.03)
Ocean	443	SRON/3modes	0.096 (0.433)	0.152 (0.638)	0.806 (0.360)	0.035 (0.038)	45.0 (54.5)	0.029 (0.032)	0.01 (0.02)
		GRASP/Components	0.390 (0.019)	0.802 (0.034)	0.174 (0.866)	0.036 (0.069)	65.0 (57.8)	0.027 (0.042)	-0.01 (-0.03)
	550	SRON/3modes	0.039 (0.543)	0.084 (1.277)	0.873 (-0.268)	0.032 (0.032)	70.0 (69.7)	0.025 (0.026)	0.00 (0.00)
		GRASP/Components	0.088 (0.094)	0.167 (0.269)	0.795 (0.651)	0.028 (0.075)	85.0 (51.6)	0.019 (0.047)	0.00 (-0.04)
	865	SRON/3modes	0.147 (0.703)	0.137 (1.216)	0.830 (-0.219)	0.042 (0.043)	60.0 (60.6)	0.032 (0.031)	0.01 (-0.01)
		GRASP/Components	-0.049 (0.580)	-0.039 (2.097)	1.012 (-1.120)	0.051 (0.084)	45.0 (39.1)	0.042 (0.056)	0.03 (-0.06)

Besides, we looked at the AERONET validation statistics for common pixels as function of regions for AOD, AODF, AODC, SSA at 550 nm and AExp (440/870) in Figures 4-13 - 4-15. In general, we observed many similarities of both algorithms. For example, the mean absolute errors (MAE) for AOD (550 nm) are relatively high over Asia, China and Sahara for both algorithms, while relatively low over Oceania, South and North America. The variations of RMSE and BIAS for AODF, AODC, AExp and SSA are quite similar for regions for 2 algorithms despite some differences in magnitude.

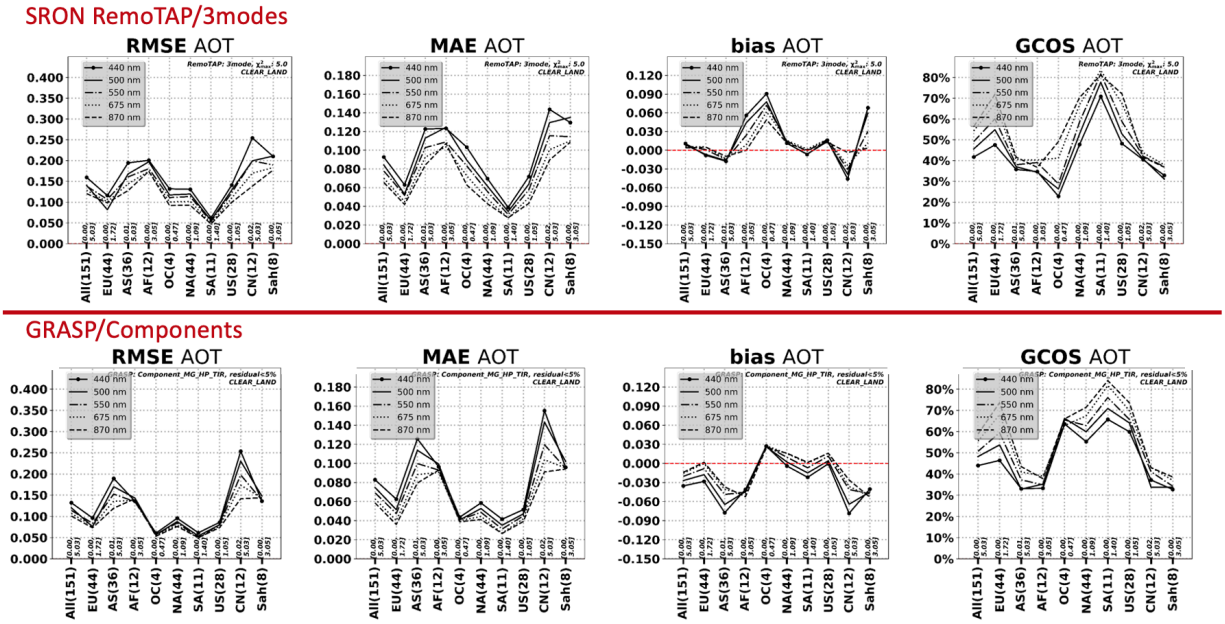

Figure 4-13: SRON RemoTAP/3modes and GRASP/Components AOD (550 nm) validation metrics for common pixels as function of regions.

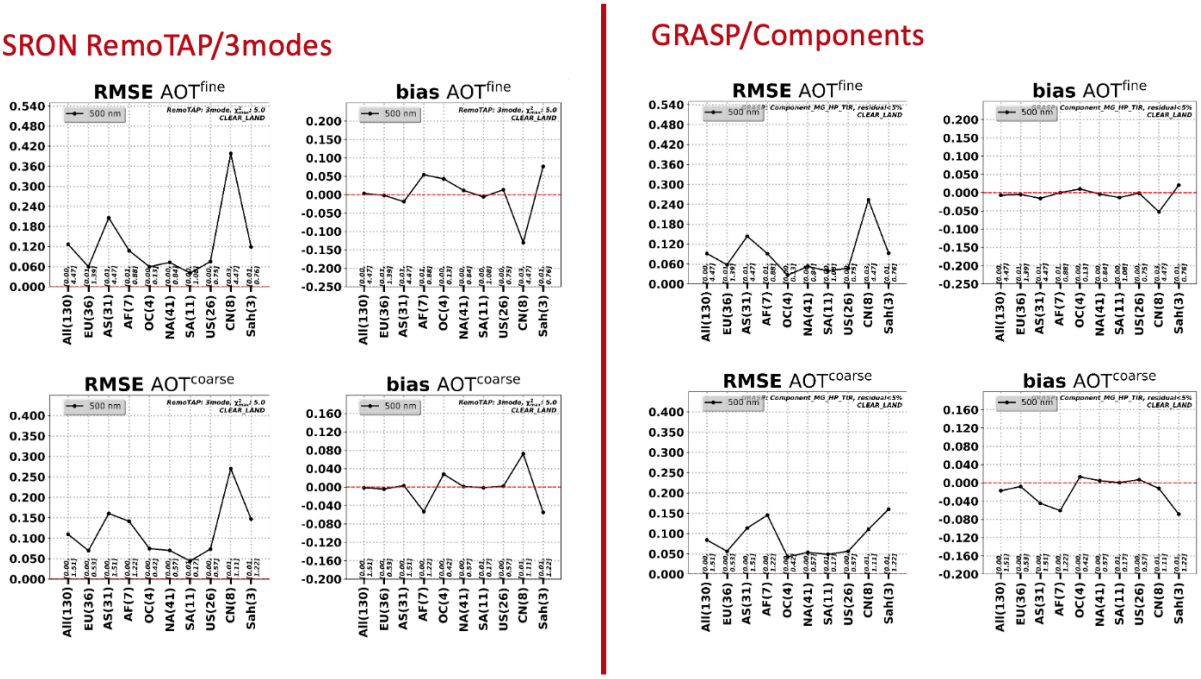

Figure 4-14: SRON RemoTAP/3modes and GRASP/Components AODF and AODC (550 nm) validation metrics for common pixels as function of regions.

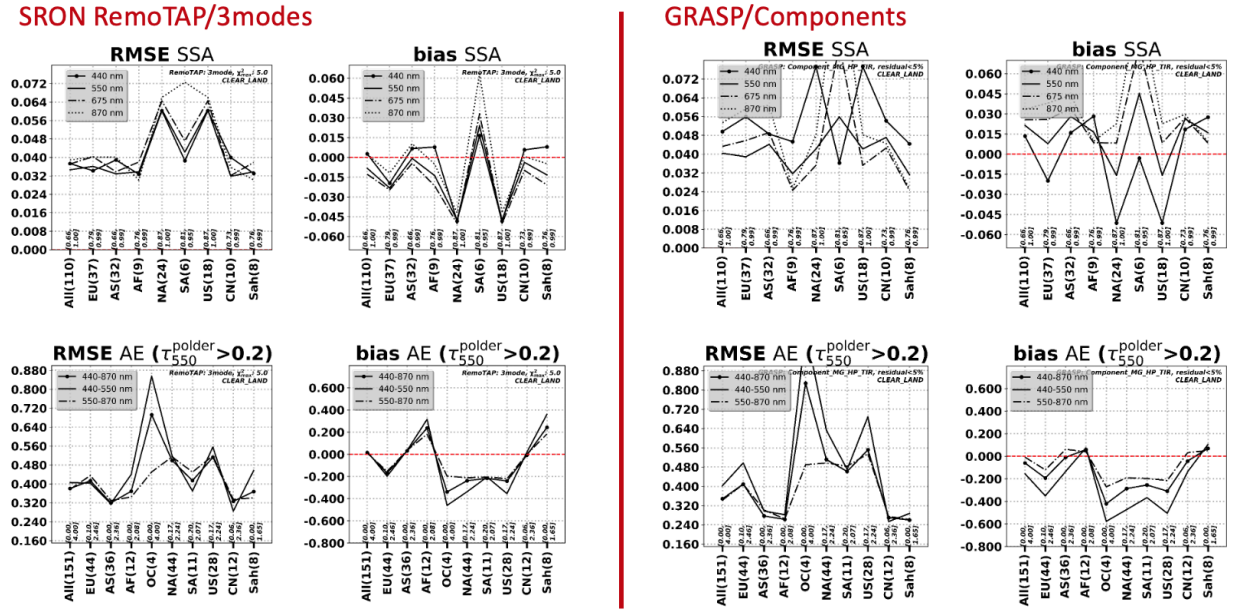

Figure 4-15: SRON RemoTAP/3modes and GRASP/Components SSA (550 nm) and AExp (440/870) validation metrics for common pixels as function of regions.

4.5 Intercomparison of regional processing

The processing of 3x3 pixels around AERONET stations has indicated improvement of agreement between SRON and GRASP with AERONET and with each other within this project. Before launching global processing, in WP3, we will process POLDER data over some specific regions. We select 7 tiles (each tile is about 600 x 600 km region) (Figure 4-16) that cover different surface types and typical aerosol conditions:

1. 138 (USA-Rocky Mountains) June-August, 2008
2. 227 (Banizoumbou) December 2007- February 2008
3. 349 (Mongu) June-August, 2008
4. 123 (Beijing) Sept.-November, 2008
5. 236 (India) March-May, 2008
6. 168.(Midway Island) Sept.-November, 2008
7. 400. (Australia) Jan – March 2008

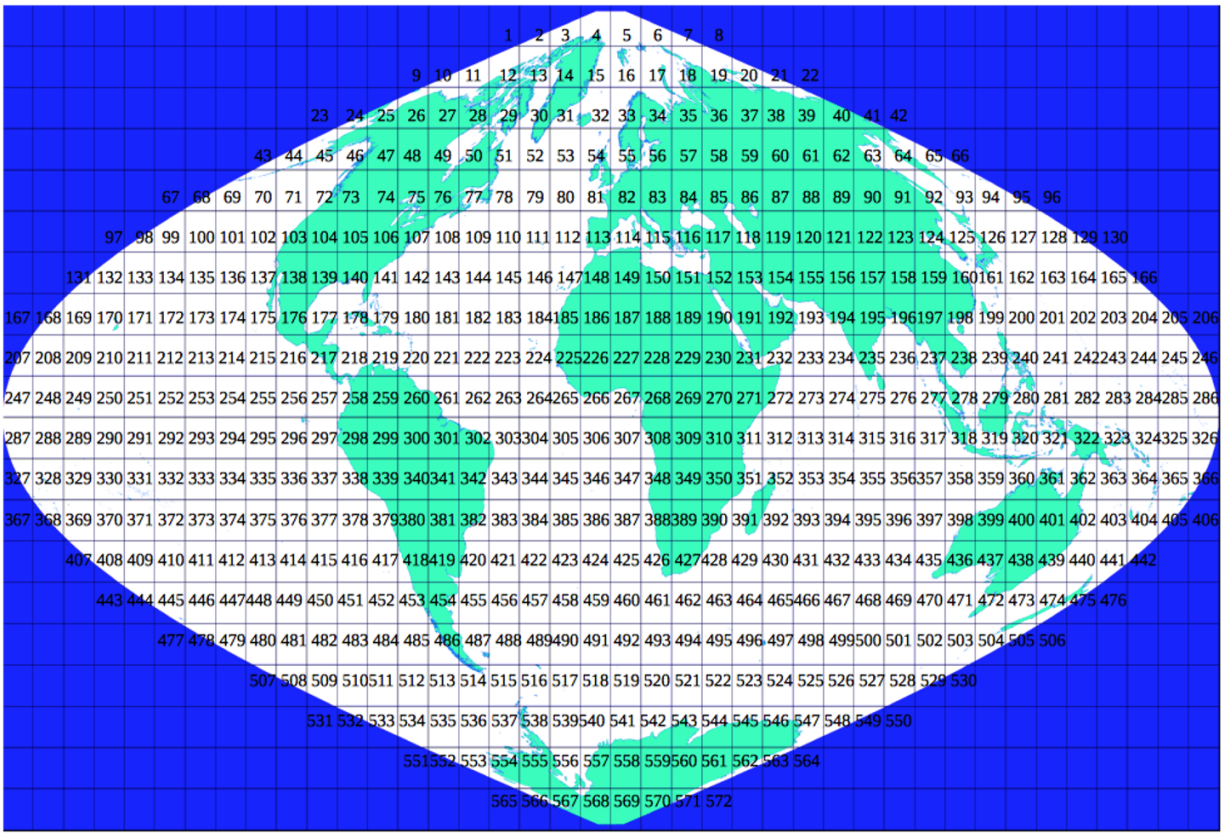

Figure 4-16: Spatial distribution of PARASOL tiles.

We process one season of each tile using the two selected methods RemoTAP/3modes and GRASP/Component. Then the results are intercompared. All tile-by-tile intercomparison results are shared in the project folder: https://drive.google.com/drive/u/1/folders/1sLnRons_KzWSiY8rGEz-M_ARdPZLdPkj. In this report we will focus on several key parameters (AOD 565 nm, AExp 443/865, and SSA 565 nm) to summarize the main features identified in the regional processing.

Figures 4-17 - 4-23 show the spatial distribution of seasonal GRASP/Component and RemoTAP/3modes AOD (565 nm), AExp (443/865), SSA (565 nm) and their differences averaged over a season between 2 methods for 7 selected Tiles respectively. Meanwhile, the pixel-to-pixel statistics between 2 methods for each tile as well as combined all 7 tiles are summarized in Table. 4-5 (AOD 565 nm), 4-6 (AExp 443/865) and 4-7 (SSA 565 nm).

Table 4-5. Summary of GRASP/Component and RemoTAP/3modes pixel-to-pixel statistics for AOD (565 nm) over 7 selected tiles.

TileID	Parameter	R	Slope	Offset	RMSE	Mean Diff. (SRON-GRASP)	GCOS (%)
123	AOD 565nm	0.937	0.942	-0.006	0.057	-0.015	67.5
138		0.571	0.795	0.049	0.106	0.029	48.5
168		0.902	0.957	0.004	0.037	-0.001	81.7
227		0.923	0.995	0.004	0.122	0.002	42.3
236		0.896	0.888	0.021	0.068	-0.012	55.2
349		0.964	0.815	0.036	0.069	-0.014	65.7
400		0.761	0.825	0.023	0.076	0.005	60.6
All		0.926	0.920	0.016	0.087	-0.003	57.7

Table 4-6. Summary of GRASP/Component and RemoTAP/3modes pixel-to-pixel statistics for AExp (443/865) when AOD (565 nm) > 0.2 over 7 selected tiles.

TileID	Parameter	R	Slope	Offset	RMSE	Mean Diff. (SRON-GRASP)	CR +/- 0.2 (%)
123	AExp (443/865)	0.717	0.684	0.338	0.301	-0.01	70.4
138		0.644	0.539	0.583	0.531	0.07	44.7
168		0.818	0.871	0.107	0.213	-0.02	86.8
227		0.745	0.882	0.200	0.288	0.13	74.8
236		0.601	0.631	0.459	0.257	0.04	78.2
349		0.590	0.748	0.414	0.231	-0.06	81.4
400		0.226	0.249	0.221	0.356	-0.04	68.5
All		0.902	0.840	0.222	0.272	0.03	76.9

Table 4-7. Summary of GRASP/Component and RemoTAP/3modes pixel-to-pixel statistics for SSA (565 nm) when AOD (565 nm) > 0.3 over 7 selected tiles.

TileID	Parameter	R	Slope	Offset	RMSE	Mean Diff. (SRON-GRASP)	CR +/- 0.03 (%)
123	SSA 565nm	0.200	0.294	0.659	0.040	-0.01	58.6
138		-0.042	-0.060	0.967	0.064	-0.02	42.5
168		0.208	0.130	0.864	0.050	0.03	47.8
227		0.733	0.489	0.464	0.038	-0.02	61.2
236		0.498	0.567	0.445	0.070	0.06	20.5
349		0.375	0.526	0.436	0.061	0.04	33.3
400		0.552	0.762	0.207	0.034	-0.02	66.6
All		0.663	0.507	0.456	0.053	0.01	45.2

We observe in general good agreement between 2 algorithms' AOD at mid-visible wavelength (565 nm). Based on all tiles > 3 millions pixels' statistics, the correlation coefficient R is around 0.92 with RMSE 0.087. The overall AOD (565 nm) difference (SRON-GRASP) is -0.003 and 57.7% pixels are within the GCOS requirement. For most of the tiles, we observe quite stable agreement that RMSE is smaller than 0.1, GCOS fraction higher than 50%, and the difference is within +/- 0.015. Meanwhile, we should note the AOD agreement varies from tile to tile. Tile 138 (USA-Rocky Mountains) shows the largest discrepancy with the (SRON-GRASP) difference about 0.029.

Since it's expected that the retrieval of AExp for low aerosol abundance is highly uncertain, we intercompare AExp for pixels where both algorithms report AOD (565 nm) higher than 0.2. The pixel-to-pixel statistics are presented in Table 4-6, and the spatial distribution is shown in Figures 4-17 - 4-23. In general, the statistics of AExp are generally not as good as that for AOD for tiles. This is probably due to the limited dynamic of AExp within a single tile. The pixel-to-pixel statistics for combined 7 tiles for ~1 million pixels indicates good agreement with R 0.90 and RMSE 0.272. Considering the accurate AExp retrieval confidence region (+/- 0.2), quantitatively ~76% pixels (AOD>0.2) satisfy the AExp requirement. For Tile 227 (Banizoumbou), where is dominant by coarse particles, RemoTAP/3modes tends to retrieve smaller particle size (higher AExp ~0.13) than GRASP/Component that agrees with our finding for AERONET validation. While it's not evident for other tiles, the overall 7 tiles difference of AExp (SRON-GRASP) is around 0.03.

For SSA at 565 nm, we present the results for AOD higher than 0.3, since the retrieval uncertainty of SSA is highly dependent on the aerosol loading. Even though the spatial pattern of SSA obtained from GRASP/Component and SRON RemoTAP/3modes are generally similar (Figures 4-17 - 4-23), the differences are evident. Based on 7 tiles ~1 million pixels intercomparison, the RMSE for SSA (565 nm) between 2 algorithms is 0.053, and the difference (SRON - GRASP) is 0.01. Meanwhile, 45.2% pixels are within the SSA confidence region (+/- 0.03). Besides, the difference (SRON - GRASP) can vary from -0.02 to +0.06. Particularly, for Tile 236 (Indian Ocean), we see clearly a huge difference (+0.06) that GRASP/Component retrieves stronger absorption than RemoTAP/3modes does. Even though both algorithms retrieve moderate AOD and smaller particles there, 55% pixels are within AOD GCOS requirement and 78% pixels satisfy AExp CR +/- 0.2. For Tile 168 (Midway Island), we also observe that GRASP/Component derives smaller (about 0.03) SSA than RemoTAP/3modes.

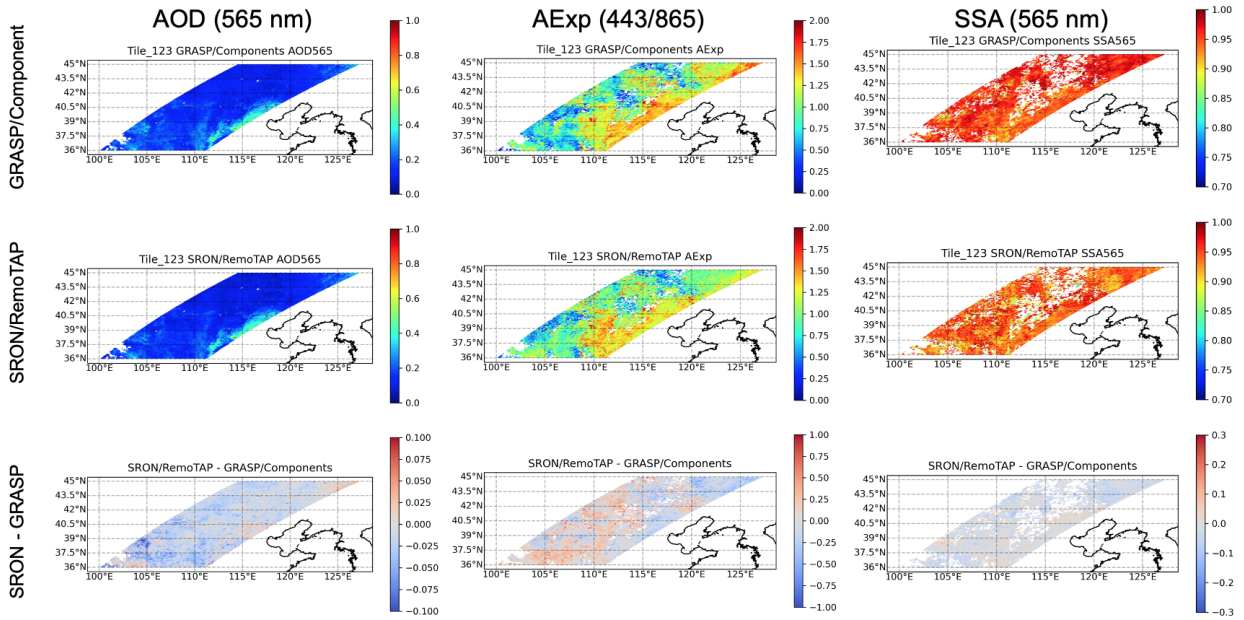

Figure 4-17. Spatial distribution of GRASP/Component and SRON RemoTAP/3modes AOD 565nm, AExp (443/865) and SSA 565nm for Tile 123 and the differences between 2 methods averaged over a season.

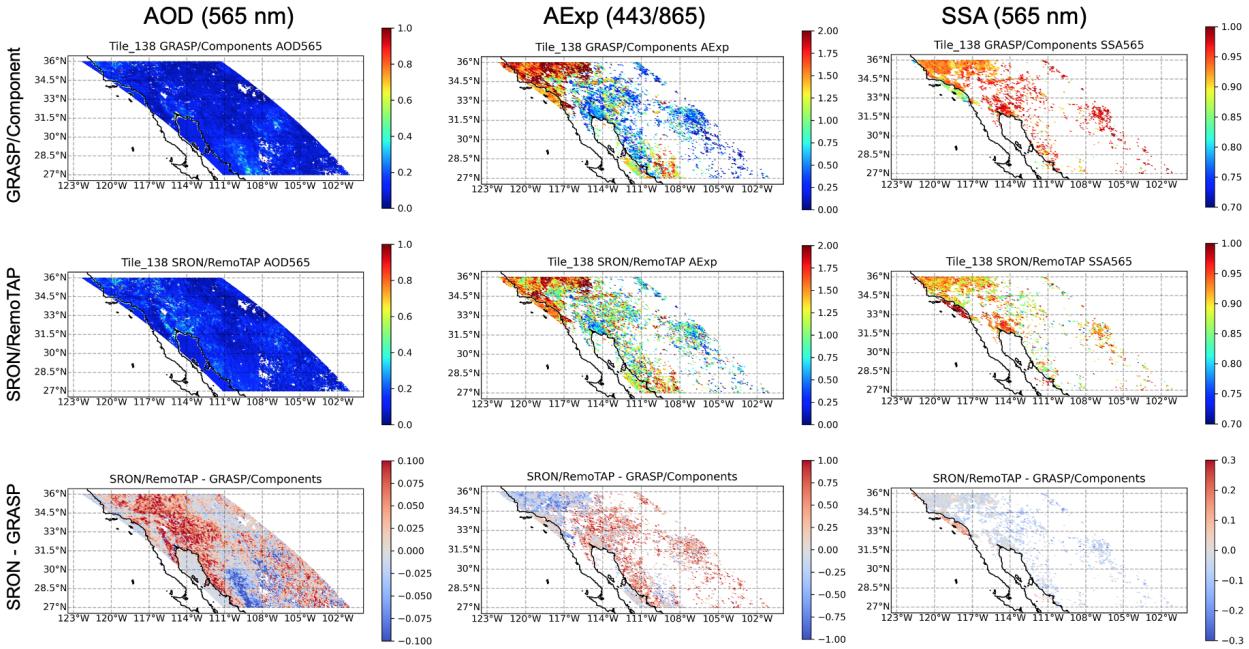

Figure 4-18. The same as Figure 4-17, but for Tile 138.

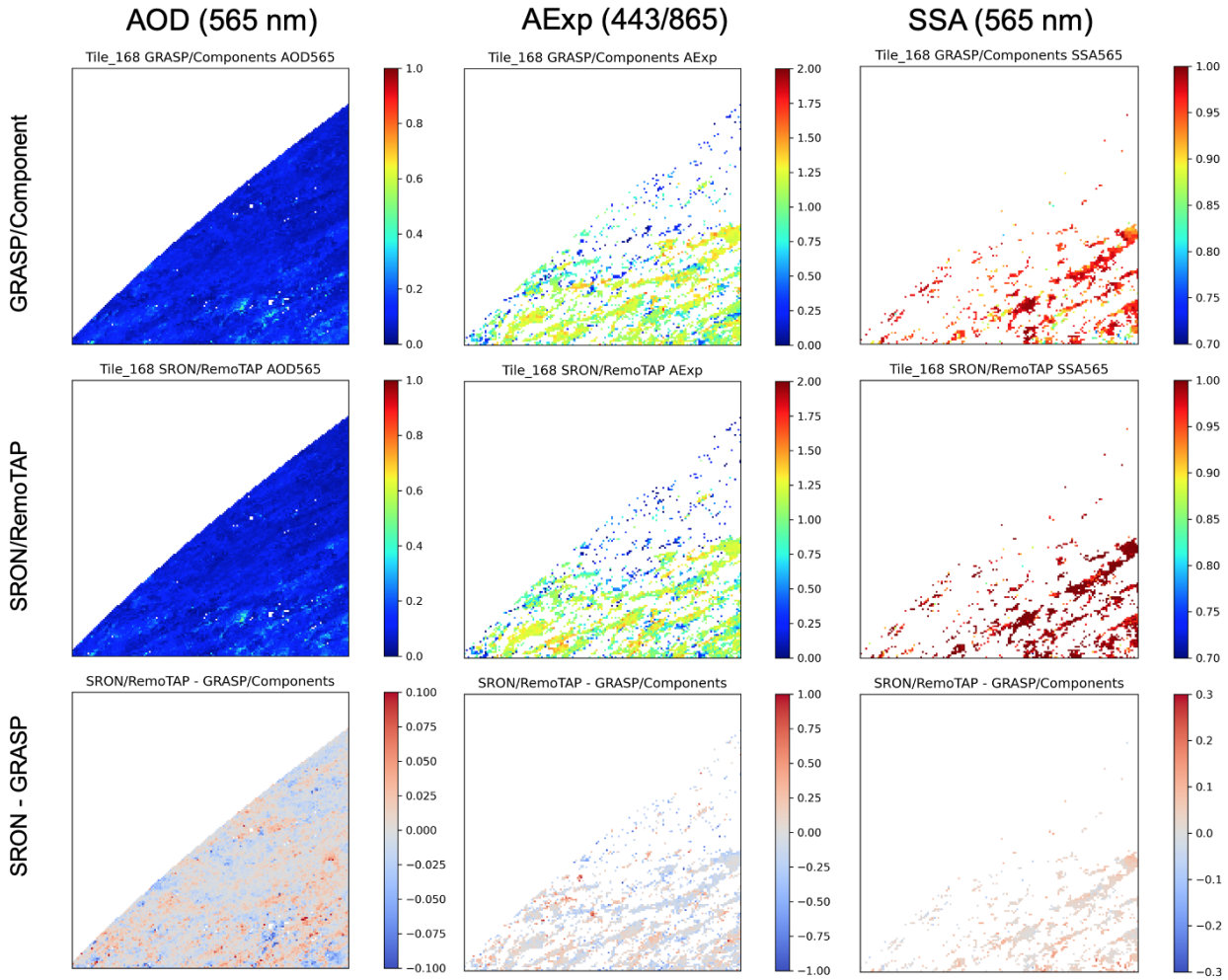

Figure 4-19. The same as Figure 4-17, but for Tile 168.

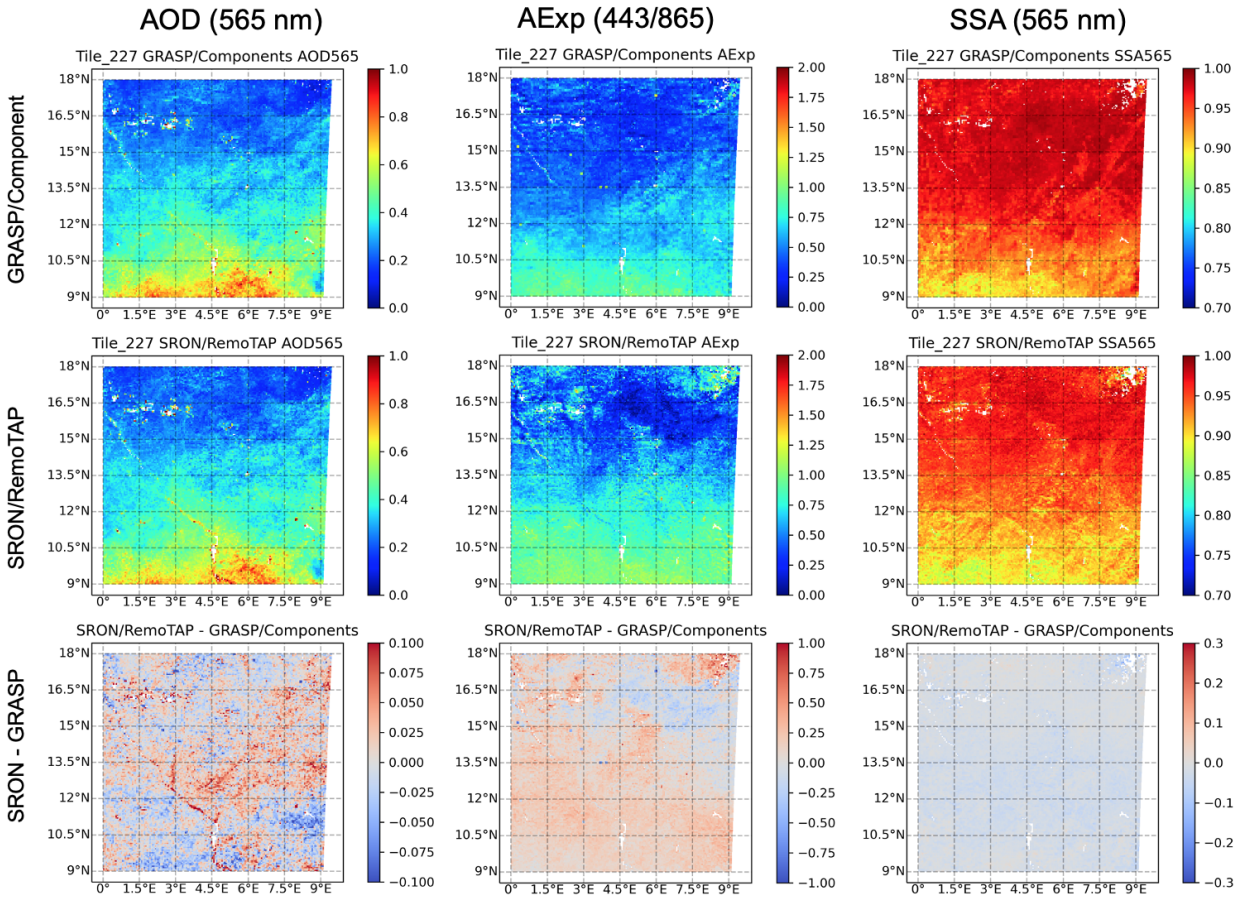

Figure 4-20. The same as Figure 4-17, but for Tile 227.

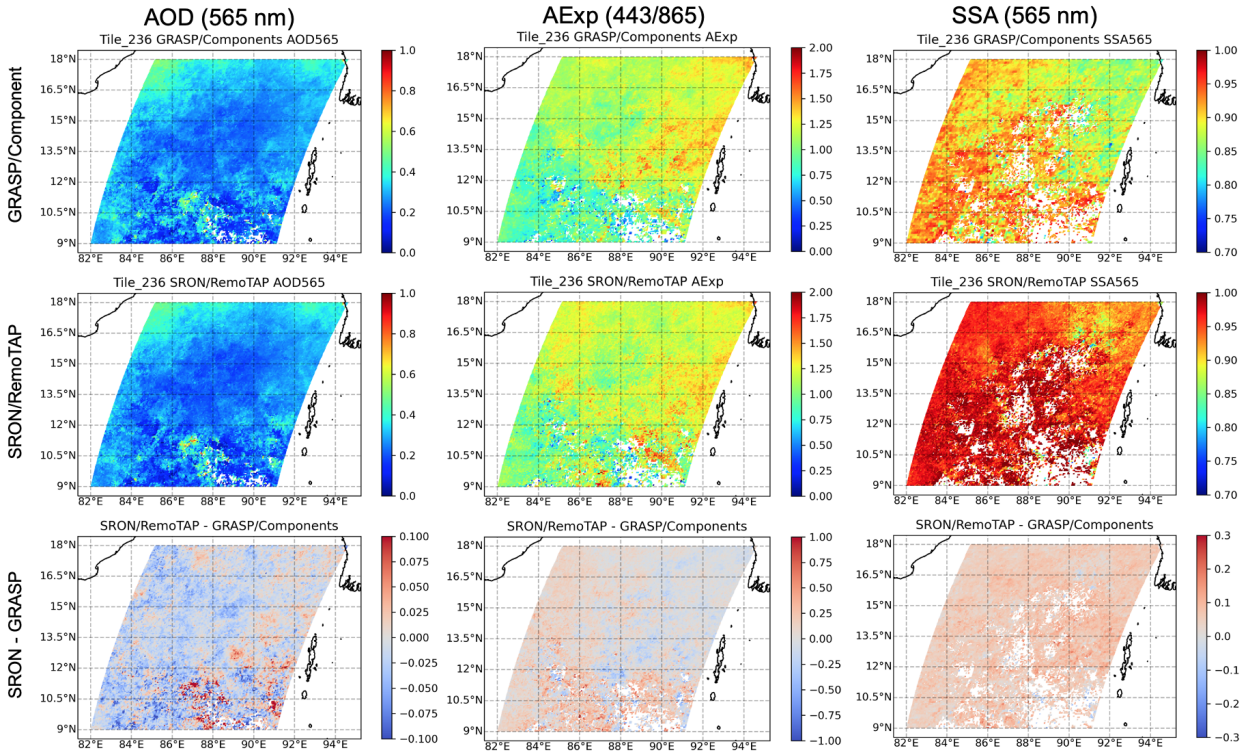

Figure 4-21. The same as Figure 4-17, but for Tile 236.

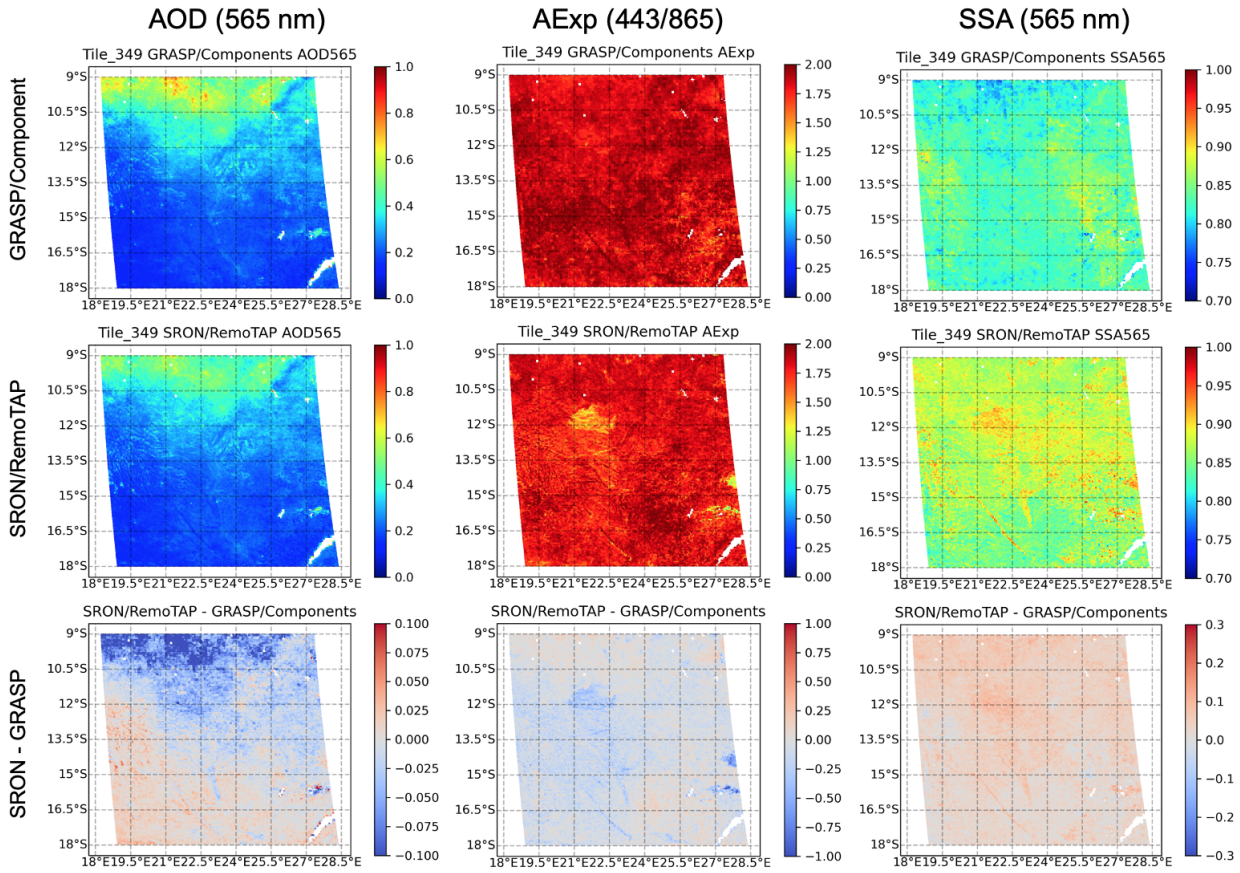

Figure 4-22. The same as Figure 4-17, but for Tile 349.

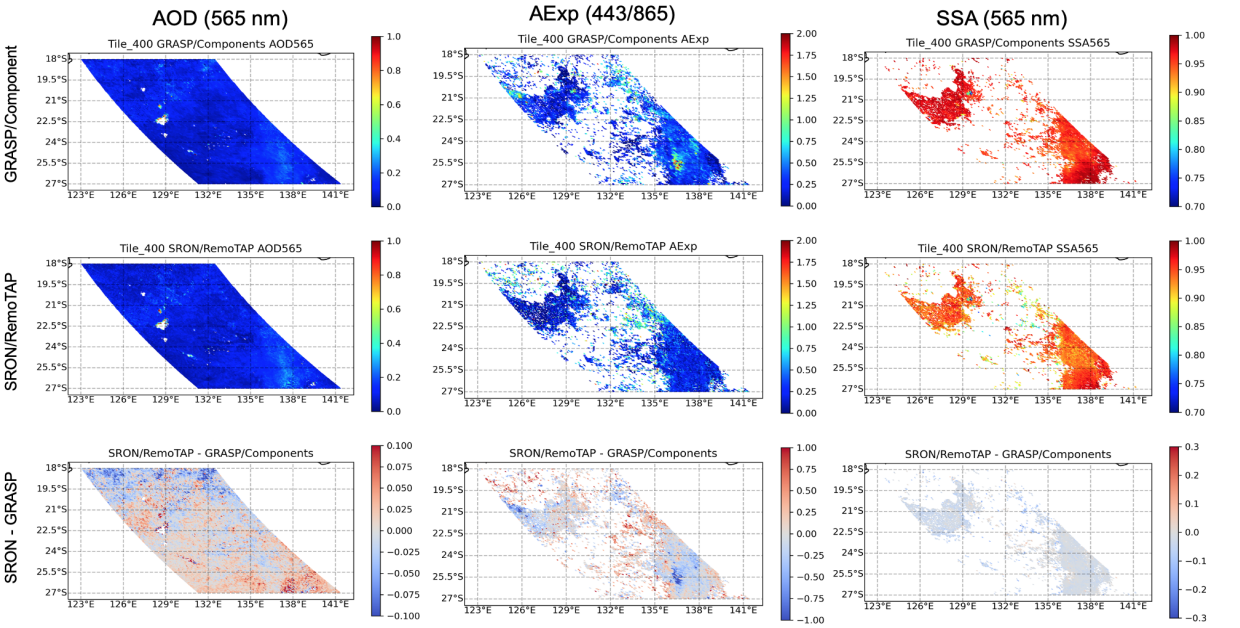

Figure 4-23. The same as Figure 4-17, but for Tile 400.

4.6 Conclusions

In WP3, we further optimized GRASP and SRON/RemoTAP algorithms and performed a detailed comparison of the optimized versions of GRASP and SRON/RemoTAP. The retrieval results are validated and intercompared over AERONET pixels as well as for 7 larger regions over the globe. Based on the harmonization and development within this project, we observed the agreement with AERONET improved significantly for both GRASP and SRON/RemoTAP. For SRON/RemoTAP, the bias of low AOD decreases from ~+0.07 (WP1) to ~+0.01, meanwhile the GCOS fraction improves from ~30% to ~53%. From the GRASP side, the improvement is mainly for the LN5Bins approach that the bias decreases to ~+0.01, which is previously of non-negligible positive bias (+0.06). In addition, we processed with a newly developed method GRASP/Component that shows overall stable and encouraging performance. Based on the AERONET validation, GRASP/Component and SRON RemoTAP/3modes approaches are selected from GRASP and SRON sides for further regional and global processings.

We validate the GRASP/Component and SRON RemoTAP/3modes retrievals with AERONET for pixels that pass the filter criteria for both algorithms. We obtained very similar results for AOD of 2 approaches: the GCOS fractions are ~53% over land and ~70% over ocean. GRASP/Component tends to slightly obtain better AE and separation of fine/coarse mode AOD, and RemoTAP/3modes obtains slightly better SSA. Overall, the performance of 2 approaches is very close in terms of AERONET validation and is significantly improved with respect to WP1. Given the variety in retrieval setups (state vector definition and different constraints) for both SRON/RemoTAP and GRASP, we do not foresee that further optimizations on these aspects will lead to significant improvements in comparison to AERONET for PARASOL retrievals. Evaluation of global retrievals may lead to new insights. Furthermore, an aspect that could be of importance is cloud filtering. This was not studied during HARPOL (as it would be a project on its own) but it is expected to affect the overall performance. Since comparison to AERONET already includes some implicit cloud filtering, the effect of improved cloud filtering would be primarily visible at a global scale.

The regional processing is done over 7 selected tiles (each tile is about 600 x 600 km region) that cover different surface types and aerosol types. The inter-comparison generally confirms the main findings obtained from AERONET retrievals. Nevertheless, we observe the agreement between 2 approaches can vary from region to region, and some issues are also identified. Based on overall more than 3 millions pixels intercomparison, a very good agreement is found for AOD (565 nm) with the pixel-level differences being within +/- 0.05 and the mean difference (SRON-GRASP) is around -0.003 and R is higher than 0.92 with RMSE around 0.087. However, the good agreement holds for most regions except for USA-Rocky Mountains, where the mean difference (SRON-GRASP) increases significantly to 0.029. The pixel-to-pixel intercomparison for AExp is also good with R 0.90, RMSE 0.272, and ~76% pixels satisfying the AExp confidence region +/- 0.2. The dispersion for SSA is large for some regions. Overall, the RMSE is around 0.053, and

~45% pixels are within the SSA +/- 0.03 confidence region. Even though the RMSE improved from WP1 0.07-0.08 to 0.05, it still implies non-negligible uncertainties in SSA retrievals.

5 WP4: Global processing using harmonized retrieval settings

In WP4 we performed global processing for the year 2008 (GRASP processed December 2007 – November 2008, SRON processed January-December 2008, so overlap for Jan-Nov 2008) using the optimized settings that have been finalized in WP3 (harmonization based on AERONET comparison). As found in WP3, for GRASP, the optimal setup corresponds to the 'Chemical Components' (CC) approach, which models the refractive index by using an internal mixture of different aerosol species and water, taking into account the relative humidity. The size distribution is described by 5 log-normal modes with fixed effective- radius and variance. For SRON/RemoTAP the optimal setup corresponds to the 3-mode approach, which describes aerosols by 3 size modes: (i) a fine mode, a coarse insoluble mode (representative for Dust) and a coarse soluble mode (representative for sea salt). For each mode the effective radius- and variance are fitted and the refractive index, described by the sum of a number of wavelength dependent function, representative for different aerosol types.

After global processing, the products have been gridded onto a 0.1 X 0.1 degrees grid to facilitate intercomparison. In this section, we first show a validation with AERONET for the global gridded products (to make sure they are consistent with the data sets processed in WP3 over AERONET sites). Next, we perform a global comparison of the SRON/RemoTAP and GRASP data sets for AOD, SSA, AE, fine- and coarse mode AOD, and retrieved surface properties. Finally, we perform a comparison of the SRPN/RemoTAP and GRASP AOD and AE products against the widely used products from MODIS.

5.1 AERONET validation of global data sets

Figure 5-1 shows the AERONET validation for the gridded global GRASP and SRON/RemoTAP products for AOD, AE, and SSA. The validation confirms our findings of WP3 (see section 4):

- For AOD both GRASP and SRON/RemoTAP show similar comparison against AERONET.
- For AE GRASP shows slightly better agreement with AERONET over land, while agreement is similar for both algorithms over ocean.
- For SSA SRON/RemoTAP shows slightly better agreement with AERONET over land, while over ocean there are not enough comparisons to draw a conclusion.

We would like to re-emphasize that the agreement with AERONET improved significantly compared to the original data sets of WP1. Also, the agreement with AERONET for AOD is at least similar (and probably better) than the agreement for MODIS products (Chen et al, 2020), which is considered typically as a reference for AOD. For AE and SSA the agreement with AERONET is, to our knowledge, better than shown by any other satellite instrument.

5.2 Comparison of global data sets

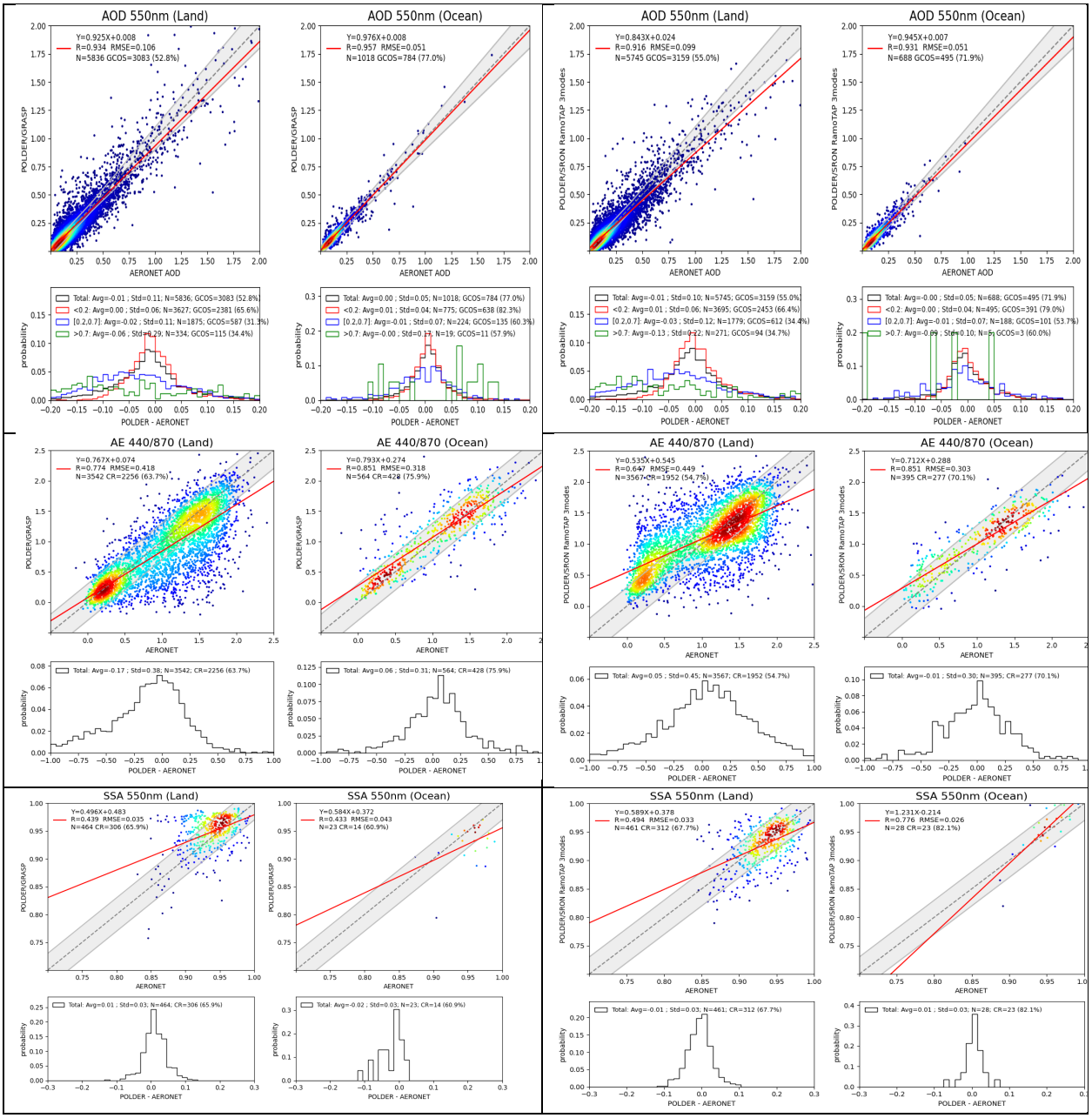

Figure 5-1: Comparison of global GRASP and SRON/RemoTAP products for AOD (upper row), Angstrom Exponent (middle row), and SSA (lower row). The 2 left columns show the comparison for GRASP products over land and ocean, respectively, and the 2 right columns show the comparison for SRON/RemoTAP.

5.2.1 Number of retrievals

Figure 5-2 show the number of retrievals for the year 2008 (Jan-Nov) for both GRASP and SRON/RemoTAP. For SRON/RemoTAP the number of valid retrievals increased significantly

compared to WP1, although in WP1 retrievals for 2006 were performed, but we expect roughly the same number of valid retrievals in each year. Despite the increase in valid RemoTAP retrievals, still there are less valid retrievals than for GRASP. The most likely explanation is that SRON/RemoTAP applies stricter filtering for clouds (RemoTAP uses MODIS, GRASP uses a PARASOL cloud mask) and goodness of fit (SRON/RemoTAP keeps retrievals with chi2 < 5, GRASP keeps retrievals with fit residual < minRes+3% over land and < minRes+10% over ocean). The largest difference in number of retrievals occurs over ocean.

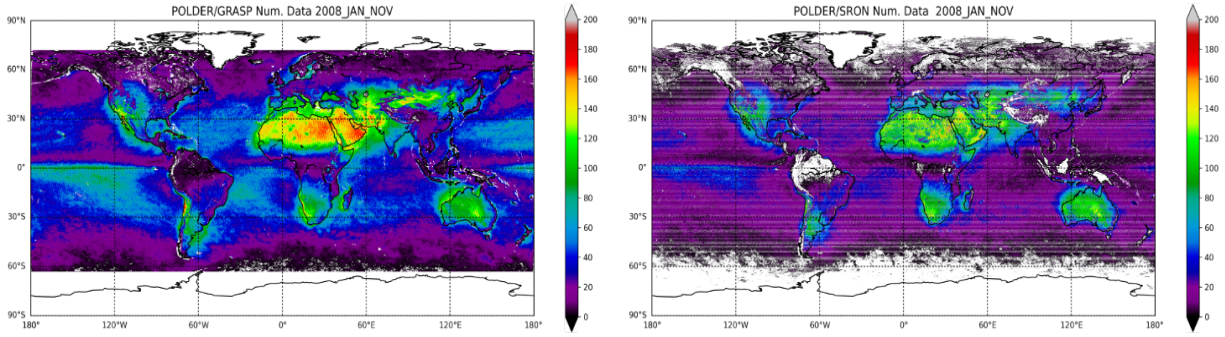

Figure 5-2: Number of valid retrievals for GRASP (left) and SRON RemoTAP (right)

5.2.2 Comparison of AOD

Figure 5-3 shows maps of the mean AOD for GRASP and SRON/RemoTAP and the map of the mean differences. Overall, GRASP and SRON/RemoTAP show the same AOD pattern with high AOD over the Sahara (Dust) and equatorial Africa (biomass burning) and the outflow of dust and biomass burning aerosol over the Atlantic ocean. Also, high AOD values are retrieved over polluted areas in east Asia, and the Ganges valley. Also interesting is the high mean AOD over Siberia, which is related to boreal forest fires. If we look at the differences between SRON/RemoTAP and GRASP, for most of the globe the differences are small. Exceptions are the Sahara/Arabia where SRON/RemoTAP AOD is higher by 0.05-0.10 and equatorial Africa where SRON/RemoTAP AOD is lower than GRASP by almost 0.15. Also notable is the difference (especially in relative sense) over the southern ocean where SRON/RemoTAP retrieves lower AOD than GRASP.

Figure 5-4 shows scatter plots of the SRON/RemoTAP AOD versus the GRASP AOD at 565nm, separately for retrievals over land and ocean. Also, histogram of the differences is shown. Over land, the RMSD is 0.12 and the difference in the mean (SRON/RemoTAP-GRASP) is 0.01. The RMSD and bias are larger at 443 nm (0.14 and 0.026, respectively) and comparable at 865 nm (not shown). [1]Over ocean, the RMSD is 0.038 nm and the bias is -0.008. The differences are

[1] Here we compare AODs at 565, 443, and 865 nm because these are wavelengths that corresponds to POLDER bands. In WP1 we used 550 instead of 565 nm because that is a common wavelength for AOD. In WP1, we also noted 440 nm but that refers actually to the same wavelength band.

slightly larger at 443 nm and slightly smaller differences at 865 nm (not shown). The agreement has been much improved compared to WP1, where the RMSD was 0.23 over land and 0.078 over ocean. So, the differences have been reduced by almost a factor 2.

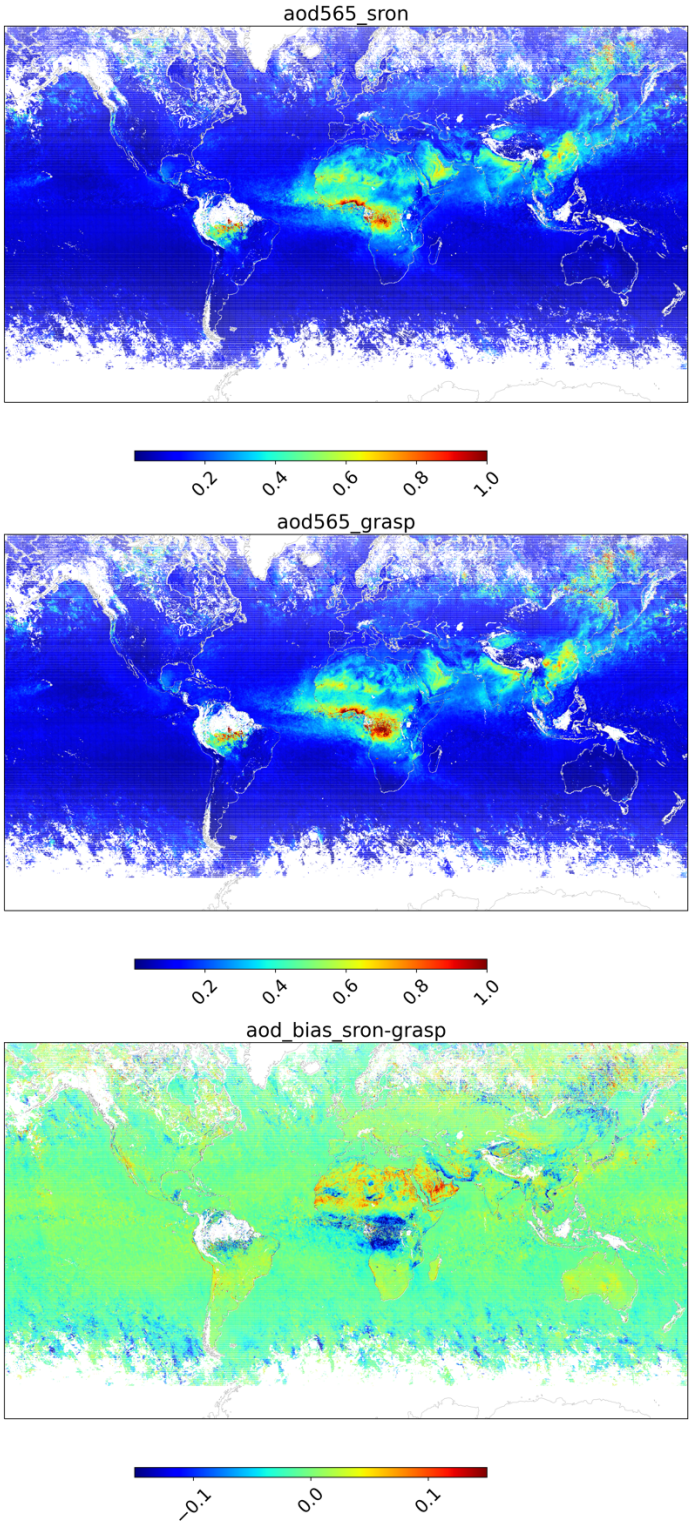

Figure 5-3: Maps of the 2008 (Jan-Nov) mean AOD for SRON/RemoTAP (upper), GRASP (middle) and the difference SRON/RemoTAP-GRASP (lower).

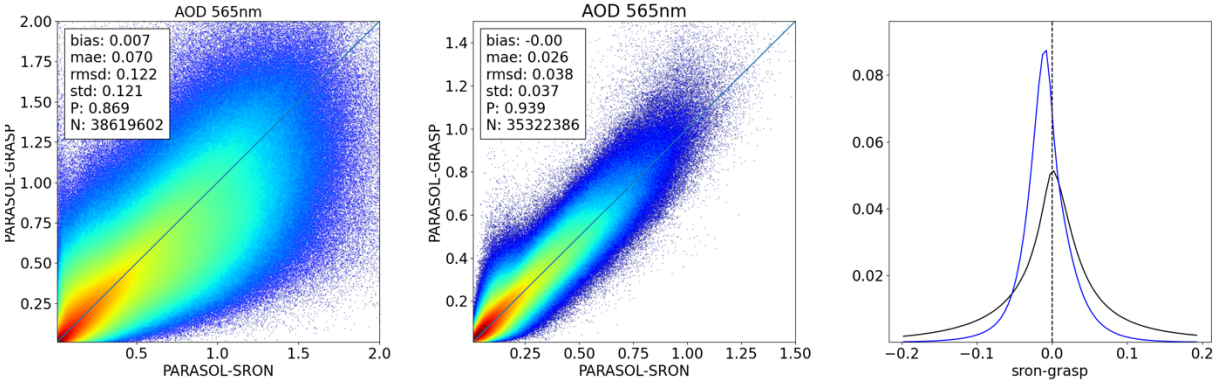

Figure 5-4: AOD (565 nm) scatter plots (GRASP versus SRON/RemoTAP) for retrievals over land (left) and ocean (middle) and a histogram of the differences (right), where the blue line corresponds to retrievals over ocean and the black line to retrievals over land

5.2.3 Comparison of Angstrom Exponent (AE), Fine- and Coarse Mode AOD

Figure 5-5 shows maps of the mean AE (440-865 nm) for GRASP and SRON/RemoTAP, respectively, and the map of the mean differences. These maps show retrievals for AOD (565nm) > 0.2. The AE maps for SRON/RemoTAP and GRASP both show a very similar overall pattern. Small AE values (larger sizes) occur over desert and over the open ocean and correspond mostly to situations dominated by Dust or Sea Salt, respectively. Larger AE values (smaller sizes) occur over areas with anthropogenic pollution (Asia, Europe, North- and South America) and over areas with biomass burning (southern Africa, South America, Indonesia, Australia). Most important differences between SRON/RemoTAP and GRASP arise over the Sahara and Middle East, where SRON/RemoTAP retrieves higher AE than GRASP. From the AERONET comparison we know that SRON/RemoTAP slightly overestimates AE at low AE values so this may be part of the reason. On the other hand, the maximum differences (where SRON/RemoTAP can be ~0.5 higher than GRASP) are not expected from the AERONET comparison.

Figure 5-6 shows scatter plots of the SRON/RemoTAP AE versus the GRASP AE, separately for retrievals over land and ocean. The upper panels show retrievals for AOD>0.2. Also, histogram of the differences is shown. Over land, for AOD > 0.2, the RMSD is 0.33 while over ocean the RMSD is 0.23. Over land, the agreement is very good for larger values of AE (small particle size) and a bit worse for lower AE values (large particles size), where SRON/RemoTAP retrieves larger AE. Over ocean, the agreement is very good for both low and high AE values. The agreement between SRON/RemoTAP and GRASP over land has been much improved compared to WP1 where we found an RMSD of 0.56 between SRON/RemoTAP and

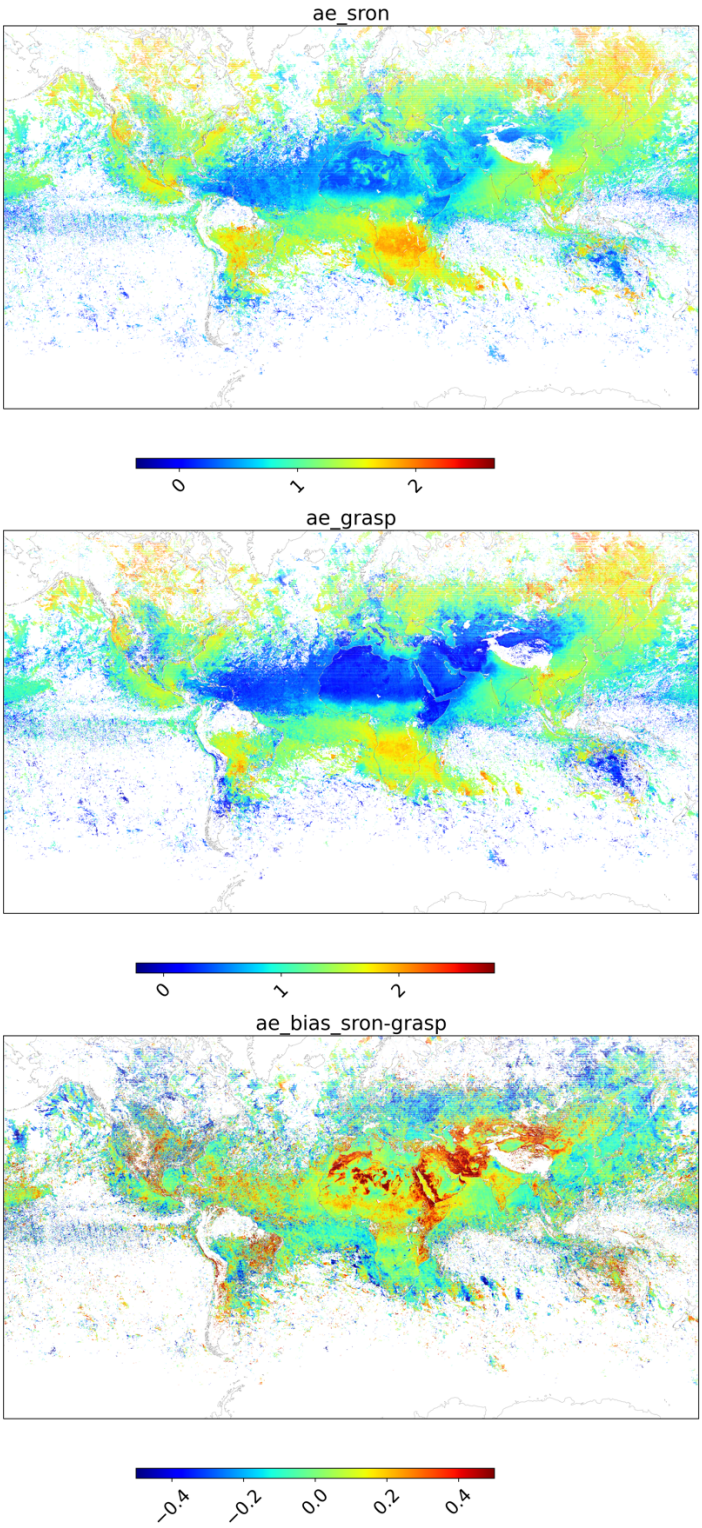

Figure 5-5: Maps of the 2008 (Jan-Nov) mean AE (440-865 nm) for SRON/RemoTAP (upper), GRASP (middle) and the difference SRON/RemoTAP-GRASP (lower). The map only includes retrievals with AOD (565 nm)> 0.2.

GRASP/HP. Over ocean, the agreement is comparable to WP1, although there we use an AOD threshold of 0.3.

When using a lower AOD threshold of 0.1 (lower panels of Figure 5-6) the agreement gets worse with RMSD values of 0.48 and 0.36 over land and ocean, respectively. Over land, the overall scatter of the data increases compared to the higher AOD threshold, while over ocean also we see some specific cases where SRON/RemoTAP retrieves small AE (close to 0) and GRASP retrieves values up to 1.5. To investigate the dependence of AE difference on AOD in more detail, Figure 5-7 shows the difference as a function of AOD. We can see the AE difference depends strongly on AOD. Over land, there is a large positive bias (~0.4) at AOD=0.10 which decreases gradually to 0 at AOD=0.4. Over ocean, there is a bias of -0.45 at AOD=0.05 which decreased more rapidly with AOD than over land. The strong dependence of AE difference on AOD results from the fact that that at small AOD, the AE calculation is very sensitive to even small errors in AOD at the different wavelengths.

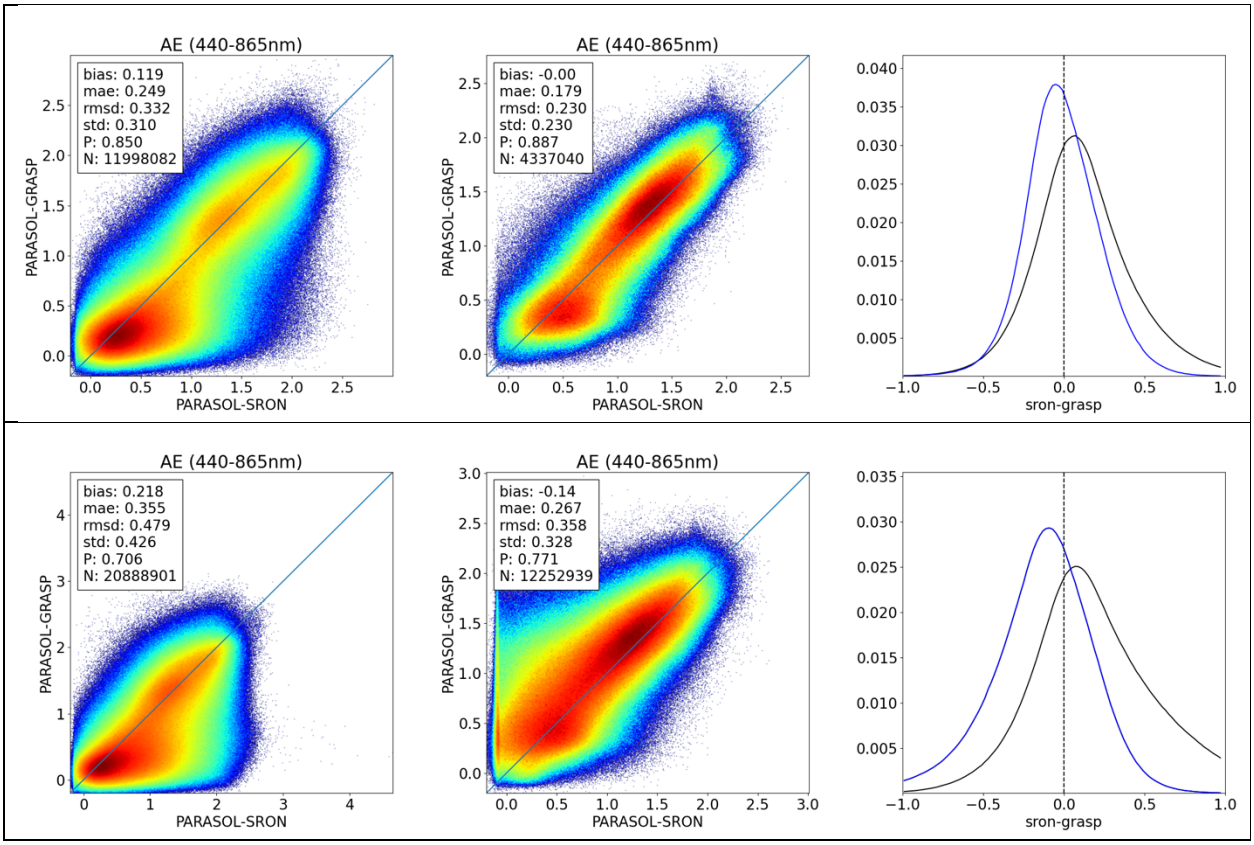

Figure 5-6: AE (440-865 nm) scatter plots (GRASP versus SRON/RemoTAP) for retrievals over land (left) and ocean (middle) and a histogram of the differences (right), where the blue line corresponds to retrievals over ocean and the black line to retrievals over land. The upper panels show retrievals for AOD>0.2 and the lower panels show retrievals for AOD > 0.1.

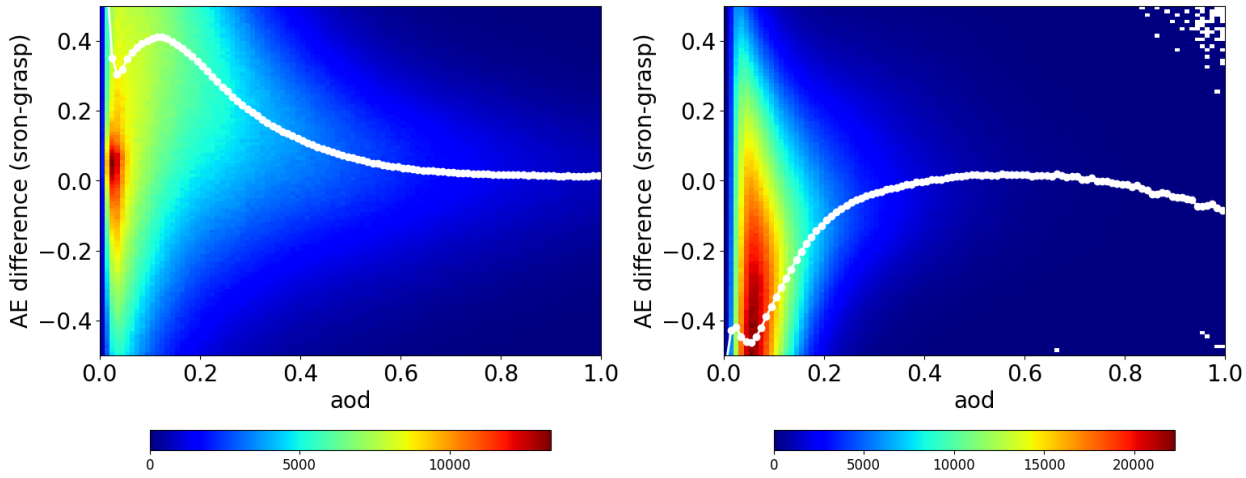

Figure 5-7: AE difference between SRON/RemoTAP and GRASP as a function of AOD over land (left) and ocean (right). The white dots show the median difference for each AOD bin. The color bar indicates the number of retrievals.

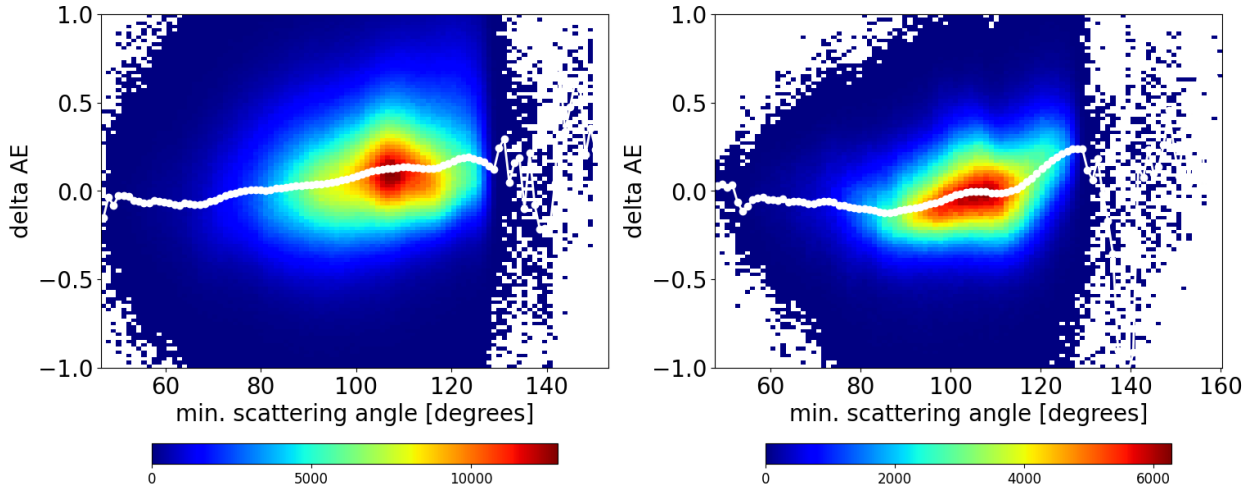

Figure 5-8: AE difference between SRON/RemoTAP and GRASP as a function of minimum scattering angle over land (left) and ocean (right). The color bar indicates the number of retrievals.

Figure 5-8 shows the AE difference between SRON/RemoTAP and GRASP as a function of minimum scattering angle. We expect that the accuracy of aerosol retrievals depends on the scattering geometry of the PARASOL measurement, where a small 'minimum scattering angle' generally corresponds to a large range of scattering angles, given that large values for scattering angle are generally available (although some exceptions may apply). From Figure 5-8 we see some dependence on minimum scattering angle. Over land, the median difference in AE becomes more positive with increasing minimum scattering angle, although the increase in difference is not very strong. Over ocean, the dependence on minimum scattering angle is even weaker for minimum scattering angles < 110°, but between 110° and 130° there is a strong increase in the difference between SRON/RemoTAP and GRASP. Indeed, we expect the largest information content for scattering angle < 110° large (Fougnie et al, 2021).

Figure 5-9 shows the comparison for the fine mode AOD and Figure 5-10 for the coarse mode AOD. Over land, the agreement for the fine mode AOD is better than for the coarse mode AOD (RMSD 0.063 vs 0.107). This means that for the total AOD, most of the differences can be explained by differences in the coarse mode AOD. Further, we see that for the fine mode AOD SRON/RemoTAP retrieves smaller values than GRASP towards higher AOD while for the coarse mode the opposite is observed. For retrievals over ocean, the RMSD for the coarse mode AOD is smaller than for the fine mode. Further, for the fine mode SRON/RemoTAP is systematically smaller than GRASP (-0.02 bias) while for the coarse mode SRON/RemoTAP is larger (0.016 bias), such that the total AOD bias between SRON/RemoTAP and GRASP is very small.

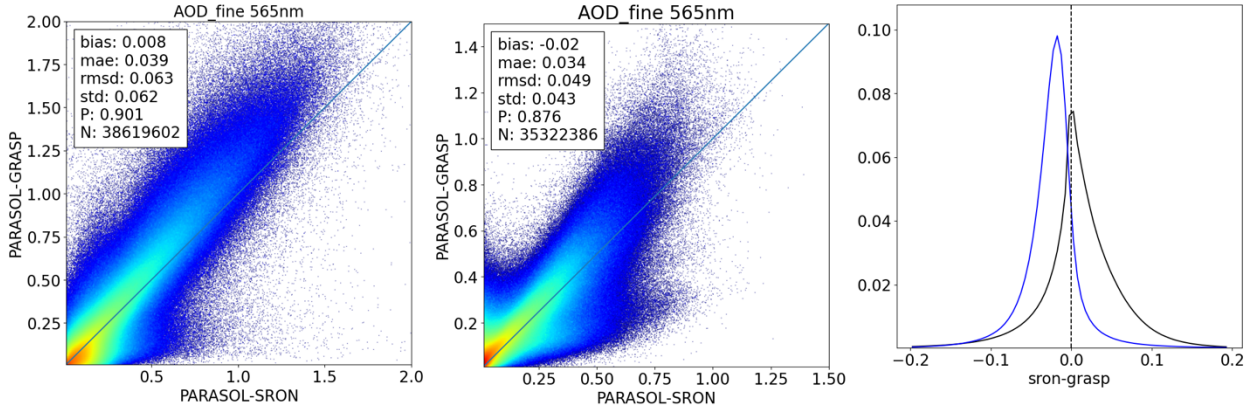

Figure 5-9: Fine mode AOD (565 nm) scatter plots (GRASP versus SRON/RemoTAP) for retrievals over land (left) and ocean (middle) and a histogram of the differences (right), where the blue line corresponds to retrievals over ocean and the black line to retrievals over land.

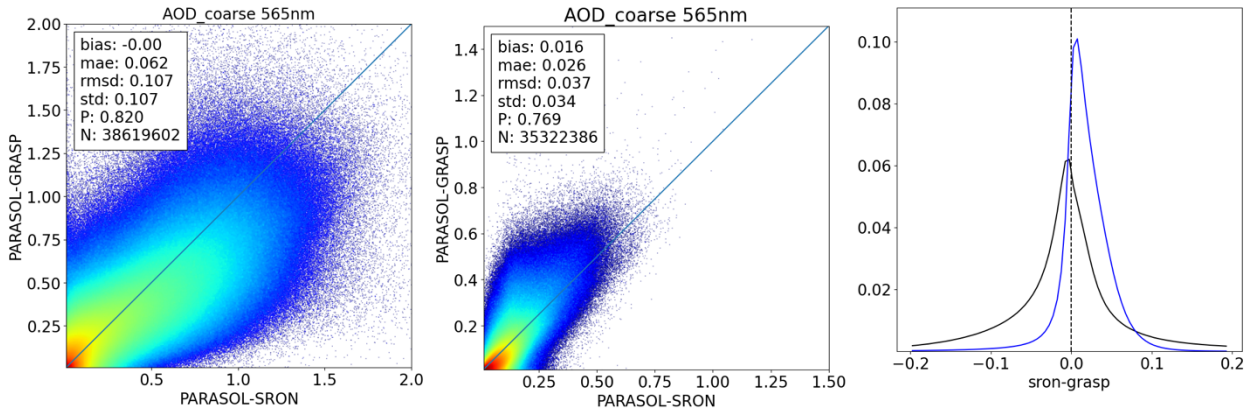

Figure 5-10: Coarse mode AOD (565 nm) scatter plots (GRASP versus SRON/RemoTAP) for retrievals over land (left) and ocean (middle) and a histogram of the differences (right), where the blue line corresponds to retrievals over ocean and the black line to retrievals over land.

5.2.4 Comparison of SSA and AAOD

Figure 5-11 shows maps of the mean SSA (565 nm) for GRASP and SRON/RemoTAP and the map of the mean differences. Overall, the maps show similar patters but there are also important differences. In general, SRON/RemoTAP retrieves higher SSA over ocean and lower SSA over land. Larger differences occur over equatorial Africa (biomass burning region) where SRON/RemoTAP retrieves significantly higher (> 0.10 difference) SSA than GRASP, over ocean but also over land (in contrast to other land regions). The difference is especially apparent over ocean. Also, over India and the Indian ocean there are notable differences in SSA between SRON/RemoTAP and GRASP. Here, over land SRON/RemoTAP retrieves a mean SSA of ~0.90 while GRASP retrieves ~0.95. Over ocean, the difference is opposite: SRON/RemoTAP retrieves SSA 0.95-1 while GRASP retrieved ~0.90. Both SRON/RemoTAP and GRASP show an unexpected sharp transition between land and ocean. A similar pattern can be seen at the west coast of the USA.

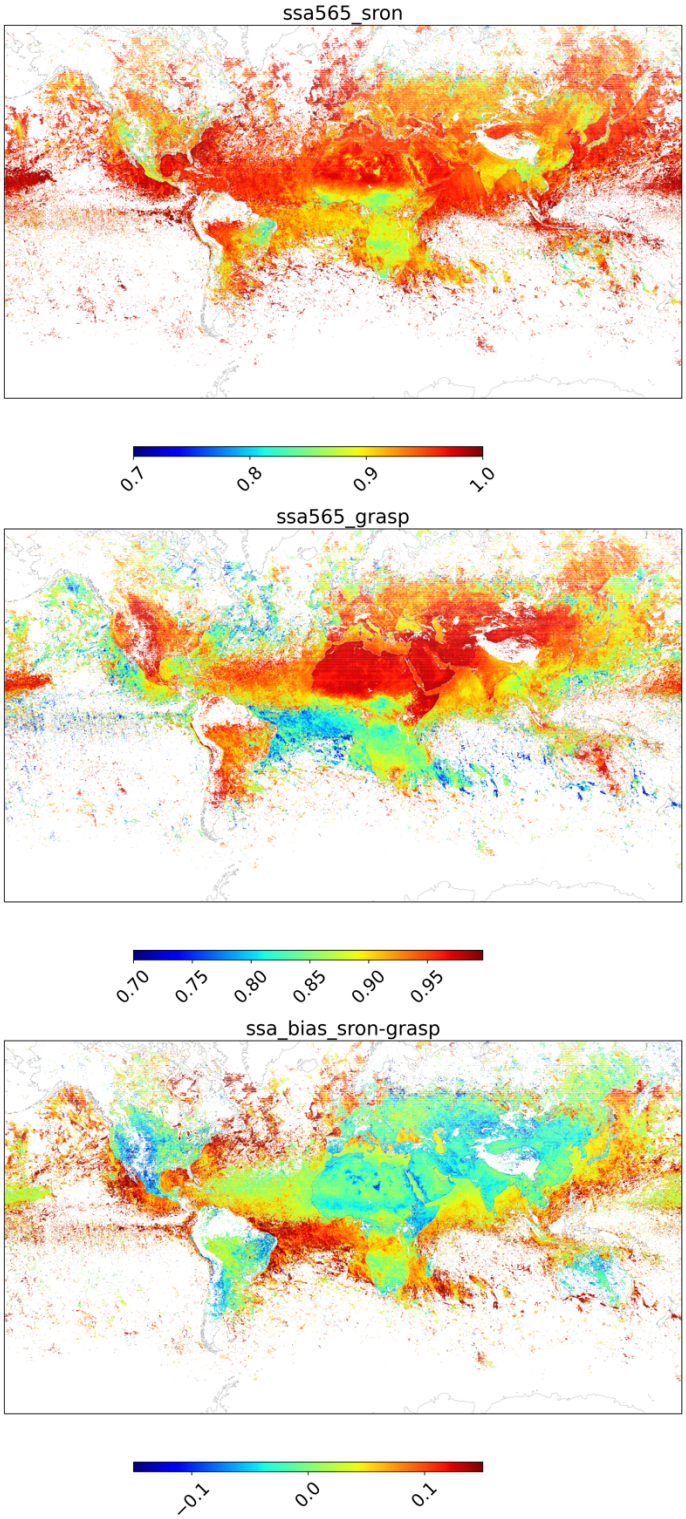

Figure 5-11: Maps of the 2008 (Jan-Nov) mean SSA for SRON/RemoTAP (uppe), GRASP (middle) and the difference SRON/RemoTAP-GRASP (lower). The map only includes retrievals with AOD (565 nm)> 0.2

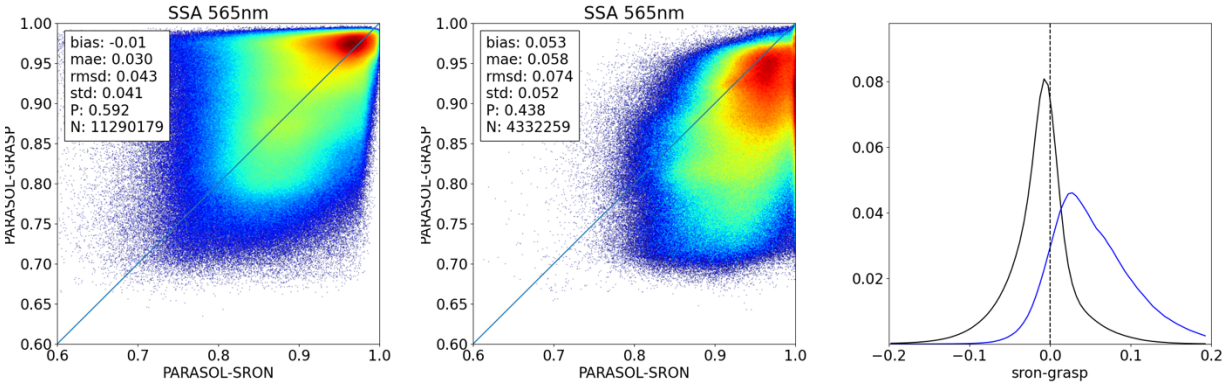

Figure 5-12: SSA (565 nm) scatter plots (GRASP versus SRON/RemoTAP) for retrievals over land (left) and ocean (middle) and a histogram of the differences (right), where the blue line corresponds to retrievals over ocean and the black line to retrievals over land. Only retrievals with AOD (565 nm)> 0.2 are included.

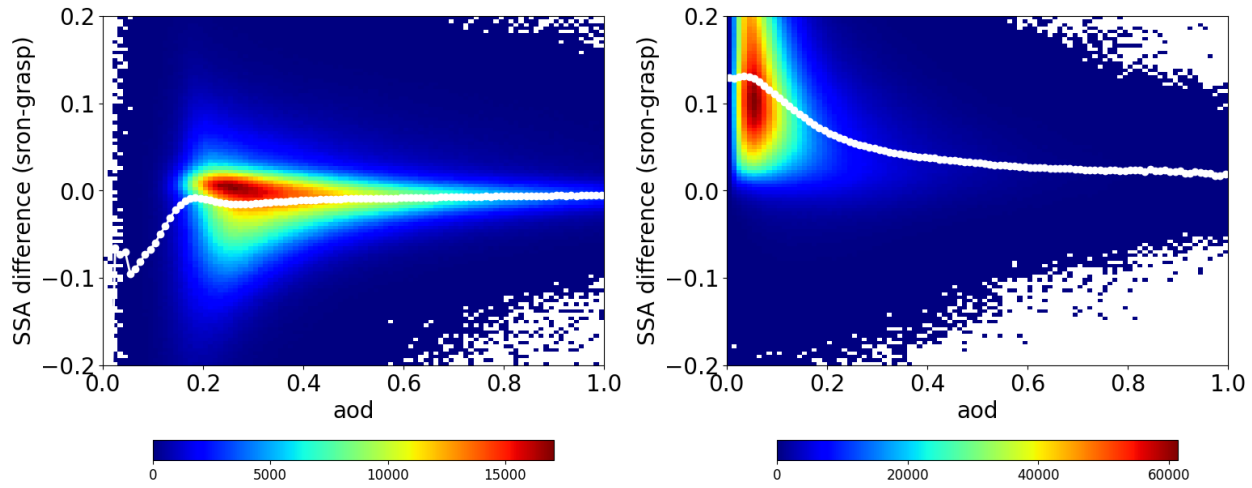

Figure 5-13: SSA difference between SRON/RemoTAP and GRASP as a function of AOD over land (left) and ocean (right). The color bar indicates the number of retrievals.

Figure 5-12 shows scatter plots of the SRON/RemoTAP SSA versus the GRASP SSA at 565 nm, separately for retrievals over land and ocean. Also, histogram of the differences is shown. Over land, the RMSD is 0.034 whereas the overall bias is < 0.01. There is some compensation between different areas, as is apparent from the world map, but overall, the agreement can be considered good over land. Over ocean the differences are substantially larger, with a RMSD and bias of 0.061 and 0.042, respectively. Here, SRON/RemoTAP retrieves higher SSA than GRASP,

as was already seen from the world map. As noted above, the AERONET SSA validation over ocean does not have sufficient points to indicate whether the difference is caused by errors in SRON/RemoTAP or GRASP. Clearly, there is a need for more SSA validation points over ocean.

Figure 5-13 shows the SSA difference (SRON/RemoTAP-GRASP) as a function of AOD (mean of SRON/RemoTAP and GRASP) for retrievals over land and ocean, respectively. Over land, we see that for AOD < ~0.15 the difference between SRON/RemoTAP and GRASP is largest where the mean difference reaches ~-0.10 for the lowest AOD values. The SSA difference decreases (in absolute sense) rapidly till AOD = ~0.15 where the SSA difference is ~-0.01 and slowly decreases further to higher AOD. Despite the fact that on average the SRON/RemoTAP SSA is lower than the GRASP SSA, we see that for a substantial number of retrievals the GRASP SSA is higher. These retrievals correspond mostly to biomass burning retrievals (see above).

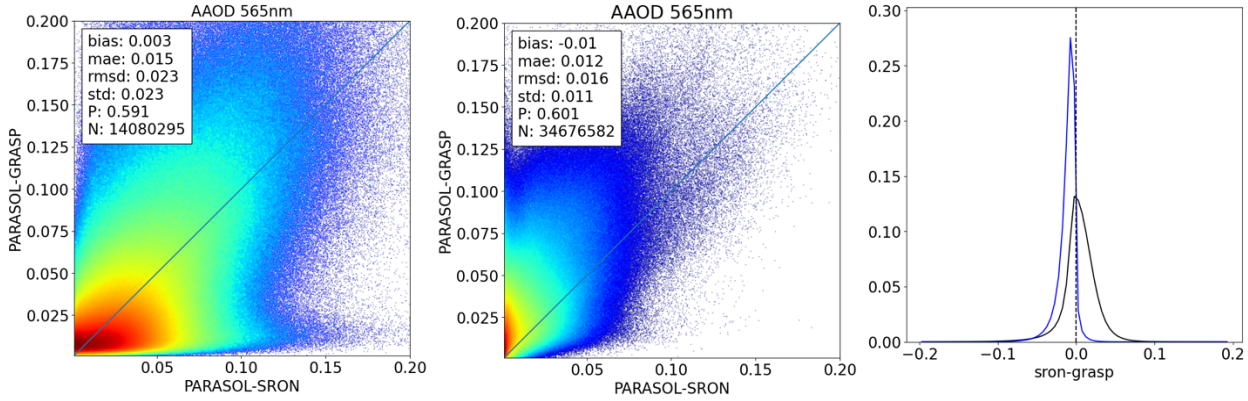

Figure 5-14: AAOD (565 nm) scatter plots (GRASP versus SRON/RemoTAP) for retrievals over land (left) and ocean (middle) and a histogram of the differences (right), where the blue line corresponds to retrievals over ocean and the black line to retrievals over land.

Figure 5-14 shows the comparison for AAOD. Over land, the overall bias is relatively small (0.003) but there is considerable scatter between SRON/RemoTAP and GRASP. Over ocean, there is a clear bias between SRON/RemoTAP and GRASP where GRASP retrieves higher AAOD than SRON/RemoTAP. This is expected because GRASP retrieves smaller SSA than SRON/RemoTAP over ocean and comparable AOD, which should result in a higher AAOD.

5.2.5 Comparison of Surface Properties

Figure 5-15 shows global maps of the mean retrieved surface Isotropic BRDF parameters for GRASP and SRON/RemoTAP and the differences between them and Figure 5-16 shows a histogram of the differences. For most of the globe, SRON/RemoTAP retrieves a higher surface BRDF than GRASP. The only exception is equatorial Africa where SRON/RemoTAP retrieved a smaller Isotropic BRDF parameter at 865 nm. The largest differences (in absolute sense) occur over the Sahara and the Arabian Peninsula. From the histogram of the differences in Figure 5-16, we see the mean difference between SRON/RemoTAP and GRASP is around 0.02 for all

wavelengths. Figure 5-17 and Figure 5-18 shows a comparison of the directional BRDF parameters and the BPDF. SRON/RemoTAP retrieves slightly larger values for the directional BRDF parameters and significantly smaller values for the BPDF. The comparison for the BPDF is worse than for the data of WP1. SRON/RemoTAP retrieves a substantially lower BPDF scaling parameter than GRASP. Like for all surface parameters, the difference is largest over the Sahara and the Arabian peninsula. This BPDF difference is unexpected given the harmonization of the surface BRDF and BPDF models between SRON/RemoTAP and GRASP, most notably by making the BRDF and BPDF description consistent in SRON/RemoTAP. To investigate the difference in the BPDF scaling parameter in more detail, Figure 5-19 shows the difference in BPDF scaling parameter as a function of the difference in isotropic BRDF parameter (490 nm). There is a very clear dependence for when the difference in isotropic BRDF parameter is in the range 0-0.05, where the difference in BPDF scaling gets more negative with increasing difference in isotropic BRDF parameter. So, a larger isotropic BRDF is compensated with a smaller BPDF scaling in SRON/RemoTAP. This can be explained by the fact that the Fresnel reflection matrix that is scaled in the BPDF model also contributes to the BRDF. This would imply the either the surface polarization is too small in SRON/RemoTAP or too large in GRASP.

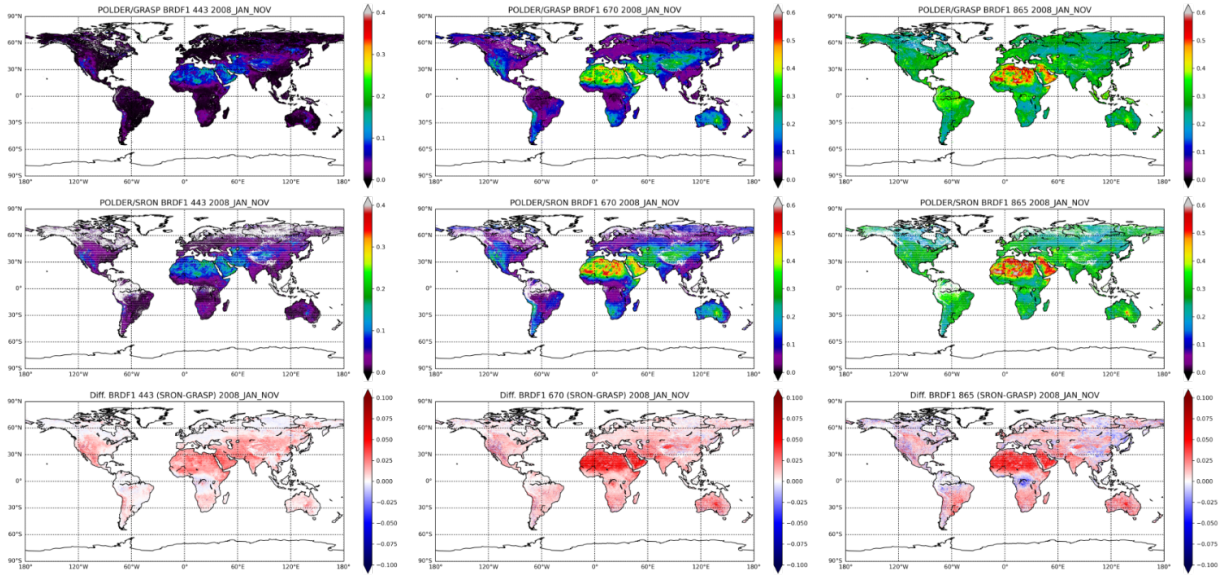

Figure 5-15: Global maps of the annual mean surface Isotropic BRDF parameter at 443 (left columns), 670 (middle columns), and 865 nm (right columns). The upper row shows the GRASP retrievals, the middle row SRON/RemoTAP retrievals, and the lower row the difference (SRON/RemoTAP-GRASP).

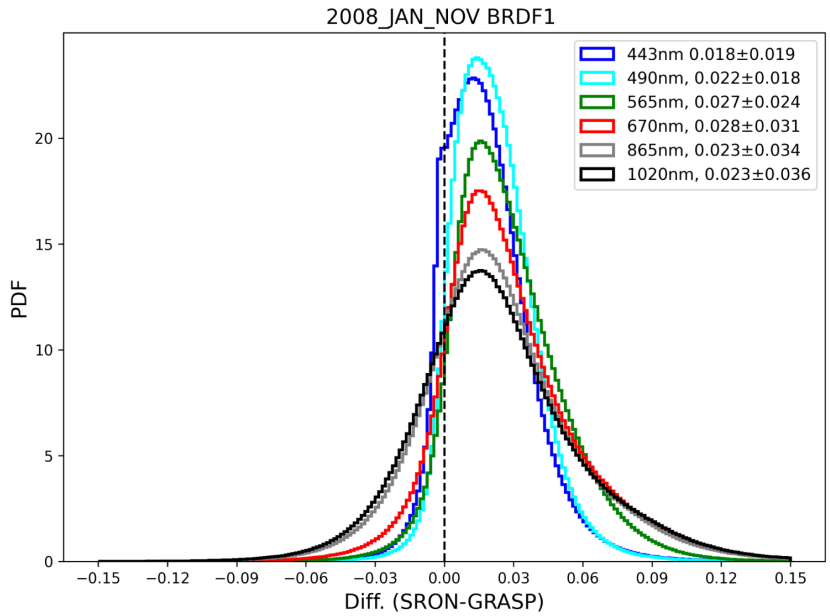

Figure 5-16: Histogram of the differences in retrieved surface Isotropic BRDF parameter at different wavelengths.

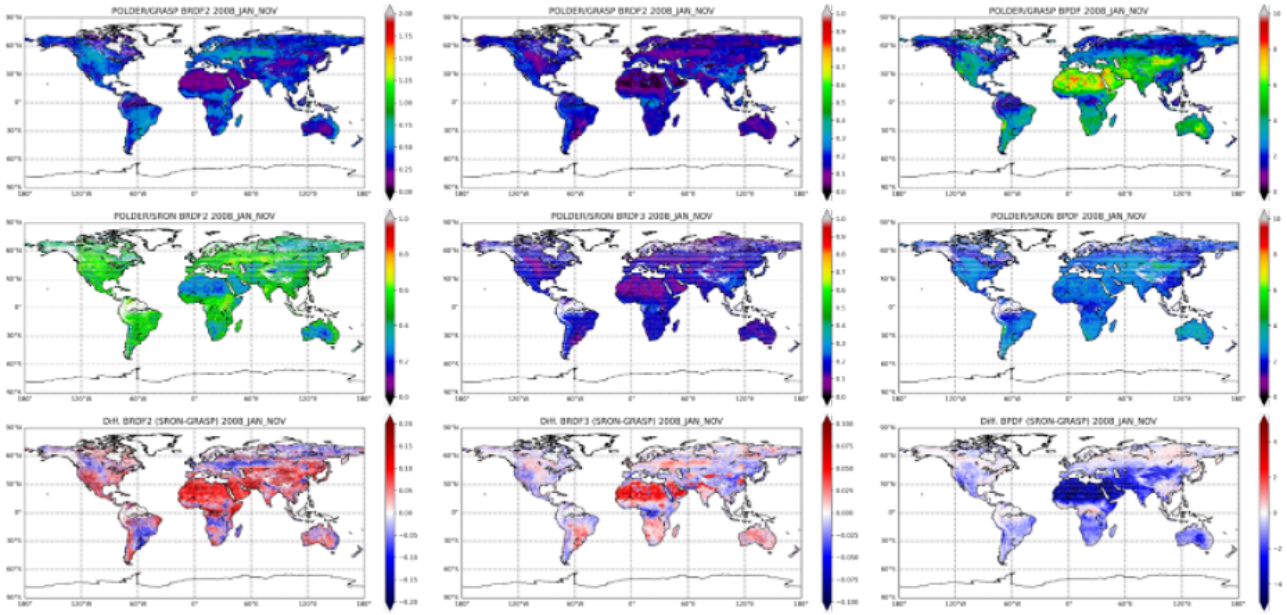

Figure 5-17: Global maps of the annual mean surface BRDF directional parameter for the Ross Thick kernel (left columns), the Li Sparse Kernel (middle columns), and the BPDF scaling parameter (right columns). The upper row shows the GRASP retrievals, the middle row SRON/RemoTAP retrievals, and the lower row the difference (SRON/RemoTAP-GRASP).

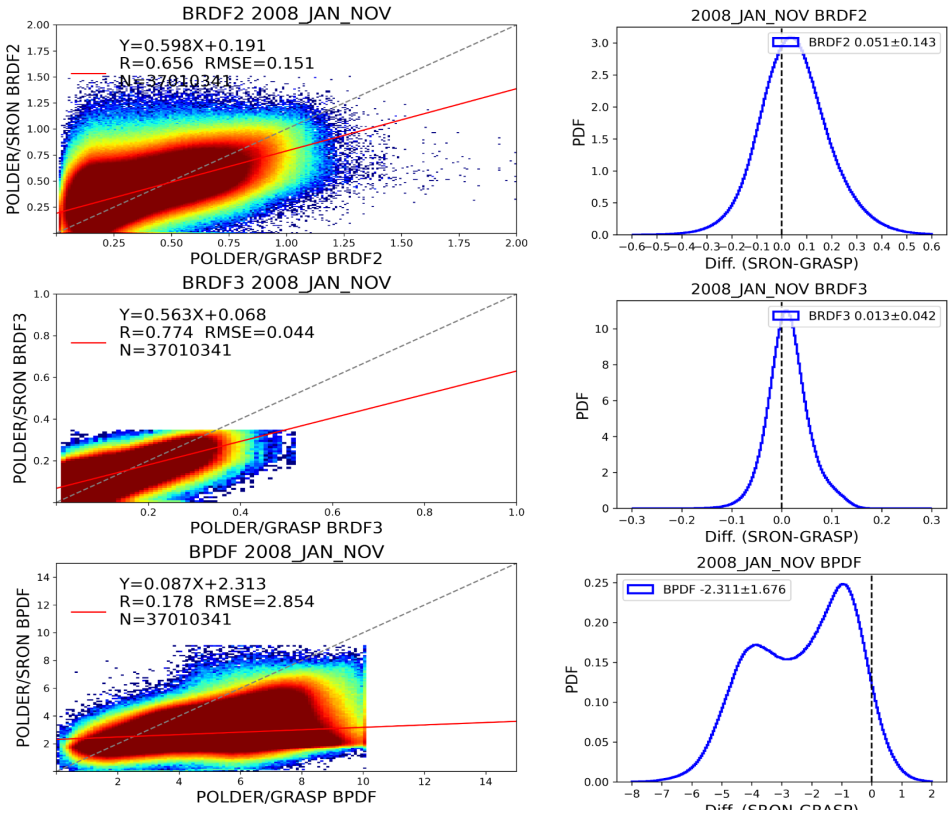

Figure 5-18: Comparison of surface BRDF geometric parameters and BPDF scaling parameter between SRON/RemoTAP and GRASP. The geometric-scattering kernel is indicated by 'BRDF2' and the volumetric-scattering kernel by 'BRDF2'

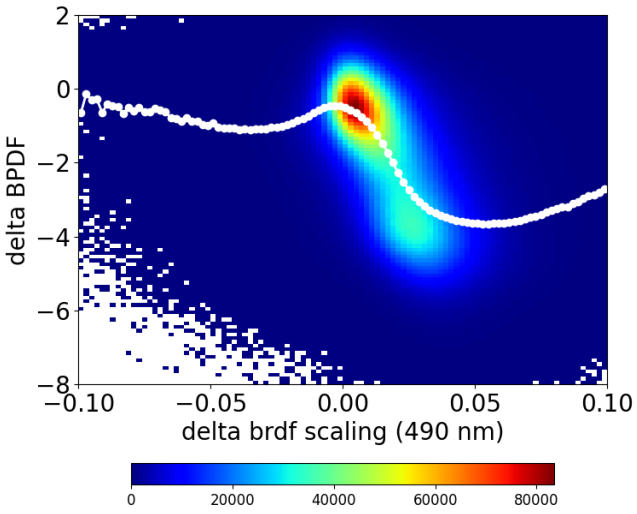

Figure 5-19: Difference in BPDF scaling parameters as a function of the difference in the isotropic BRDF parameter (490 nm). Differences represent SRON/RemoTAP – GRASP. The color bar indicates the number of retrievals

Figure 5-20 shows the difference in AOD between SRON/RemoTAP and GRASP as a function of difference in retrieved Isotropic BRDF parameter (at 490 nm) and the difference in BPDF scaling parameter. It can be seen that for cases where SRON/RemoTAP retrieves a smaller

Isotropic BRDF parameter than GRASP, it also retrieves a smaller AOD. The difference in AOD increases to -0.10 when the difference in Isotropic BRDF is also -0.10. For cases where SRON/RemoTAP retrieves a higher Isotropic BRDF parameter, there is no clear dependence of AOD differences on difference in Isotropic BRDF. There is also a clear dependence of the AOD difference on difference in the BPDF scaling parameter. As notes above, SRON/RemoTAP retrieves much smaller values for the BPDF scaling than GRASP. When the BPDF difference is ~-8, SRON/RemoTAP retrieves on average a higher AOD value than GRASP by ~0.10. These cases correspond mostly to the Sahara and the Arabian Peninsula. On the other hand, when SRON/RemoTAP retrieves higher BPDF than GRASP (mostly over higher latitudes), it retrieves smaller AOD, where the mean difference is ~-0.05.

Figure 5-21 shows the difference in SSA between SRON/RemoTAP and GRASP as a function of difference in retrieved Isotropic BRDF parameter (at 490 nm) and the difference in BPDF scaling parameter. For SSA, we see in particular a large effect on isotropic BRDF parameter, where the SSA difference can be almost up to 0.10 when the difference in isotropic BRDF parameter is -0.10. The dependence on BPDF is smaller and especially apparent when SRON/RemoTAP retrieves higher BPDF than GRASP.

Figure 5-22 shows the difference in AE between SRON/RemoTAP and GRASP as a function of difference in retrieved isotropic BRDF parameter (at 490 nm) and the difference in BPDF scaling parameter. Here we see a strong dependence on BPDF scaling parameter. For large negative differences, i.e. when SRON/RemoTAP retrieves smaller BPDF than GRASP, there is a large positive difference in AE. These cases correspond mostly to the Sahara where indeed SRON/RemoTAP retrieves higher AE than GRASP (see Figure 5-5). Given that the AERONET comparison indicates a positive AE bias in SRON/RemoTAP over the Sahara, a possible explanation is that SRON/RemoTAP retrieves a surface reflection matrix with too small polarization. In future work, the SRON/RemoTAP team will investigate whether an improved retrieval of surface BPDF will lead to a better AE retrieval over the Sahara.

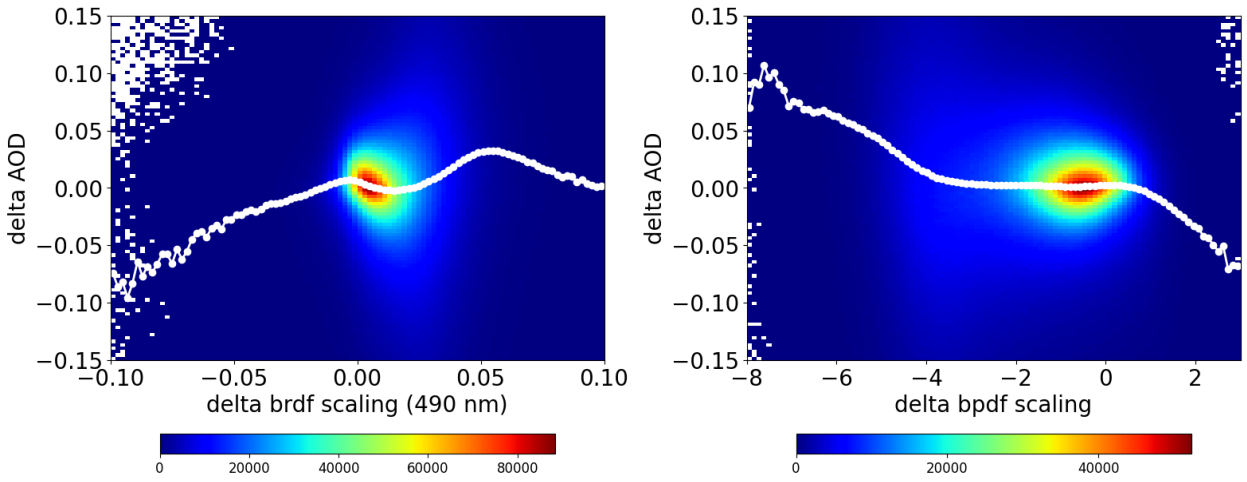

Figure 5-20: Dependence of the AOD difference (SRON/RemoTAP – GRASP) on difference in the Isotropic BRDF parameter at 490 nm (left) and the BPDF scaling parameter (right). The color bar indicates the number of retrievals

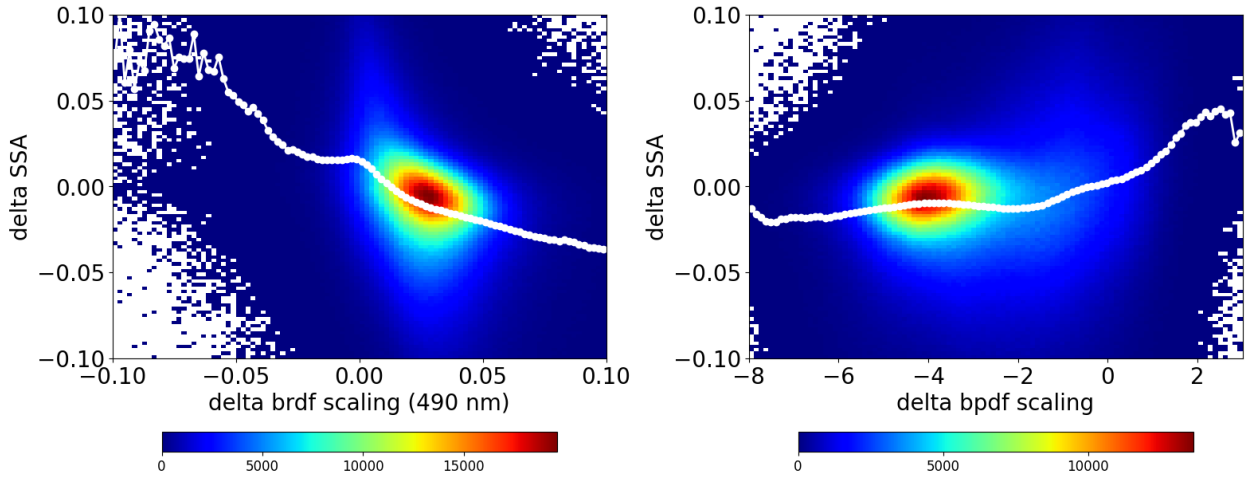

Figure 5-21: Same as

Figure 5-20: Dependence of the AOD difference (SRON/RemoTAP – GRASP) on difference in the Isotropic BRDF parameter at 490 nm (left) and the BPDF scaling parameter (right). The color bar indicates the number of retrievals

but for differences in SSA. Only cases with AOD(565nm)>0.2 are included. The color bar indicates the number of retrievals.

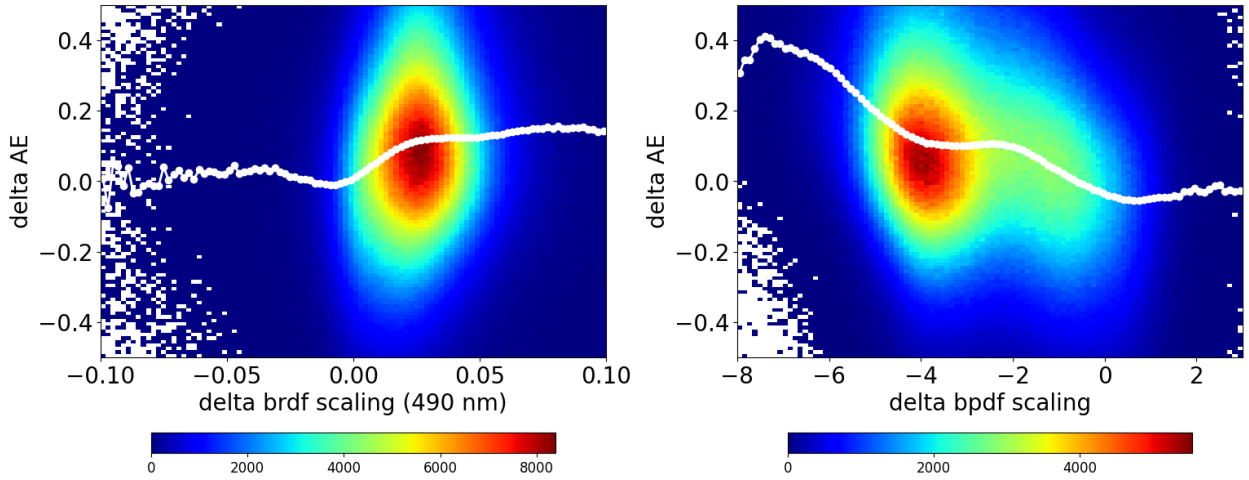

Figure 5-22: Same as

Figure 5-20: Dependence of the AOD difference (SRON/RemoTAP – GRASP) on difference in the Isotropic BRDF parameter at 490 nm (left) and the BPDF scaling parameter (right). The color bar indicates the number of retrievals

but for differences in AE. Only cases with AOD(565nm)>0.2 are included. The color bar indicates the number of retrievals.

5.3 Comparison to MODIS

The MODIS Dark Target (DT) (Levy et al, 2013) and Deep Blue (DB) (Hsu et al, 2013) AOD products are the most widely used aerosol products. Here, we compare AOD and AE retrieved

from POLDER by both SRON/RemoTAP and GRASP to the MODIS DT and DB products. Figure 5-23 shows the comparison for AOD over land and ocean. Over land, GRASP agrees somewhat better with MODIS than SRON/RemoTAP but the agreement between GRASP and SRON/RemoTAP is significantly better (see Figure 5-4) than the agreement between both algorithms with MODIS. Over ocean, the agreement of both GRASP and SRON/RemoTAP with MODIS is similar as the agreement between GRASP and SRON/RemoTAP, although GRASP compares slightly better with MODIS than SRON/RemoTAP. The better agreement between GRASP and SRON/RemoTAP over land than the agreement of both algorithms with MODIS may suggest a more accurate AOD product over land for the POLDER algorithms than for MODIS. Also, the agreement with AERONET for both POLDER algorithms over land seems somewhat better than the agreement with AERONET for MODIS (Chen et al., 2020).

Figure 5-24 shows maps of the annual mean AOD for the different products and the differences between them. Qualitatively, the maps for the 3 products look very similar. For the differences over land, both GRASP and SRON/RemoTAP show very similar patterns against MODIS, with a strong positive difference over most of Africa, India, and China, a somewhat weaker positive difference over Europe and the US, and some small spots of negative differences (e.g. over South America). Over the global ocean, SRON/RemoTAP shows a small (0.01-0.02) negative difference against MODIS, whereas GRASP shows a small positive difference at mid-latitudes and a small negative difference in most of the Tropics.

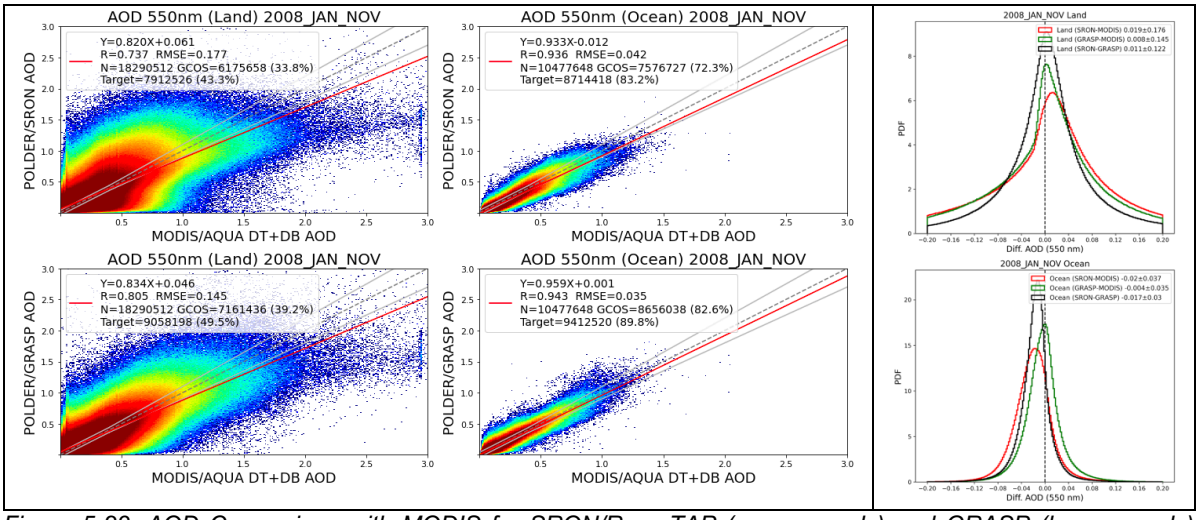

Figure 5-23: AOD Comparison with MODIS for SRON/RemoTAP (upper panels) and GRASP (lower panels). Left panels show comparison over land, middle panels comparison over ocean, and right panels histograms of the differences. For MODIS the DT and DB aerosol products have been combined.

Figure 5-25 shows the AE comparison of both PARASOL products with the MODIS DT product over land and ocean. Over land, we can clearly see that the MODIS-DT AE tends to be centered around a number of discrete values. This is probably a result of the MODIS retrieval approach based a discrete set of aerosol models. Both for SRON/RemoTAP and GRASP there is a large difference with the MODIS-DT AE and the agreement between SRON/RemoTAP and GRASP, shown in Figure 5-6, is much better than the agreement of both products with MODIS. This is

expected because MODIS has limited information content on aerosol size over land which results in poor comparison of MODIS-DT AE against AERONET (Chen et al., 2020). The same conclusions hold for the AE comparison with the MODIS-DB product over land (not shown). Over ocean, the agreement between the PARASOL products and MODIS is better than over land but still much worse than the agreement between SRON/RemoTAP and GRASP (Figure 5-6). This suggests that also over ocean both PARASOL algorithms provide a more accurate AE than MODIS, as expected.

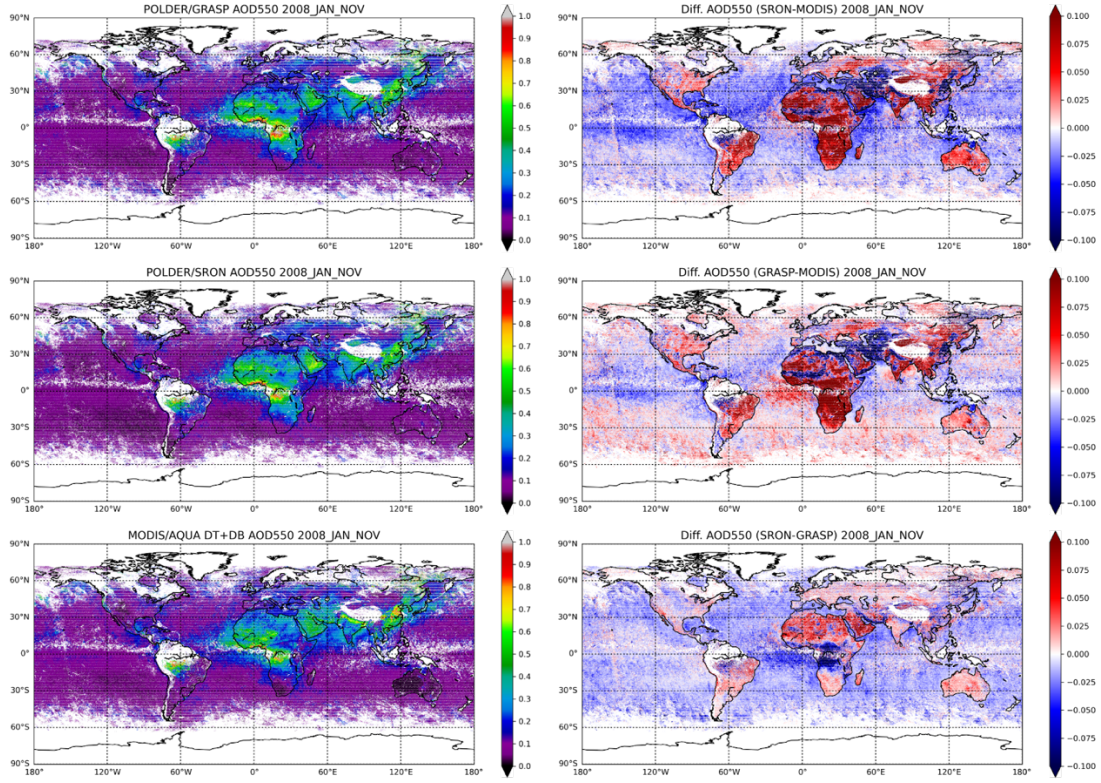

Figure 5-24: Maps of annual mean AOD for GRASP (upper left), SRON/RemoTAP (middle left), and MODIS (lower left) as well as the differences GRASP-MODIS (upper right), SRON/RemoTAP-MODIS (middle right) and SRON/RemoTAP-GRASP) lower right.

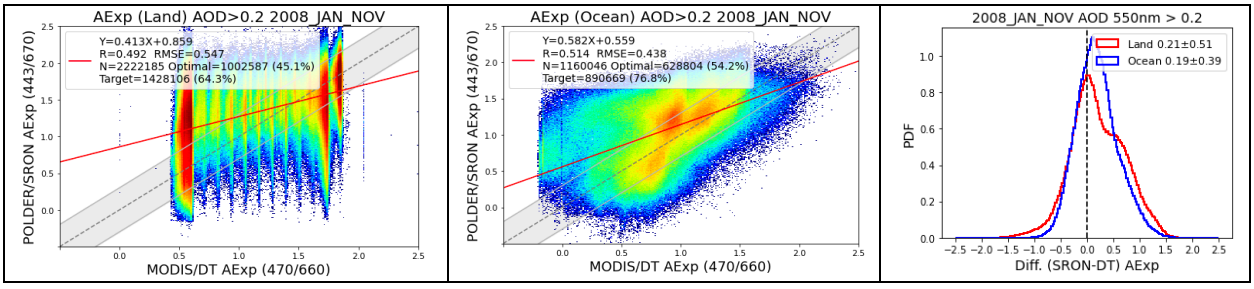

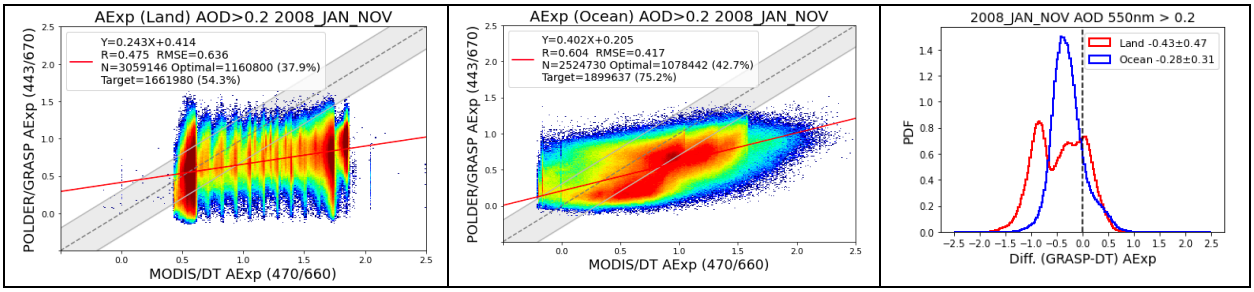

Figure 5-25: AE Comparison with MODIS-DT for SRON/RemoTAP (upper panels) and GRASP (lower panels). Left panels show comparison over land, middle panels comparison over ocean, and right panels histograms of the differences.

5.4 Conclusions

In WP4 we performed global processing of one year of PARASOL data with both SRON/RemoTAP and GRASP. The retrieved L2 data products were further processed to a gridded product at 0.1° x 0.1° resolution. First the global products were compared against AERONET and the findings of WP3, where we processed PARASOL data over AERONET stations only, were confirmed.

The global comparison of the GRASP and SRON/RemoTAP products can be summarized as follows:

- AOD: The agreement has been improved substantially over land and ocean compared to WP1 by almost a factor of 2. The RMSD values are 0.12 and 0.037 over land and ocean, respectively. The largest differences occur over the biomass burning region in equatorial Africa. The global mean values are virtually unbiased with respect to each other.
- Angstrom Exponent: Also, here the agreement has been substantially improved compared to WP1. For AE the RMSD between SRON/RemoTAP and GRASP is 0.33 over land and 0.23 over ocean when only retrievals with AOD>0.2 are included. When taking retrievals with AOD>0.1, the RMDS increases to 0.48 over land and 0.36 over ocean. Towards lower AOD, significant differences occur between the 2 data products because the AE calculation becomes very sensitive to even small errors in AOD at the different wavelengths when the AOD is small. The differences show some correlation with the scattering geometries of the multi-angle measurements.
- Fine and Coarse AOD: Over land, the agreement is better for fine mode AOD (RMSD=0.063) than for coarse mode AOD (RMSD=0.11) and over ocean vice versa (RMSD=0.049 for fine mode and 0.037 for coarse mode). Over ocean, the fine and coarse mode have opposite biases (~0.02) that compensate each other in the total AOD.
- SSA and AAOD: Good agreement over land (RMSD=0.030) for retrievals with AOD > 0.2. Over ocean the agreement is poor with a bias of 0.053 (where SRON/RemoTAP retrieves higher SSA) and an RMSD of 0.053. As expected, the differences increase towards low AOD, both over land and ocean. For the AAOD, the agreement is reasonable over lands and biased over ocean, where GRASP retrieves higher AAOD than SRON/RemoTAP (as expected from the lower SSA).

- The surface BRDF products show reasonable agreement, where for the majority of cases SRON/RemoTAP retrieves higher BRDF than GRASP. The differences in the BPDF are substantial, where SRON/RemoTAP retrieves smaller BPDF than GRASP in most cases. The differences in AOD are correlated with differences in BPDF.

We also compared the GRASP and SRON/RemoTAP AOD and AE products against MODIS. For AOD over land, the agreement of either GRASP or SRON/RemoTAP with MODIS is worse than the agreement between the 2 PARASOL algorithms themselves. Over ocean, the agreement is very similar among the 3 products for AOD. For AE, the agreement between GRASP and SRON/RemoTAP is much better than the agreement of both products with MODIS, especially over land. This is expected because the PARASOL measurements have a much larger information content on aerosol size than MODIS (e.g. Mishchenko and Travis, 1997; Hasekamp and Landgraf, 2007)

To the best of our knowledge, the agreement between GRASP and SRON/RemoTAP is unprecedented. The good agreement between the 2 products gives confidence in the quality of both products.

6 Summary

Within the HARPOL project, we have performed a systematic intercomparison of the 2 main algorithms for aerosol retrieval from Multi-Angle Polarimeter (MAP) measurements, GRASP and SRON/RemoTAP. The project started in WP1 with and evaluation of the existing GRASP and SRON/RemoTAP PARASOL products at the start of the project. In WP2 (comparison for synthetic measurements) and WP3 (comparison over AERONET stations) several improvements have been implemented in both GRASP and SRON/RemoTAP and different definitions of the aerosol properties in the retrieval state vector have been investigated. Based on the intercomparisons in WP2 and WP3 optimal setups have been defined for both algorithms. For GRASP, the Chemical Component (CC) setup was selected which models the refractive index by using an internal mixture of different aerosol species and water, taking into account the relative humidity. The size distribution is described by 5 log-normal modes with fixed effective- radius and variance. For SRON/RemoTAP a setup was selected which describes aerosols by 3 size modes: a fine mode, a coarse insoluble mode (representative for Dust) and a coarse soluble mode (representative for sea salt). For each mode the effective radius- and variance are fitted and the refractive index, described by the sum of a number of wavelength dependent function, representative for different aerosol types. Finally, in WP4 the selected versions of GRASP and SRON/RemoTAP were used to process a year of global PARASOL data and the results have been compared.

Table 6-1 shows a summary of the validation with AERONET for the new improved products of GRASP and SRON/RemoTAP, as well as for the initial data products at the start of the project (WP1). We can see that both the GRASP and SRON/RemoTAP AOD retrievals (both land and ocean) improved significantly compared to the WP1 products and now both show good agreement with AERONET (similar performance for GRASP and SRON/RemoTAP). For SSA both products also improved over land compared to WP1 and now both show reasonable comparison against AERONET (SRON/RemoTAP slightly better than GRASP). Over ocean, not enough validation points are available to draw a conclusion for SSA. For AE over land SRON/RemoTAP improved significantly compared to the WP1 product whereas GRASP already showed good performance for AE in WP1. For AE over ocean, GRASP improved compared to WP1 whereas for SRON/RemoTAP the performance remained the same. Overall, for AE GRASP performs slightly better than SRON/RemoTAP.

Table 6-2 shows a summary of the global comparison between GRASP and RemoTAP. Over land, the agreement improved significantly compared to WP1, where the improvement in RMSD is almost a factor 2 for all 3 products (AOD, SSA, AE). Over ocean, the agreement for AOD improved also by almost a factor 2 and now show very good agreement between GRASP and SRON RemoTAP, with an RMSD of 0.038. SSA retrieval over ocean remains problematic, with still a large difference between GRASP and SRON/RemoTAP. For AE, the comparison was already good in WP1 and is similar for the new products.

Overall, both the GRASP and SRON/RemoTAP PARASOL products improved significantly during the HARPOL project. This has increased the fidelity of both algorithms and the corresponding products can be considered state-of-the art. For AOD, the performance is at least comparable to, and probably better than that of current reference products (from MODIS)

and for SSA and AE both GRASP and SRON/RemoTAP PARASOL retrievals provide the most accurate available satellite products.

Table 6-1: RMSE and percentage of retrievals that fall within the GCOS requirements of Table 2-1(indicated as 'GCOS') for AERONET comparison of GRASP and SRON/RemoTAP for AOD, SSA, and AE, for the new products (GRASP-CC and SRON/RemoTAP-3 modes) and the initial products of WP1 (GRASP-HP and SRON/RemoTAP-2 modes). The comparison includes only retrievals for common pixels.

			New Product		Initial Product (WP1)	
property	**surface**	**Algorithm**	**RMSE**	**GCOS**	**RMSE**	**GCOS**
AOD (565 nm)	Land	GRASP	0.10	54%	0.16	34%
		SRON/Remotap	0.10	54%	0.18	33%
SSA (440 nm)	Land	GRASP	0.049	50%	0.056	40%
		SRON/RemoTAP	0.041	57%	0.055	41%
AE (440-865nm)	Land	GRASP	0.367	n/a	0.382	n/a
		SRON/RemoTAP	0.387	n/a	0.63	n/a
AOD (565 nm)	Ocean	GRASP	0.047	77%	0.13	32%
		SRON/RemoTAP	0.057	71%	0.12	46%
SSA (440 nm)	Ocean	GRASP	0.055	56%	0.056	40%
		SRON/RemoTAP	0.032	56%	0.055	40%
AE (440-865nm)	Ocean	GRASP	0.224	n/a	0.39	n/a
		SRON/RemoTAP	0.285	n/a	0.27	n/a

Table 6-2: RMSD and bias between GRASP (CC) and SRON/RemoTAP for global retrievals for the year 2008 (Jan-Nov) for the properties AOD, SSA, and AE. The table shows both the comparision of the new products and the initial products from WP 1. For GRASP we show the WP1 comparison for GRASP-HP.

		New Product		Initial Product (WP1)	
Property	**Surface**	**RMSD**	**bias**	**RMSD**	**bias**
AOD (565 nm)	Land	0.12	0.007	0.22	0.03
SSA (440 nm)	Land	0.043	-0.01	0.083	0.06
AE (440-865nm)	Land	0.33	0.12	0.58	0.33
AOD (565 nm)	Ocean	0.038	0.00	0.073	-0.02
SSA (440 nm)	Ocean	0.074	0.053	0.08	0.06
AE (440-865nm)	Ocean	0.23	0.00	0.22	0.01

7 Recommendation for Future Research

Within the HARPOL project the SRON/RemoTAP and GRASP aerosol products retrieved from Multi-Angle Polarimetric (MAPs) PARASOL observations, have been substantially improved compared to the original data sets at the start of the project. SRON/RemoTAP and GRASP have very similar performance against AERONET, with some small differences in performance for Angstrom Exponent (AE – where GRASP compares slightly better to AERONET) and Single Scattering Albedo (SSA – where SRON/RemoTAP compares slightly better to AERONET). Overall, both SRON/RemoTAP and GRASP compare well with AERONET, although the performance depends on the region. For AE, Australia is a difficult region for both algorithms. Furthermore, both algorithms tend to underestimate AOD at high AOD, which is in particularly visible over China.

Away from the AERONET stations, differences between SRON/RemoTAP and GRASP can be substantially larger, with systematic differences in a different direction than expected from the AERONET comparison. Most notably, over ocean GRASP retrieves smaller SSA than SRON/RemoTAP. Both GRASP and SRON/RemoTAP show at some locations an unexpected sharp transition between land and ocean for SSA. For Angstrom exponent, both algorithms compare well for moderate and high AOD (>0.2). For low AOD, retrieval of both AE and SSA becomes more challenging and needs improvement. For AOD, a relatively large bias between SRON RemoTAP and GRASP occurs over the Rocky Mountains (SRON RemoTAP higher by ~0.03) and also over equatorial Africa.

The issue of cloud screening has not been investigated during HARPOL. First of all, AERONET measurements have been cloud screened already and hence a comparison between PARASOL and AERONET involves already an implicit cloud screening. Furthermore, because we have compared SRON/RemoTAP and GRASP for common pixels, effectively the combination of both cloud screening approaches has been used.

Based on our findings in the HARPOL project, and general product needs in the aerosol user community, we formulate the following recommendations for follow-on studies related to aerosol remote sensing:

- Further development and improvement of the SRON/RemoTAP and GRASP algorithms (and preferably more MAP aerosol algorithms). Although the comparison with AERONET of POLDER retrievals from both SRON/RemoTAP and GRASP is state-of-the-art, there are still limitations (improvements needed in absorption for GRASP and Angstrom Exponent for SRON/RemoTAP). In addition, it is important to focus algorithm intercomparisons not only on AERONET stations but perform global intercomparison as a good agreement at AERONET stations is no guarantee for global agreement.
- For upcoming European MAP missions (3MI, CO2M) perform a systematic comparison of the operational product to a product produced by one or (preferably)

more alternative scientific algorithms. This requires support to the alternative scientific algorithms for further development and improvement.

- For upcoming ESA MAP missions, perform a systematic comparison of aerosol products against MAP aerosol products from non-ESA missions (most notably the PACE mission with 2 MAP instruments).
- For PARASOL, perform global processing of the full archive (2005-2013) with the optimized versions of both GRASP and SRON/RemoTAP. This will be a very important data set for the aerosol-climate community as aerosol emissions have changed a lot in that period for different regions in the world.
- Evaluate the effect of different cloud screening algorithms. This should include cloud screening algorithms from the MAP instruments themselves and additional available instrumentation (high resolution radiometers like MODIS and METimage).
- Develop advanced methods for quality flagging. Currently quality flagging relies on goodness-of-fit only and involves typically a binary (good/bad) decision. Different parameters should be included in a quality flag and the flag should have different levels of quality so different users can decide to use different levels of the quality flag.
- Develop higher level data products that are needed by the scientific and broader user community. Examples of such products are: PM2.5, Cloud Condensation Nuclei (CCN), chemical composition, Direct Radiative Effect of Aerosols (DREA).
- Develop operational retrievals for aerosols above clouds. Investigate the possibilities and limitations of aerosol retrieval in partly cloudy scenes.
- Facilitate a better connection between the satellite community and the aerosol-modeling (climate / air quality, global / regional), in particular focused on the use (e.g. in data assimilation) of advanced data products that come available from MAP retrievals (absorption, size, refractive index, shape).
- Invest in a better validation infrastructure for ‘new’ aerosol products like Single Scattering Albedo (SSA), size distribution, refractive index (chemical composition). AERONET validation of these products are restricted to high AOD cases (> 0.4 at 440 nm) which will occur less in the coming decade because of expected reduced aerosol emissions.
- Develop synergetic aerosol products from multiple satellites. In particular, the combination of Earthcare with MAP aerosol retrievals is of interest. Unfortunately, Earthcare and MAP measurements are not performed at the same time but methods should be investigated to combine the different measurements (e.g. Earthcare with 3MI in a 9h30 orbit and with PACE in a 1h00 pm orbit).
- Investigate the capability to provide aerosol optical properties outside the spectral range of the level-1 measurements used for the retrieval. This is important when using aerosol products for light-path correction in Greenhouse gas retrievals

(CO2M) and also for the computation of radiative fluxes (direct aerosol radiative effect).

8 References

Chen, C., Dubovik, O., Henze, D. K., Chin, M., Lapyonok, T., Schuster, G. L., Ducos, F., Fuertes, D., Litvinov, P., Li, L., Lopatin, A., Hu, Q. and Torres, B.: Constraining global aerosol emissions using POLDER/PARASOL satellite remote sensing observations, Atmos. Chem. Phys., 19(23), 14585–14606, doi:10.5194/acp-19-14585-2019, 2019.

Chen, C., Dubovik, O., Fuertes, D., Litvinov, P., Lapyonok, T., Lopatin, A., Ducos, F., Derimian, Y., Herman, M., Tanré, D., Remer, L., Lyapustin, A., Sayer, A., Levy, R., Hsu, N. C., Descloitres, J., Li, L., Torres, B., Karol, Y., Herrera, M., Herreras, M., Aspetsberger, M., Wanzenboeck, M., Bindreiter, L., Marth, D., Hangler, A., and Federspiel, C.: Validation of GRASP algorithm product from POLDER/PARASOL data and assessment of multi-angular polarimetry potential for aerosol monitoring, Earth Syst. Sci. Data, 12(4), 3573–3620, doi:10.5194/essd-12-3573-2020, 2020.

Di Noia, A., Hasekamp, O. P., van Harten, G., Rietjens, J. H. H., Smit, J. M., Snik, F., Henzing, J. S., de Boer, J., Keller, C. U., and Volten, H.: Use of neural networks in ground-based aerosol retrievals from multi-angle spectropolarimetric observations, Atmos. Meas. Tech., 8, 281–299, https://doi.org/10.5194/amt-8-281-2015, 2015.

Di Noia, A., Hasekamp, O. P., Wu, L., van Diedenhoven, B., Cairns, B., and Yorks, J. E.: Combined neural network/Phillips–Tikhonov approach to aerosol retrievals over land from the NASA Research Scanning Polarimeter, Atmos. Meas. Tech., 10, 4235–4252, https://doi.org/10.5194/amt-10-4235-2017, 2017.

Dubovik, O. and King, M. D.: A flexible inversion algorithm for retrieval of aerosol optical properties from Sun and sky radiance measurements, J. Geophys. Res. Atmos., 105(D16), 20673–20696, doi:10.1029/2000JD900282, 2000.

Dubovik, O., Holben, B., Eck, T. F., Smirnov, A., Kaufman, Y. J., King, M. D., Tanré, D. and Slutsker, I.: Variability of Absorption and Optical Properties of Key Aerosol Types Observed in Worldwide Locations, J. Atmos. Sci., 59(3), 590–608, doi:10.1175/1520-0469(2002)059<0590:VOAAOP>2.0.CO;2, 2002.

Dubovik, O., Sinyuk, A., Lapyonok, T., Holben, B. N., Mishchenko, M., Yang, P., Eck, T. F., Volten, H., Muñoz, O., Veihelmann, B., van der Zande, W. J., Leon, J.-F., Sorokin, M. and Slutsker, I.: Application of spheroid models to account for aerosol particle nonsphericity in remote sensing of desert dust, J. Geophys. Res., 111(D11), D11208, doi:10.1029/2005JD006619, 2006.

Dubovik, O., Herman, M., Holdak, A., Lapyonok, T., Tanré, D., Deuzé, J. L., Ducos, F., Sinyuk, A. and Lopatin, A.: Statistically optimized inversion algorithm for enhanced retrieval of aerosol properties from spectral multi-angle polarimetric satellite observations, Atmos. Meas. Tech., 4(5), 975–1018, doi:10.5194/amt-4-975-2011, 2011.

Dubovik, O., Lapyonok, T., Litvinov, P., Herman, M., Fuertes, D., Ducos, F., Torres, B., Derimian, Y., Huang, X., Lopatin, A., Chaikovsky, A., Aspetsberger, M. and Federspiel, C.: GRASP: a versatile algorithm for characterizing the atmosphere, SPIE Newsroom, doi:10.1117/2.1201408.005558, 2014.

Fan, C., Fu, G., Di Noia, A., Smit, M., HH Rietjens, J., A Ferrare, R., Burton, S., Li, Z. and P Hasekamp, O., 2019. Use of a neural network-based ocean body radiative transfer model for aerosol retrievals from multi-angle polarimetric measurements. *Remote Sensing*, *11*(23), 2019.

Bertrand Fougnie, Julien Chimot, Margarita Vázquez-Navarro, Thierry Marbach, Bojan Bojkov, Aerosol retrieval from space – how does geometry of acquisition impact our ability to characterize aerosol properties, Journal of Quantitative Spectroscopy and Radiative Transfer, Volume 256, 2020,107304, ISSN 0022-4073, https://doi.org/10.1016/j.jqsrt.2020.107304.

Fu, G. and Hasekamp, O.: Retrieval of aerosol microphysical and optical properties over land using a multimode approach, Atmos. Meas. Tech., 11(12), 6627–6650, doi:10.5194/amt-11-6627-2018, 2018.

Fu, G., Hasekamp, O., Rietjens, J., Smit, M., Di Noia, A., Cairns, B., Wasilewski, A., Diner, D., Seidel, F., Xu, F., Knobelspiesse, K., Gao, M., da Silva, A., Burton, S., Hostetler, C., Hair, J., and Ferrare, R.: Aerosol retrievals from different polarimeters during the ACEPOL campaign using a common retrieval algorithm, Atmos. Meas. Tech., 13, 553–573, https://doi.org/10.5194/amt-13-553-2020, 2020.

Giles, D. M., Sinyuk, A., Sorokin, M. G., Schafer, J. S., Smirnov, A., Slutsker, I., Eck, T. F., Holben, B. N., Lewis, J. R., Campbell, J. R., Welton, E. J., Korkin, S. V. and Lyapustin, A. I.: Advancements in the Aerosol Robotic Network (AERONET) Version 3 database – automated near-real-time quality control algorithm with improved cloud screening for Sun photometer aerosol optical depth (AOD) measurements, Atmos. Meas. Tech., 12(1), 169–209, doi:10.5194/amt-12-169-2019, 2019.

Hasekamp, O.P. and Landgraf, J. : Linearization of vector radiative transfer with respect to aerosol properties and its use in satellite remote sensing. Journal of Geophysical Research: Atmospheres, 110(D4), doi.org/10.1029/2004JD005260, 2005.

Hasekamp, O. P. and Landgraf, J.: Retrieval of aerosol properties over land surfaces: Capabilities of multiple-viewing-angle intensity and polarization measurements, Appl. Opt., 46(16), 3332–3343, doi:10.1364/AO.46.003332, 2007.

Hasekamp, O. P., Litvinov, P. and Butz, A.: Aerosol properties over the ocean from PARASOL multiangle photopolarimetric measurements, J. Geophys. Res., 116(D14), D14204, doi:10.1029/2010JD015469, 2011.

Hasekamp, O. P., Gryspeerdt, E. and Quaas, J.: Analysis of polarimetric satellite measurements suggests stronger cooling due to aerosol-cloud interactions, Nat. Commun., 10(1), 1–7, doi:10.1038/s41467-019-13372-2, 2019.

Hsu, N. C., Jeong, M.-J., Bettenhausen, C., Sayer, A. M., Hansell, R., Seftor, C. S., Huang, J., and Tsay, S.-C.: Enhanced Deep Blue aerosol retrieval algorithm: The second generation, J. Geophys. Res.-Atmos., 118, 9296–9315, https://doi.org/10.1002/jgrd.50712, 2013.

Li, L., Dubovik, O., Derimian, Y., Schuster, G. L., Lapyonok, T., Litvinov, P., Ducos, F., Fuertes, D., Chen, C., Li, Z., Lopatin, A., Torres, B. and Che, H.: Retrieval of aerosol components directly from satellite and ground-based measurements, Atmos. Chem. Phys., 13409–13443, doi:10.5194/acp-19-13409-2019, 2019.

Li, X. and Strahler, A. H.: Geometric-Optical Bidirectional Reflectance Modeling of the Discrete Crown Vegetation Canopy: Effect of Crown Shape and Mutual Shadowing, IEEE Trans. Geosci. Remote Sens., 30(2), 276–292, doi:10.1109/36.134078, 1992.

Litvinov, P., Hasekamp, O. and Cairns, B.: Models for surface reflection of radiance and polarized radiance: Comparison with airborne multi-angle photopolarimetric measurements and implications for modeling top-of-atmosphere measurements, Remote Sens. Environ., 115(2), 781–792, doi:10.1016/j.rse.2010.11.005, 2011a.

Litvinov, P., Hasekamp, O., Cairns, B. and Mishchenko, M.: Semi-empirical BRDF and BPDF models applied to the problem of aerosol retrievals over land: testing on airborne data and implications for modeling of top-of-atmosphere measurements, in book: Polarimetric Detection, Characterization and Remote Sensing, Springer, Dordrecht., 2011b.

Lacagnina, C., Hasekamp, O. P., Bian, H., Curci, G., Myhre, G., van Noije, T., Schulz, M., Skeie, R. B., Takemura, T. and Zhang, K.: Aerosol single-scattering albedo over the global oceans: Comparing PARASOL retrievals with AERONET, OMI, and AeroCom models estimates, J. Geophys. Res., 120(18), 9814–9836, doi:10.1002/2015JD023501, 2015.

Lacagnina, C., Hasekamp, O. P. and Torres, O.: Direct radiative effect of aerosols based on PARASOL and OMI satellite observations, J. Geophys. Res., 122(4), 2366–2388, doi:10.1002/2016JD025706, 2017.

Levy, R. C., Mattoo, S., Munchak, L. A., Remer, L. A., Sayer, A. M., Patadia, F., and Hsu, N. C.: The Collection 6 MODIS aerosol products over land and ocean, Atmos. Meas. Tech., 6, 2989– 3034, https://doi.org/10.5194/amt-6-2989-2013, 2013.

Maignan, F., Bréon, F. M., Fédèle, E. and Bouvier, M.: Polarized reflectances of natural surfaces: Spaceborne measurements and analytical modeling, Remote Sens. Environ., 113(12), 2642–2650, doi:10.1016/j.rse.2009.07.022, 2009.

Mishchenko, M.I., and L.D. Travis, 1997: Satellite retrieval of aerosol properties over the ocean using polarization as well as intensity of reflected sunlight. J. Geophys. Res., 102, 16989-17013, doi:10.1029/96JD02425.

O'Neill, N. T., Eck, T. F., Smirnov, A., Holben, B. N. and Thulasiraman, S.: Spectral discrimination of coarse and fine mode optical depth, J. Geophys. Res. Atmos., 108(17), doi:10.1029/2002jd002975, 2003.

Ross, J.: The radiation regime and architecture of plant stands, Dr W. Junk Publishers., The Hague, Netherlands., 1981.

Stap, F. A., Hasekamp, O. P., and Röckmann, T.: Sensitivity of PARASOL multi-angle photopolarimetric aerosol retrievals to cloud contamination, Atmos. Meas. Tech., 8, 1287–1301, https://doi.org/10.5194/amt-8-1287-2015, 2015.

Schaaf, C., Wang, Z. (2015). MCD43C1 MODIS/Terra+Aqua BRDF/AlbedoModel Parameters Daily L3 Global 0.05Deg CMG V006 [Data set]. NASA EOSDIS Land Processes DAAC. Accessed 2021-06-16 from https://doi.org/10.5067/MODIS/MCD43C1.006

Schutgens, N., Dubovik, O., Hasekamp, O., Torres, O., Jethva, H., Leonard, P. J. T., Litvinov, P., Redemann, J., Shinozuka, Y., de Leeuw, G., Kinne, S., Popp, T., Schulz, M., and Stier, P.: AEROCOM/AEROSAT AAOT & SSA study, part I: evaluation and intercomparison of satellite measurements, Atmos. Chem. Phys., 21(9), 6895-6917, https://doi.org/10.5194/acp-21-6895-2021, 2021.

Tsikerdekis, A., Schutgens, N. A. J. and Hasekamp, O. P.: Assimilating aerosol optical properties related to size and absorption from POLDER/PARASOL with an ensemble data assimilation system, Atmos. Chem. Phys., 21(4), doi:10.5194/acp-21-2637-2021, 2021.

Wu, L., Hasekamp, O., van Diedenhoven, B., and Cairns, B.: Aerosol retrieval from multiangle, multispectral photopolarimetric measurements: importance of spectral range and angular resolution, Atmos. Meas. Tech., 8, 2625–2638, https://doi.org/10.5194/amt-8-2625-2015, 2015.

Wu, L., Hasekamp, O., van Diedenhoven, B., Cairns, B., Yorks, J.E. and Chowdhary, J., 2016. Passive remote sensing of aerosol layer height using near-UV multiangle polarization measurements. Geophysical research letters, *43*(16), doi.org/10.1002/2016GL069848, 2016.